~~CONFIDENTIAL~~

TECHNICAL MEMORANDUM

UB
NASA TM X-1423

(NASA-TM-X-1423) FEASIBILITY STUDY OF A TUNGSTEN WATER-MODERATED NUCLEAR ROCKET. 4: NEUTRONICS P.G. Klann, et al (NASA) Mar. 1968 163 p

N72-74700

Unclas
00/99 40224

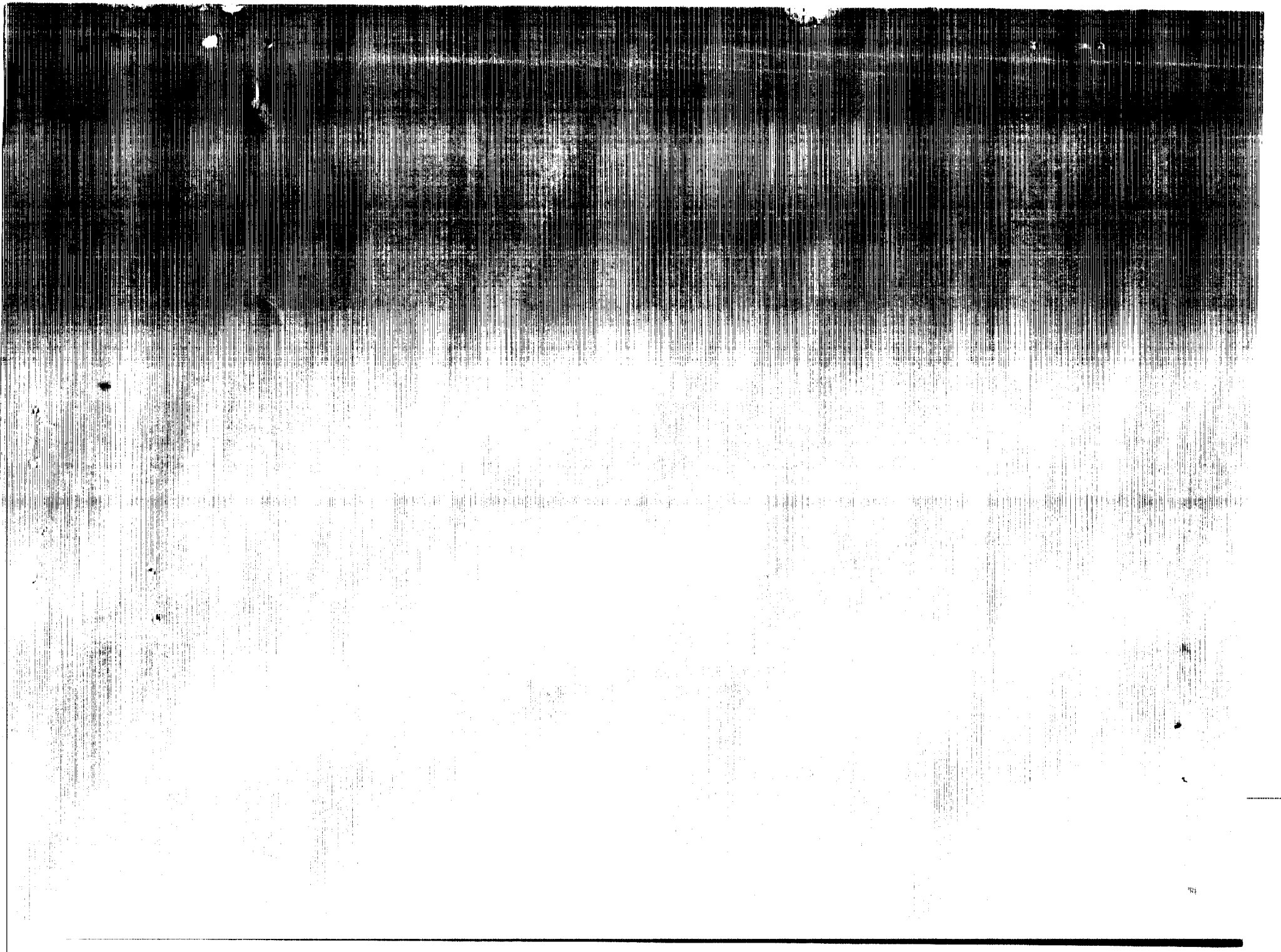

[redacted]

NASA TM X-1423

FEASIBILITY STUDY OF A TUNGSTEN WATER-MODERATED NUCLEAR ROCKET

IV. NEUTRONICS

By Paul G. Klann, Wendell Mayo, Edward Lantz, and Walter A. Paulson

Lewis Research Center
Cleveland, Ohio

[redacted]

[redacted]

[redacted]

[redacted]

NATIONAL AERONAUTICS AND SPACE ADMINISTRATION

[redacted]

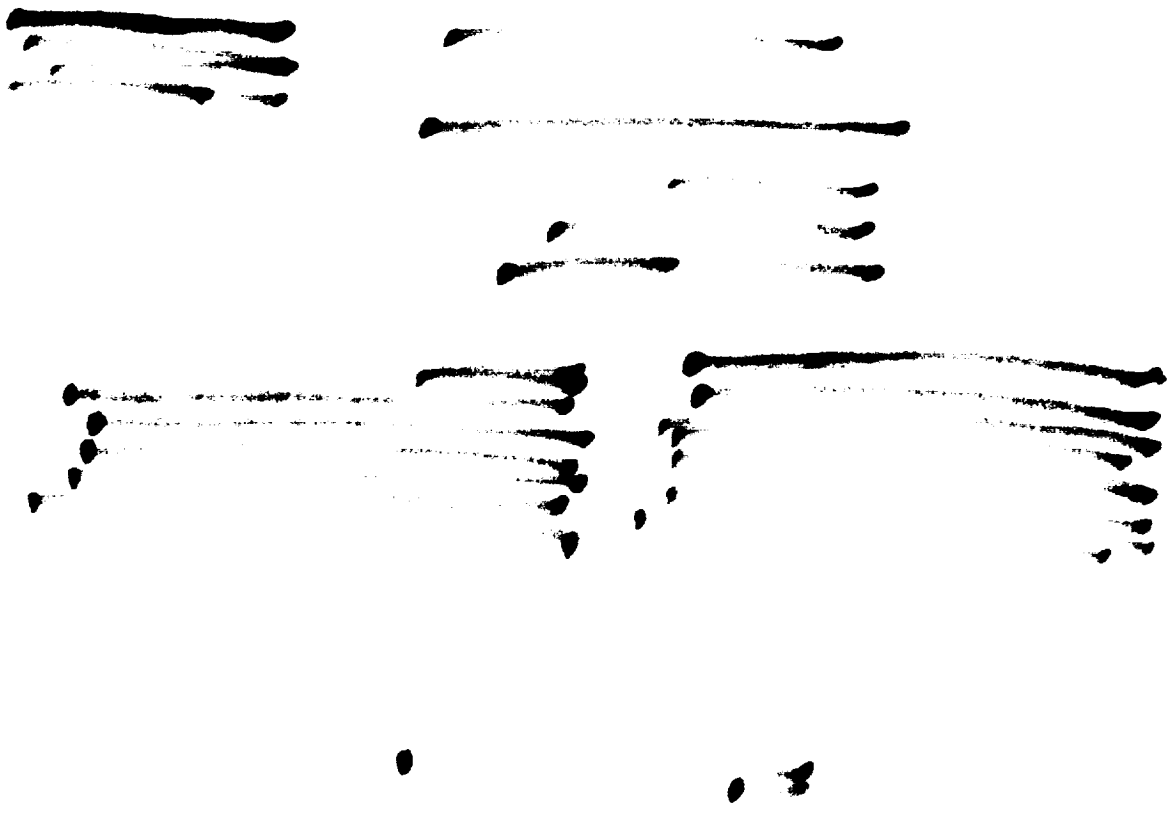

PREFACE

The concept of a nuclear rocket system based on the use of a tungsten water-moderated reactor (TWMR) was originated at the Lewis Research Center. The TWMR is a thermal reactor that uses water as the moderator, uranium dioxide as the fuel, and tungsten enriched in tungsten 184 as the fuel element structural material. As is common to all nuclear rocket systems, hydrogen is used as the propellant to maximize specific impulse. The reactor (see illustration) consists of a tank containing a number of pressure tubes that are attached to tube sheets at the inlet and outlet ends of the reactor. The pressure tubes contain the fuel elements. The space inside the tank between the tubes is filled with water, which serves both as the neutron moderator and as a coolant for the structure. Heat is generated in the water by neutrons and gamma rays and is also transferred to the water by heat leakage from the hot fuel elements, each of which is located in a pressure tube. The removal of heat is provided by pumping the water through the core and a heat exchanger in a closed loop. The water is regeneratively cooled in the heat exchanger by the hydrogen propellant, which flows from a supply tank through the nozzle and heat exchanger into the core. As the hydrogen flows through the core pressure tubes and through the fuel elements, it is heated to a high temperature and is expanded out the nozzle to produce thrust.

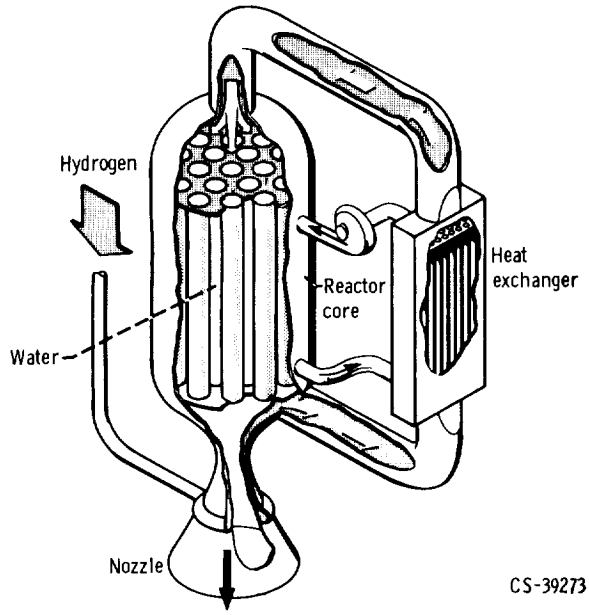

The potential advantages of the concept lie in the following areas: The use of tungsten provides a high-temperature material with good thermal shock resistance, tensile and compressive strength, thermal conductivity, and resistance to corrosion by the hydrogen propellant. The properties of tungsten also permit the fabrication of fuel elements with very thin cross sections for good heat transfer. The use of water as the moderator provides a good coolant for the pressure vessel and structural members and reduces core size and weight over that obtained for most moderator materials. In this concept, the fuel element assemblies are structurally independent of each other and thus permit individual development of these assemblies.

A program was undertaken at Lewis to investigate the engineering feasibility and performance of the TWMR nuclear rocket system. The results of these investigations, which are summarized in part I (NASA Technical Memorandum X-1420) of this series of reports, are presented in detail in the other six parts of the series as follows: II. Fueled Materials (NASA Technical Memorandum X-1421); III. Fuel Elements (NASA Technical Memorandum X-1422); IV. Neutronics (NASA Technical Memorandum X-1423); V. Engine System (NASA Technical Memorandum X-1424); VI. Feed System and Rotating Machinery (NASA Technical Memorandum X-1425); VII. System Dynamics (NASA Technical Memorandum X-1426).

CONTENTS

FEASIBILITY STUDY OF A TUNGSTEN WATER-MODERATED NUCLEAR ROCKET

IV. NEUTRONICS (U)

by Paul G. Klann, Wendell Mayo, Edward Lantz, and Walter A. Paulson

Lewis Research Center

SUMMARY

As part of an overall effort to evaluate the tungsten water-moderated reactor (TWMR) concept for rocket application, the neutronic feasibility of the reference design was investigated both analytically and experimentally. Results of these studies show that sufficient reactivity is available to allow for both a negative water temperature reactivity coefficient and a tailored power distribution in the reference core.

An important program objective was to show that the neutronics and the radiation heating of these reactors are understood to the degree that reasonably accurate calculations can be made. It was found that the reactivity of these cores can be calculated within a few percent. Also, very good analytical-experimental agreement was obtained for the power distribution within a fuel assembly. The calculated values for the gross radial and axial power densities were quite good throughout most of the core, but they were in error by as much as 10 to 15 percent close to the beryllium reflector. This error should not be construed as an absolute error however, since no serious attempt was made to calculate accurate gross power distributions in the interest of saving computer time. In the calculation of the in-core gamma heating, it was found that the heterogeneity of the reactor must be accounted for. Some improvements in the methods are required to calculate accurate temperature reactivity coefficients and the decay constant of the fundamental mode, but, in general, the results of the experimental-analytical comparisons show that the neutronics of these cores is understood.

INTRODUCTION

A neutronics program was undertaken as part of the overall study effort on the tung-

sten water-moderated reactor (TWMR). This program consisted of generating sufficiently detailed information from reactor analysis and critical experiments to show the neutronic feasibility of the concept.

The general procedure followed was first to obtain and update the nuclear cross-section data. Then computer programs were acquired and developed to predict reactivity, power density distributions, and kinetics parameters. Finally critical experiments were performed that established the validity of results obtained by calculational methods in predicting operating characteristics and parameters. In order to obtain a consistent set of parameters for the overall rocket system, a specific reference design was selected; however, cores other than the reference design were also studied.

The most important criterion in determining the neutronic feasibility of a nuclear rocket reactor concept is the amount of excess reactivity obtainable with a uranium concentration that allows sufficient high-temperature strength in the fuel element. Excess reactivity in a reactor design permits power density tailoring, negative temperature coefficients of reactivity, minimizing reflector thickness, and/or a choice of reflector materials. Other uses can always be found for any surplus of excess reactivity. In fact, a reactor concept may not be considered feasible without a reasonable surplus of excess reactivity.

At the start of the TWMR program, it was not known whether the reactivity of these heterogeneous reactors could be calculated with good accuracy. Neutron cross sections for different tungsten isotopes were not well known. Thus, the reactor physics effort preceding the work described in this report was devoted primarily to determination of tungsten cross sections. After cross sections were considered reasonably well known, computer programs were obtained that provided results with accuracy comparable to that of the cross sections. These programs, which are described herein, were used to develop a reference design and then a set of critical experiments.

One of the primary purposes of the experiments was to verify the calculated excess reactivity, but other purposes were to measure power distributions and moderating water temperature coefficients. Calculations were compared with experiments throughout the program. Many of these comparisons are included.

Although determination of excess reactivity available for a reactor concept gives an indication of neutronic feasibility, it does not guarantee that a reactor of a specific size and power can be built. Reactivity requirements for the reference reactor are defined, therefore, to show compatibility with available excess reactivity.

The feasibility of the concept also depends on its dynamic behavior. The value of certain parameters such as temperature coefficients, prompt neutron lifetime, and effective delayed neutron fraction were required for these studies. Techniques for calculating these parameters are evaluated in this report.

Another factor vital to the feasibility and design of the TWMR is the radiation heating in the water and tungsten regions of the core. A Monte Carlo code was developed to pre-

dict the gamma heating. Experiments were run in a specially instrumented critical reactor to obtain comparative experimental data. A discussion of this computer program is included.

The following Lewis personnel have contributed to the material presented in this report: Robert E. Sullivan, John L. Anderson, Jr., Clayton E. Barber, Marvin R. Clark, Colin A. Heath, and Robert M. Westfall.

CRITICAL EXPERIMENTS, ANALYSES, AND RESULTS

The neutronic feasibility of the tungsten water-moderated reactor (TWMR) concept depends on the core having sufficient available reactivity to accommodate power tailoring, temperature defect, and burnup within metallurgically imposed limits on fuel-element loading. In addition, capabilities of the proposed liquid poison control systems to shut down and regulate the reactivity excess adequately, together with intrinsic core reactivity coefficients, must be demonstrated.

This feasibility study was based on (1) results of a series of critical experiments conducted on water- and beryllium-reflected cores with the basic design features of the reference-design reactor, and (2) analytical interpretation of these results by using updated nuclear data and sophisticated reactor analysis methods. The experimental program consisted of acquisition of criticality data, measurement of excess reactivities, reactivity coefficients, temperature coefficients, and the measurement of gross and detailed power distributions. Basic design principles and margins of the reference-design reactor are corroborated by the critical experiment program and supporting reactor analyses. Analytical methods developed in support of the experimental program are sufficiently generalized and have sufficient physical basis to permit analysis of larger and smaller reactor designs with a fair degree of confidence.

In addition to corroborating the reactor physics, the nuclear feasibility study was concerned with obtaining information for design of ancillary equipment. The specification of the moderator heat-exchanger design for the TWMR system required accurate data on the rate of gamma heat deposition in the water and tungsten regions of the core. A gamma heating program was therefore developed to calculate the rate of gamma heat deposition as a function of position in the core when the spatial distribution of fission power generation was known. Data were obtained to check the validity and the precision of this program by measuring the rate of gamma heat deposition and the rate of fission power generation throughout the beryllium-reflected core. This report shows that the distribution and magnitude of the deposition rate of gamma heating in the unzoned beryllium-reflected

core can be calculated within the precision required to establish the design of heat-exchanger components for the water cooling loop.

REFERENCE-DESIGN TWMR

Configuration and Fuel-Element Design

The reference-design TWMR (fig. 1) contains 121 fuel elements in a hexagonal array, with a pitch of 8.016 centimeters, with the 6 outer corner elements removed. The core is light-water moderated and beryllium reflected on the sides and at the inlet end. Each fuel element consists of 26 fuel stages, each 3.81 centimeters long and each consisting of 10 concentric fueled cylinders (table 1), the largest of which has an outer diameter of 5.034 centimeters. The fueled cylinders are cermets of separated tungsten (W) and enriched uranium dioxide (UO_2) clad with separated tungsten. The separated tungsten has an isotopic composition (in weight percent) of 87-percent W^{184}, 10-percent W^{183}, 1.6-percent W^{182}, and 1.4-percent W^{186}. The fuel stages are supported by an axially continuous unfueled support tube of separated tungsten. The active core length is 106.998 centimeters. The tungsten support tubes containing fueled stages are inserted inside 6.35-centimeter-diameter aluminum pressure tubes, within which the hydrogen propellant is heated. Circulating water occupies the volume between the pressure tubes and acts as a neutron moderator as well as a coolant for the pressure tubes.

The spatial power generation in the core will be tailored so that all the fuel elements will be operating near the limit of their heat-transfer capability. The power tailoring of the reference-design core will be accomplished by substituting natural tungsten for separated tungsten in core regions where it is desirable to depress the power. The radial power distribution will be flattened by replacing separated tungsten support tubes with natural tungsten support tubes in the 19 central fuel elements in the core. The axial power distribution will be peaked toward the inlet of the core by replacing the separated W-UO_2 cermet material in stages 12 to 21 (45.4 to 86.7 cm from inlet end) with 30-percent natural tungsten and 70-percent separated W-UO_2 cermet material.

Soluble Poison Control System

The reference-design reactor will be controlled by varying the concentration of the cadmium sulfate ($CdSO_4$) - water solution in control tubes located in the center of each of the water triflutes between the fuel elements. During reactor operation, there will be a continuous flow of poison solution (fig. 2) down the central inlet pipe within the control

tube and out the annular passage between the pipe and the control tube. An ion exchanger will reduce the concentration of the poison flowing in the system, while a pressurized supply of concentrated poison solution will increase the concentration.

EXPERIMENTAL CORES

Critical experiments to obtain data on the TWMR concept were conducted by the General Atomic Division of General Dynamics Corporation at San Diego (refs. 1 to 8) and by the General Electric Company at the National Reactor Testing Station, Idaho Falls (refs. 9 and 10). Critical experiments conducted by General Atomic were concerned with obtaining data on the 121-fuel-element 1500 megawatt reference-design core. Additional information was obtained from experiments by General Electric in connection with a 37-fuel-element core. This configuration, however, was not of primary interest in this feasibility study.

Critical Experiments at General Atomic

Critical configurations. - Critical configurations measured at the Nuclear Rocket Facility at General Atomic consisted of 121 fuel elements in hexagonal array with the 6 corner fuel elements removed (fig. 3(a)). The active core length was 106.363 centimeters. The fuel elements were contained in 6.502-centimeter-diameter, 0.163-centimeter-wall, watertight aluminum pressure tubes, spaced on triangular lattice pitches; light-water moderators surrounded the aluminum pressure tubes.

Measurements were made with the configurations fully reflected by light water at 7.62- and 7.37-centimeter lattice pitches (cores I and II). In addition, measurements were also made with the 7.62-centimeter-pitch configuration reflected with a 7.30-centimeter-thick beryllium side reflector, backed with 0.635-centimeter boral sheeting, and a 10.16-centimeter-thick beryllium bottom reflector (core IV). The purpose of the boral sheeting was to decouple the water exterior to the beryllium reflector from the core, since this additional water is not present in the reference design.

Two zoned configurations were built, using the 7.62-centimeter-pitch, beryllium-reflected configuration, by adding natural tungsten to the fuel elements in specific regions of the core. The first configuration (core V) was radially zoned by the addition of 0.0254-centimeter natural tungsten foil wrapped around the U^{238} rings in the 19 central fuel elements. The second configuration (core VI) was radially and axially zoned by the further addition of 0.127-centimeter natural tungsten sleeves that fit over the innermost fuel rings of stages 11 to 19, 45 to 85.5 centimeters from the bottom of each fuel-element

core. This method of zoning the mockup resulted in a good simulation of the zoned reference-design core. These cores are summarized in table 2.

General Atomic mockup fuel elements. - The reference-design fuel-element matrix, clad, and support components were constructed of a reference-design mixture of tungsten isotopes enriched in low neutron-absorbing W^{184} isotope to make efficient use of the allowable fuel concentrations in the thermal spectrum of the core. Since appreciable quantities of this reference-design tungsten mixture were not available, mockup fuel elements were used for the critical experiments. These fuel elements were constructed of natural tungsten, aluminum, U^{235}, and U^{238} and combined to match neutronic, spectral, and geometric characteristics of the reference-design fuel element analytically. This analytical match was made by using sophisticated nuclear analysis techniques that incorporated recently reviewed and updated nuclear cross-section data.

A 5-ring mockup fuel element was selected on the basis of the available fuel material to simulate the 10-ring reference-design fuel element. The main structural components of this mockup element consisted of five core-length pieces of thin-wall aluminum tubing whose diameters were graduated so that the tubes could be concentrically assembled. The mockup fuel element (fig. 3(b)) was constructed by wrapping each aluminum tube with twenty-four 4.128-centimeter-wide, 0.0127-centimeter-thick natural tungsten bands, overlaid and clamped by 4.128-centimeter-wide, 0.107-centimeter-thick uranium-aluminum alloy rings containing approximately 35 weight percent uranium enriched to 93.15 weight percent in U^{235}. The bands were separated by 0.318-centimeter-wide corrugated aluminum spacers, which also held the aluminum tubes concentrically alined. The outer fuel-element tube assembly (fig. 3(b)) was further wrapped with twenty-four 4.128-centimeter-wide, 0.0076-centimeter-thick bands of tungsten and encased in 4.128-centimeter-wide, 0.102-centimeter-thick U^{238} metal rings (separated by the 0.318-cm-wide Al spacers).

The fuel element (fig. 3(b)) was assembled by threading the smallest diameter aluminum tube into the aluminum endplate; the successively large tubes were next slipped over the inner tube in turn, each being held concentric by the aluminum spacers. The top aluminum endplate was then threaded on the center tube. The completed fuel element was inserted into the 6.162-centimeter-inner-diameter watertight aluminum pressure tube. The fuel-element assemblies were then spaced on the desired lattice pitch.

Each mockup fuel element thus consisted of twenty-four 4.128-centimeter-high stages separated by 0.318-centimeter spacers, each stage (fig. 3) of which was composed of five distinct rings that were composites of aluminum, natural tungsten and uranium-aluminum alloy. The outer ring also contained U^{238}. Dimensions of the mockup fuel stage are listed in table 3.

In order to obtain experimental confirmation of the analytically established mockup of the reference fuel element, several kilograms of calutron-separated tungsten isotopes

were obtained from Oak Ridge. These isotopes were used to fabricate five special fuel stages, which were substituted for five of the mockup stages in the center fuel assembly of the mockup core. The resulting change of reactivity was then measured. Since the isotopic composition of the reference fuel stage could not be duplicated exactly by the special stages, the special stages were fabricated of removable isotopic tungsten rings. Varying the number of rings in the special stages permitted bracketing of the composition and the expected worth of the reference stages. The mockup fuel stage worth lay between the compositions that bracketed the reference composition. The measured deviation between the mockup fuel stages and the special fuel stages could be calculated to within 0.5-percent reactivity $\Delta k/k$. This close agreement gave strong support to the method of treating the individual tungsten isotopes in the calculations used in establishing the mockup fuel elements. This experiment is discussed in greater detail in the section EXPERIMENTAL COMPARISON OF GENERAL ATOMIC MOCKUP FUEL STAGES WITH SPECIAL REFERENCE-DESIGN FUEL STAGES.

Soluble poison system. - Excess reactivity from each critical configuration was offset by cadmium nitrate ($CdNO_3$) - water poison solution in the control tubes located at the midpoint of each triangular lattice of fuel elements (fig. 3(a)). Control tubes consisted of nickel-plated aluminum with an inner diameter of 1.27 centimeters and and a wall thickness of 0.0794 centimeter. The $CdNO_3$ solution was used in place of the reference cadmium sulfate ($CdSO_4$) solution to reduce the potential hazard of large-scale corrosion of the aluminum though pin holes in the nickel plating. This poison system was a static simulation of the proposed reference-design control system.

Experimental program. - The experimental program consisted of acquisition of criticality data on water-reflected, beryllium-reflected, and zoned-beryllium-reflected core measurements of core excess reactivity, reactivity coefficients, gross and detailed power distributions, and circumferential power distributions around fuel elements in various locations. The temperature coefficient was determined in a series of steps from 20° to 80° C for both the unzoned and zoned cores. In addition, the prompt neutron lifetime was inferred from pulsed neutron measurements.

Critical Experiments at General Electric

Initial planning of the TWMR rocket study program did not include acquisition of criticality data on a small 37-fuel-element critical assembly. An opportunity was presented, however, to obtain valuable data on this core size at small cost by making use of the General Electric 630-A Low Power Test Facility (ref. 11).

Critical configurations. - The critical configuration measured at the General Electric facility consisted of a 37-fuel-element hexagonal array (fig. 4). The active core length

was 69.342 centimeters. Fuel elements were contained in 6.35-centimeter-outer-diameter, 0.165-centimeter-thick-wall, watertight aluminum pressure tubes spaced on a 7.87-centimeter pitch, and the pressure tubes were surrounded by a light-water moderator. Measurements were made with a light-water reflector at the bottom and the top, and with a 9.525-centimeter-thick beryllium reflector backed by additional water on the six sides of the core. For one set of measurements, a 0.635-centimeter-thick boral sheet was placed adjacent to the beryllium reflector to decouple this additional water, which is not present in the reference design, from the core.

General Electric test fuel element. - The main structural components of the fuel element, shown in figure 5, consisted of a central 0.165-centimeter-thick-wall aluminum tube, three 0.0152-centimeter-thick-wall nichrome mandrel cylinders, and an outer 0.066-centimeter-thick-wall stainless-steel cylinder. The cylinders were of graduated diameters to permit nesting, and the nichrome mandrel cylinders included protrusions preformed into them to separate the band wrappings. The cylinders were held concentric in the fuel-element assembly by the aluminum endplates. The aluminum tube and nichrome cylinders were each wrapped along the length with nine 7.303-centimeter-wide bands made of enriched 0.00254-centimeter U^{235} and natural tungsten foil to form nine axial stages. These nine bands were spaced 0.508 centimeter apart by the protrusions preformed in the nichrome tubing mandrels. An additional layer of aluminum was wrapped over the nine bands of the largest nichrome tube mandrel. Lastly, each nichrome mandrel was encased in a full-length sheath of U^{238} (not shown in the figure), and the stainless-steel cylinder was wrapped with nine 7.303-centimeter-wide tungsten bands spaced to overlay the layers wrapped on the nichrome mandrels.

The fuel element was assembled by sliding the nichrome mandrels and the stainless-steel cylinder over the center aluminum tube, then concentrically positioning the mandrels with an end fitting associated with the aluminum tube (fig. 5). The assembly was completed by sliding the upper fitting into place and tightening the wing nut on an extension to the center aluminum tube.

Soluble poison system. - Excess reactivity of the 37-fuel-element configuration was held down by the aqueous $CdSO_4$ solution contained in control poison tubes located at midpoints of the triangular lattice of fuel elements (fig. 4). The control poison tubes consisted of a 1.905-centimeter-outer-diameter, 0.124-centimeter-thick-wall aluminum tube lined with 1.588-centimeter-outer-diameter, 0.1588-centimeter-thick wall polypropylene tubing to prevent corrosion of aluminum by the $CdSO_4$ solution. During measurement of the moderator temperature coefficient and power distribution, 48 control poison tubes were in the core, the remaining six poison tube positions were occupied by control rod guides.

Experimental program. - The experimental program conducted at General Electric consisted of measurements of excess reactivity of the core, reactor control system reactivity, gross fission power distribution, and detailed total and epicadmium fine

radial and axial power distributions on the center fuel element. In addition, circumferential power distributions around fuel elements were obtained on fuel elements situated at representative core locations. The moderator temperature coefficient was measured in the 37-fuel-element assembly with the 9.525-centimeter beryllium reflector backed by a water reflector and also with a 0.635-centimeter boral sheet interposed between the beryllium reflector and the water.

ANALYTICAL COMPARISON OF GENERAL ATOMIC MOCKUP AND REFERENCE-DESIGN CORES

Composition and Geometry of Mockup Fuel Element

The 5-ring General Atomic mockup fuel element was designed to have a fuel loading identical to that of the reference-design fuel element, with enriched tungsten simulated by a combination of natural tungsten, aluminum, and depleted U^{238}. This combination contained about one-sixth the number of tungsten atoms of the reference-design material, or about the maximum of natural tungsten that could be accommodated commensurate with matching reference-design thermal absorption. Aluminum was used as the structural material because of its small thermal capture cross section and its lack of resonance absorption. In addition, the effect of inelastic scattering from the enriched tungsten of the reference-design element on the slowing-down length in the core was approximated by varying the amount of aluminum in the mockup fuel element. The depleted U^{238} was added to increase resonance absorption to that of the reference-design composition.

Because of the constraints imposed by the fixed thickness dimension and composition of uranium-aluminum alloy used for the mockup fuel element, it was not possible to design a completely suitable 5-ring element with equally spaced fuel rings and the exact outer dimension of the reference-design fuel element. However, 5-ring equally spaced design was achieved when the outside U^{238} ring of the mockup fuel element was set at a diameter 1.6 percent less than the outer diameter of the tungsten radiation shield of the original reference-design fuel element. The dimensions and composition of the reference-design fuel element and the mockup fuel element are listed in tables 1 and 3.

Comparison of Major Reactor Parameters Calculated for Mockup and Unzoned Reference Cores

The unzoned reference-design and mockup fuel elements were analytically compared

in two geometrically identical cores using the method discussed in the section General Atomic Design Method. Both calculated cores contained 121 fuel elements spaced in a hexagonal array on a pitch of 8.016 centimeters and were reflected by the beryllium-water reflector specified for the reference-design core. The cadmium poison was omitted for these calculations.

A comparison of major reactor parameters for the reference-design core and the mockup core is shown in table 4. The fast parameters are flux-weighted averages over the slowing-down spectra from 2.38 eV to 14.9 MeV. The thermal parameters are flux-weighted averages over the thermal spectra from 0 to 2.38 eV.

It can be seen in table 4 that an adequate match has been achieved for the majority of nuclear parameters. The most important deviation occurs in macroscopic fission cross sections that differ by about 6.5 percent in the thermal energy region. This difference arises because it is not possible to match both the total fuel loading and the fuel self-shielding factor of the reference-design fuel element with a 5-ring fuel element in which the fuel thickness and loading of the rings are independently fixed. Therefore, the mock-up core is effectively more heavily loaded than the reference-design core. This difference in the effective loading is reflected in a slightly harder spectrum and a greater depression in the thermal spectrum of the mockup core. The effect of this deviation on the infinite multiplication factor k_∞ was slight and resulted in about a 1-percent deviation between the reference-design and mockup cores. (All symbols are defined in appendix A.)

A difference in the Fermi age between the mockup core and reference-design core was also calculated. The Fermi age in the mockup core was approximately 5 percent less than that of the reference-design core over the entire slowing-down range. The effect of this difference in high energy leakage is small, as will be seen by comparison of effective reactivities.

The epithermal and thermal macroscopic capture cross sections for the tungsten isotopes and U^{238} in the mockup and reference-design cores are compared in table 5. These data indicate that resonance absorption of the separated tungsten specified for the reference-design core is adequately simulated in the mockup core by a combination of natural tungsten and U^{238}. The deviation in total epithermal capture cross section is about 9 percent. Because of the 12-percent discrepancy in thermal capture cross section in the opposite direction, it was not possible to increase resonance absorption of the reference-design core by increasing the U^{238} content of the mockup fuel element.

Calculational geometry used for comparison calculations is shown in figure 6. Ten broad-group-diffusion-theory one-dimensional spatial calculations were used to obtain eigenvalues by the buckling iteration technique. The group structure is shown in table 6. A two-dimensional calculation of the mockup showed that the one-dimensional buckling iteration technique is adequate; results of the calculations are listed in table 7. Calculated excess reactivities of the unpoisoned reference-design core and the mockup core

differ by about 1 percent. A detailed total neutron balance, given in table 8, shows that the total capture and overall leakage of the mockup core agree well with the reference-design core.

In conclusion, calculations show that the mockup fuel element is a good neutronic simulation of the reference-design fuel element. Therefore, experiments performed with mockup fuel elements yield data that are directly applicable to the cold reference-design core and data that may be extrapolated to other important design points.

Zoned Reference Core Simulation

A simulation of each zone of the zoned reference core was built by adding natural tungsten to the mockup core. The zoned reference core is summarized in figure 7. The dimensions, fuel loadings, and pitch are those of the reference-design core. The axial zoning in the reference core is accomplished by the use of a mixture of 30-volume-percent natural tungsten and 70-volume-percent enriched tungsten in the middle axial regions (zones 1 and 2) for all tungsten components of the reference-design fuel stage (except the inner and outer support tubes and the radiation shield). Radial zoning in the same core is accomplished by the use of natural tungsten for the outer support tube and radiation shield in the central radial regions (zones 2 and 3). Since zoning in the reference core is accomplished by variation of the tungsten enrichment, the total tungsten atom densities (as well as all the other atom densities) remain the same in all four regions of the zoned reference-design core. The homogenized atom densities of each zone of the reference-design core are given in table 9(a). Zone 4 has the same atom densities as the unzoned reference-design core.

The simulation of the reference-design core was based on matching the two group parameters (fast and thermal) in each equivalent zone of the mockup core with particular attention to the neutron capture cross section Σ_c in each group. The simulation was accomplished by adding natural tungsten in two ways: in the middle axial mockup region (zones 1 and 2), a 0.127-centimeter tungsten foil was added to the outside of innermost fuel ring; in the central radial mockup regions (zones 2 and 3), a 0.0259-centimeter tungsten foil was added to the outside of the U^{238} ring. The homogenized atom densities in each mockup zone are given in table 9(b).

The addition of the 0.127-centimeter tungsten foil in a central part of the mockup fuel elements increased the resonance capture of the mockup fuel element without a prohibitive increase in the thermal capture, as required to match the reference mixture of 30 to 70 volume percent in zone 1. The additional tungsten was shielded in the thermal energy region by the thermal absorption of the mockup fuel.

A comparison between the mockup and reference neutronic parameters is given in

table 10 for zones 1 to 4. The values in table 10(b) for the unzoned region, zone 4, differ from the values in table 4 calculated for the original simulation because of added refinements in the analytical methods used to calculate the zoned cores. The zone 1 simulation (table 10(a)) was, in general, as good as the unzoned simulation (table 10(b)) with two exceptions: the values of the Fermi age τ (and consequently the neutron transport cross section Σ_{tr}) deviate by approximately 10 percent in the fast range; the values of the neutron fission cross section Σ_f deviate by approximately 10 percent in the thermal range, as compared with unzoned deviations of approximately 5 and 7 percent, respectively. The increased deviation in the value of τ resulted from the fact that the total tungsten loading in the reference-design core was unchanged between zones 1 and 4, while the mockup loading was increased in zone 1 as compared with zone 4. Thus, the inelastic scattering of the additional tungsten in zone 1 of the mockup core lowered the Fermi age; in the reference zone 1, however, it remained relatively unchanged, as expected.

The increased deviation in the thermal value of Σ_f (and consequently in f, the thermal utilization) in zone 1 was caused by the addition of tungsten to the center of the mockup fuel element. Although this device made possible a good match of the values of Σ_c, as noted earlier in this section, it leads to less shielding of the mockup fuel compared with the reference core, in which the tungsten and fuel are mixed. The deviations noted in τ and Σ_f both represented a slightly more reactive mockup zone when compared with the reference-design core and thus led to conservative estimates of what may be accomplished in axial power zoning.

The addition of a 0.0254-centimeter tungsten foil to the outside of the U^{238} ring in the mockup core is a close physical approximation to the reference core change in which a natural tungsten support tube and radiation shield were used. Consequently, the calculated results for zone 3 in the mockup core, as given in table 10(c) show good agreement to the equivalent reference-design zone. Comparison of the zone 3 mockup reference deviations and the deviations in the simulation of zone 4 shows that the zone 3 simulation is as good in virtually every parameter. An increase to 5 percent in the deviation of the thermal value of Σ_{tr} in zone 3 arose from small differences in the spatially independent neutron current spectrum. The same neutron current difference existed between the mockup and reference in zone 4; its effect on the value of Σ_{tr} was compensated for by the 4-percent deviation in the neutron scattering cross section Σ_s, which did not exist in zone 3.

A Fermi age mockup reference deviation increase in zone 3 over that in zone 4 again occurred because of the additional tungsten loading in the mockup. The increase is from 4.6 to 6.1 percent.

A combination of the axial and radial mockup zoning methods was used in the mockup central core region (zone 2) and compared with a combination of the axial and radial reference methods in zone 2 of the reference core. The results are shown in table 10(d). The parameter deviations between the mockup and reference zone may be ascribed to reasons just noted.

The mockup zoning schemes used gave a good simulation without incurring unreasonable refabrication costs. The tungsten additions to the 121-element core were 78.0 kilograms in the 0.127-centimeter form and 15.8 kilograms in the 0.0254-centimeter form.

ANALYTICAL METHODS

Cross Sections

Nuclear data available at the latter part of 1964 and the beginning of 1965 were reviewed, assessed, and compiled for aluminum, tungsten isotopes, beryllium, cadmium, U^{235}, and U^{238} (refs. 12 to 18). Resulting data were then incorporated into cross-section libraries of the GAM II and GATHER II cross-section programs (refs. 19 to 21) used in nuclear analysis of the thermal TWMR. The water and boron cross sections already contained in GAM II and GATHER II programs were used with only minor revisions. The same basic cross-section data were used in both General Atomic design method and the Lewis TWMR design method.

General Atomic Design Method

Spectrum calculation. - The spectrum was determined by using the GAM II slowing-down program (ref. 19) and the GATHER II thermalization program (ref. 21). The GAM II slowing-down program was used to calculate infinite media spectra and group-averaged cross sections for the homogenized Wigner-Seitz cell over the energy range 14.9 MeV to 2.38 eV. The GATHER II thermalization program was used to calculate cell homogenized spectra and group-averaged cross sections in the energy range below 2.38 eV. The Nelkin kernel for hydrogen bound in water was used in the GATHER II program to calculate group transfer cross sections for water in the region below 2.38 eV. High energy and thermal cell disadvantage factors were then determined by using the computed cross sections for the 10-group energy structure shown in table 6 using P_1S_4 theory in the GAPLSN (ref. 22) multigroup transport theory program. All the cell details are explicitly represented except cadmium poison, which was homogenized into the moderator using the separately computed disadvantage factors discussed under Poison tube disadvantage

factors. A "white-boundary" condition was imposed on the GAPLSN calculations by surrounding the cell with an optically thick pure isotropic scatterer. The GAPLSN calculated self-shielding factors, with the exception of those in the resonance energy region, are then incorporated into a second GAM II-GATHER II calculation to obtain final homogenized cross-section data for the 10 broad groups.

Resonance absorption. - In the close-spaced lattices typical of the TWMR core, fuel elements are coupled in the resonance region because the presence of one fuel element depletes resonance flux available to neighboring fuel elements. In the GAM II program (ref. 19), which calculates resonance absorption by the Nordheim method, coupling between elements was taken into account by modifying the escape probability of the isolated element by the tabulated Dancoff-Ginsburg correction factor. In this case, ordinary cylinder collision-probability tables were used in the resonance calculation. The outer radius of the outermost tungsten ring and the U^{238} ring was used to define the surface of these respective absorbing lumps. The lumped absorber atom density for tungsten and U^{238} was determined by homogenization of the respective materials within the outer radius of the outermost tungsten and U^{238} ring. A more accurate method of accounting for fuel-element interaction of neighboring fuel elements is to calculate escape probability from the entire Wigner-Seitz cell using cell transport theory with cell boundary conditions. The cell escape probability as a function of cross section is then substituted for that of the isolated element in the resonance escape calculation. Comparative calculations between the two methods have indicated agreement to within a few percent between escape probabilities obtained by the direct cell method and those found by the isolated element method in which Dancoff factors are applied. The simpler isolated element method was generally used for criticality calculations in this report.

Poison tube disadvantage factors. - Transport theory calculations are required to obtain precise disadvantage factors for poison tube cadmium solutions. A one-dimensional GAPLSN transport calculation (ref. 22) applied to a cylindrical approximation of the actual hexagonal fuel-poison tube arrangement was used to obtain basic five-thermal-group disadvantage factors. The poison tube was centered, and the moderator and fuel were represented as annular rings surrounding the poison tube. The cylindrical transport results were then adjusted to actual geometry by multiplicative group-dependent geometric factors. These group-dependent geometric factors were obtained as the ratio of a GAMBLE (ref. 23) two-dimensional cell diffusion calculation applied to a realistic poison tube geometry and a one-dimensional GAZE diffusion calculation (ref. 24) in connection with the cylindrical approximation just mentioned. Adjusted thermal group disadvantage factors were then weighted by respective group absorption rates and averaged to obtain the mean thermal group disadvantage factor as a function of poison concentration. This disadvantage factor was then applied to the cadmium poison homogenized into the moderator of the Wigner-Seitz cell.

Eigenvalue calculation. - The broad-group homogenized cross sections for the 10-energy-group structure obtained in spectrum calculations were used in eigenvalue calculations of water- and beryllium-reflected cores. Eigenvalues were computed by the one-dimensional diffusion theory GAZE II code (ref. 24), which used a buckling iteration technique. The buckling iteration technique consists of sequential radial, axial, and radial GAZE II calculations in which the buckling computed from the previous calculation is used as transverse buckling in the following calculation. To start the process, an assumed axial buckling is entered in the radial one-dimensional GAZE II calculation. The value for radial buckling obtained from this calculation is then entered as the transverse radial buckling for the subsequent axial GAZE II calculation, and a value for the axial buckling is obtained. A final radial GAZE II calculation is then completed with this axial transverse buckling. This procedure was shown to converge the effective multiplication factor k_{eff} for these cores to an error in the multiplication factor k of less than 10^{-4}.

Lewis TWMR Design Method

Spectrum calculation. - The LTWMR design method used General Atomic codes to determine the neutron spectrum. The GAM II slowing-down code was used to calculate buckling-dependent spectra and group-averaged cross sections in a homogenized Wigner-Seitz cell over the energy range from 14.9 MeV to 0.532 eV. The GATHER thermal spectrum code was used to calculate cell homogenized thermal spectra and group-averaged cross sections for the energy range below 0.532 eV. The Nelkin kernel for hydrogen bound in water was used in the GATHER program to calculate group transfer cross sections in the region below 0.532 eV.

Spatial flux-weighted homogeneous cell cross sections were then determined by using the GAM II and GATHER II cross sections for the 15-group energy structure shown in table 11. These cross sections were obtained from the results of an S_4P_0 transport theory calculation by using the TDSN program (ref. 25) in which the cell details were explicitly represented, and a white-boundary condition, which is the "isotropic reflection" option in TDSN, was applied to the outer boundary. Since resonance self-shielding factors are automatically incorporated in the Nordheim resonance calculation performed in the GAM II program, it is thought that the aforementioned procedure for obtaining spatial flux-weighted cross sections for the resonance region effectively results in self-shielding the resonance energy region twice. Calculations have shown the magnitude of the effect of this apparent double self-shielding is small for configurations in the range under present consideration.

Resonance absorption. - Ordinary cylinder collision probability tables were used in the Nordheim resonance calculation in the GAM II program for the tungsten isotopes and

U^{238}. The outer radius of the outermost tungsten ring and the radius of the U^{238} ring were used to define the surface of the resonance neutron absorbing lump. The lumped absorber atom density for each resonance absorbing isotope was determined by homogenization of the respective materials within the outer radius of the outermost tungsten and U^{238} ring. While Dancoff corrections can be included in the Lewis TWMR calculational technique, they were omitted because fuel elements were spaced sufficiently far apart in the configurations calculated to make the fuel element coupling by fast neutrons negligible.

Poison tube disadvantage factors. - Thin-wall aluminum tubes containing $CdNO_3$ poison solution, located at the midpoints of triangular water gaps between fuel elements, were homogenized into the cylindrical cell geometry of the Wigner-Seitz cell. The poison was represented as an annulus with area equal to the cross-sectional poison tube area. This annulus formed the bounding outer zone of the explicit cell model used in the TDSN multigroup problem discussed in the section Spectrum calculations. Poison tube disadvantage factors were therefore incorporated in cell calculations through the 15-group spatial flux-weighted cell cross sections obtained from the TDSN results.

Eigenvalue calculations. - The LTWMR method has been used herein to analyze two configurations. One configuration is the 37-fuel-element General Electric mockup core discussed in the section DESCRIPTION OF EXPERIMENTAL CORES while the other is the TWMR reference design, described in the section DESCRIPTION OF REFERENCE-DESIGN TWMR. While details of these configurations differ, the same general approach is used in performing eigenvalue calculations.

Homogenized core cross sections are obtained as previously explained: the homogenized reflector (Be and H_2O) 15-group cross sections are obtained by using GAM-GATHER calculations (ref. 20). The cylindrical radius of the core is chosen as the radius corresponding to the core volume of the number of unit cells in the core. Eigenvalues are computed by the transport theory TDSN program in one dimension by using the buckling iteration technique outlined previously.

General Atomic Refined Analytical Method

The precritical predictions of the soluble poison concentrations necessary for criticality of the mockup cores I to IV (table 2) were obtained by using the General Atomic design method. Comparison of the precritical predictions with experiment showed that the General Atomic design method consistently underestimated the eigenvalue and excess reactivity by about 2-percent $\Delta k/k$. A detailed analysis of the approximated factors in the General Atomic design method was completed to pinpoint the sources of the disagreement. As a result, a refined analytical technique was evolved that resulted in agreement to within 0.5 percent in eigenvalue between calculation and experiment.

The procedures used in the refined analytical method follow the same basic outline as the General Atomic design method and differ only in the extent of the approximation employed to obtain component parts of the overall calculation.

The special features incorporated by the refined method for core I calculations and an estimate of the effect on reactivity of including each component separately are enumerated in the following paragraphs. In actual calculations, the effects are not separable.

The thermal disadvantage factors for cadmium were obtained from a two-dimensional transport calculation of the unit cell by using the Sn transport code 2DXY (ref. 26). The internal curved boundaries were represented in x-y geometry by a stepped approximation, and the calculation employed five thermal groups. It is estimated that this refinement was worth about 0.05-percent $\Delta k/k$.

The thermal disadvantage factors of all other constituents of the cell were obtained by using the two-dimensional (R-Z) S_n code DDF (ref. 27). The 0.317-centimeter spacer gap between the fuel stages was explicitly represented in this calculation, the self-shielded cadmium was represented by a thin ring along the circumference of the cell. These refinements were estimated to be worth 0.7- and 0.3-percent $\Delta k/k$ individually.

The resonance treatment was improved by using the GAROL code (ref. 27) below 1 keV. The GAROL code allowed for resonance overlap, a 0.4-percent $\Delta k/k$ effect; self-shielding of the U^{235} in the resonance region, a 0.1-percent $\Delta k/k$ effect; and inclusion of interstitial aluminum, a -0.8-percent $\Delta k/k$ effect. The code took specific account of the moderator region of the cell, a 0.1-percent $\Delta k/k$ effect.

Two-dimensional GAMBLE (ref. 23) diffusion theory calculations were made for the core in place of the one-dimensional GAZE (ref. 24) buckling iterations used in the General Atomic design method. This refinement contributed about 0.7 percent in reactivity.

The refined analytical method involves time-consuming calculations both from the viewpoint of man-hours and machine time. Therefore, this method was only used to check out core I and to calculate the zoned cores V and VI.

COMPARISON OF ANALYTICAL DATA AND EXPERIMENTAL RESULTS IN GENERAL ATOMIC MOCKUP CORES

The critical configurations built at General Atomic to obtain data on the tungsten water-moderated systems as well as the parallel calculations performed in connection with these measurements to corroborate analytical methods developed by General Atomic were discussed in the preceding section.

Eigenvalue and Excess Reactivity

The General Atomic design method calculations were used to predict the poison concentration required to make the reactor critical in advance of the initial approach to criticality for each reactor configuration. Results of these calculations were the best predictions of soluble poison concentration required for criticality that could be obtained with moderate expenditure of digital computer time with the current state of knowledge. These results are summarized in table 12. These calculations, as previously explained, were made by using updated cross-section data, the best available cross-section codes, and fairly sophisticated techniques. Deviations apparent between analysis and experiment must therefore be attributed to uncertainties remaining in cross-section data and/or failure of some somewhat standard approximations made in the analysis. Subsequent to the critical experiments, further refinements were made in the calculations and closer agreement with experiment was obtained.

Excess reactivity of the experimental configurations was measured by two methods. In the first method, water-filled poison tubes were substituted for representative groups of poison-filled tubes in the core, and associated reactivity changes were measured. Measured reactivities were then weighted by the occurrence of each representative group, and the results were added (with appropriate corrections for stainless-steel rods and source tube) to obtain total excess reactivity of the core held down by the cadmium.

In the second method, the maximum cadmium inventory was uniformly loaded into the core, and a subcritical pulsed neutron measurement of shutdown reactivity was made. The cadmium inventory was then uniformly reduced, the core was pulsed, and the measurement was repeated. This procedure was repeated until the core was near critical. These experimental data were then used to check values obtained by the poison tube substitution method previously.

7.62-Centimeter-pitch, fully water-reflected, 121-element core (core I). - The precritical prediction of soluble poison concentration necessary for criticality of core I was 0.0953 mole of $CdNO_3$ per liter of poison solution. With this poison inventory in the core, the critical reactor loading was 9 elements short of the predicted 121-fuel-element loading. By using the measured worth of a fuel element in the outer ring, the estimated multiplication for the 121-element core at this cadmium concentration was 1.021. The core was reloaded with a 0.1255 molar solution, and criticality was then attained with the 121-fuel-element loading. Thus, precritical calculations underestimated k_{eff} by 2.1 percent.

Excess reactivity measured by the poison substitution method was 14.39 dollars or 10.24-percent $\Delta k/k$ for core I, while calculated excess reactivity was 11.54 dollars or 8.22-percent $\Delta k/k$. The calculated effective delayed neutron fraction β_{eff} was 0.00712. Thus, a discrepancy of -2.0-percent $\Delta k/k$ was found in excess reactivity between calcu-

lation and experiment. This discrepancy is of the same magnitude as the discrepancy found for the poisoned core eigenvalue calculations. Postcritical analysis, with the General Atomic refined method using two-dimensional GAMBLE diffusion theory calculations for the entire core, brought agreement to within 0.5 percent between the calculated and measured eigenvalues.

7.37-Centimeter-pitch, fully water-reflected, 121-element core (core II). - The precritical prediction of the soluble poison concentration in the poison tubes for criticality of this configuration was estimated as 0.0431 mole of $CdNO_3$ per liter of solution. This prediction took into account the 2-percent underestimation of the eigenvalue determined in testing the previous configuration. The calculated eigenvalue for this core was 0.9863. The measured k_{eff} for this configuration was 1.008.

Excess reactivity measured for this core by the poison substitution method was 6.61 dollars or 4.78-percent $\Delta k/k$, as compared with a calculated excess reactivity of 3.40 dollars or 2.46-percent $\Delta k/k$. The value calculated for β_{eff} was 0.00724. Therefore, a discrepancy of -2.3-percent $\Delta k/k$ exists between calculated and measured excess reactivities for this core.

7.37-Centimeter-pitch, fully water-reflected, unpoisoned, 85-element core (core III). - The 7.37-centimeter-pitch core (core III) was initially loaded with no $CdNO_3$ in the poison tubes in order to obtain experimental data on an unpoisoned core. These data were then compared with the calculated eigenvalue for this core to ascertain whether poison tubes were being taken into proper account in poisoned configurations. A symmetrical loading of 85 fuel elements without poison tubes had an eigenvalue of 1.0056, while calculations of core III predicted 0.9899. The difference between analysis and experiment was -1.6 percent for the unpoisoned core, which indicated that the primary discrepancy in the eigenvalue does not lie in treatment of the cadmium poison.

7.62-Centimeter-pitch, bottom-and-side beryllium-reflected, 121-element core (core IV). - Precritical calculations to predict the required $CdNO_3$ concentration in the poison tubes for criticality of this core were made in a nearly identical fashion as for previously discussed cores. In the present calculations, however, two deviations were made from the General Atomic analytical design method. The first difference was the use of the two-dimensional x-y transport calculations previously mentioned to obtain thermal cadmium disadvantage factors. The second difference was the result of positioning a 0.635-centimeter boral sheet exterior to the 7.303-centimeter beryllium - 0.952-centimeter polyethylene composite side reflectors to decouple the beryllium-reflected core from the external water region surrounding the core. The treatment of this plate required the generation of extrapolation distances for the radial diffusion theory calculation by separate transport theory calculations.

Precritical prediction of the soluble poison concentration necessary for criticality of this core was calculated to be 0.232 mole of $CdNO_3$ per liter of solution. In this calcula-

tion, the final GAZE diffusion theory solution was converged to a k_{eff} of 0.98 to allow for the expected discrepancy between the experiment and the General Atomic analytical design method already discussed. The measured k_{eff} of this core was 1.0024 with the final $CdNO_3$ concentration of 0.2202 mole per liter. The calculated eigenvalue for this core was 0.986, which resulted in a difference of -1.6 percent between calculation and measurement. The reduced error is caused by the inclusion of two-dimensional disadvantage factors discussed previously for cadmium in the calculation. Excess reactivity measured by the poison substitution method for this core was 20.55 dollars or 14.43-percent $\Delta k/k$, while calculated excess reactivity was 17.81 dollars or 12.50-percent $\Delta k/k$. The calculated β_{eff} was 0.00702. The -1.92-percent disparity between calculation and experiment is again of the same order as errors noted for calculations of critical poison loadings and excess reactivity for the configurations just discussed.

The excess reactivity of this core was reanalyzed in conjunction with the calculation of the 7.62-centimeter-pitch radially zoned core (core V) discussed in the next section by using the General Atomic refined calculational method. The recalculated excess reactivity was 19.89 dollars or 14.0-percent $\Delta k/k$, which agrees very well with the measured value. The disadvantage factors used in this calculation were those obtained from a calculation of the unzoned core with the poison tubes containing 0.1704 mole per liter of $CdNO_3$ solution. Thus, the results do not reflect the effect of the difference of cadmium concentration on the disadvantage factors.

7.62-Centimeter-pitch, bottom-and-side beryllium-reflected, radially zoned, 121-element core (core V). - This core is identical with core IV, just described, except that an additional 0.0254-centimeter tungsten ring has been added on the outside of the U^{238} ring in each of the 19 central fuel elements. Criticality was obtained with a poison concentration of 0.1704 mole per liter. The measured k_{eff} for this concentration was 1.0089.

The criticality calculations used the General Atomic refined method and two-dimensional (R-Z) GAMBLE diffusion theory calculations discussed earlier. The final calculated eigenvalue for the radially zoned core with 0.1704 mole cadmium per liter $CdNO_3$ solution was 1.0010. Agreement to within 0.8 percent was thus obtained. This is the same sort of agreement as was obtained for the water-reflected core (core I), which tends to confirm the accuracy of the refined methods.

The excess reactivity measured for this core by the poison substitution method was 18.43 dollars or 13.09-percent $\Delta k/k$. The calculated value of β_{eff} was 0.00710. The calculated excess reactivity obtained by removing the cadmium from the two-dimensional diffusion theory GAMBLE calculation used to establish the critical eigenvalue and reconverging the problem was 17.34 dollars or 12.31-percent $\Delta k/k$. Thus, agreement to within 0.78 percent was obtained between the General Atomic refined calculation and experiment.

7. 62-Centimeter-pitch, bottom-and-side beryllium-reflected, axially and radially zoned, 121-element core (core VI). - All the fuel elements were modified by installing a 0. 1270-centimeter tungsten ring on the outside of the innermost fuel ring of stages 11 to 19, 45 to 85. 5 centimeters from the core bottom. The 0. 0254-centimeter tungsten added to the outside of the U^{238} ring was left in place on the 19 central fuel elements.

Criticality was achieved with a cadmium concentration of 0. 1278 mole per liter. The measured k_{eff} for this core was 1. 00096. The calculated k_{eff} of 1. 00056 was obtained by using the refined methods and two-dimensional (R-Z) GAMBLE diffusion theory calculations. Thus, excellent agreement is obtained with the refined method, even for the geometrically complicated zoned core.

An excess reactivity of 14. 24 dollars or 10. 01-percent $\Delta k/k$ was measured by the poison substitution method. The calculated value of β_{eff} was 0. 00703, which compares to within 0. 2 percent with the 13. 92 dollars or 9. 79-percent $\Delta k/k$ calculated as outlined for core V.

Conclusions - Eigenvalue and Excess Reactivity Comparisons

It is seen in table 12 that a discrepancy of about -2 percent was noted between the General Atomic design method calculation and experiment for both $CdNO_3$ poisoned and the unpoisoned cores. The discrepancy cannot be primarily attributed to errors in calculation of poison tube disadvantage factors since the discrepancy is essentially independent of the level of poisoning. It is also shown in table 12 that calculated and measured values of the criticality data and excess reactivity data consistently differ by about -2 percent for both water and beryllium reflectors.

Therefore, since the General Atomic analytical design method incorporates all the important physics features in a straightforward manner and since this method consistently underpredicts measured criticality data by about 2 percent, it is apparent that the method can be used with confidence for reactor scoping studies over the range of interest for TWMR cores. The validity of the General Atomic design method is further demonstrated by the close agreement (0. 5 percent) between calculation and experiment when detailed calculations of approximated factors are included in the analysis, thus indicating that the sources of the disagreement can be pinpointed. The close agreement obtained when refined calculations are performed is shown in table 12. As previously noted refinement of the analysis to obtain this good agreement requires expenditure of an immoderate number of man-hours and computer time. Therefore, in a design program for a TWMR core, the refined calculations would only be completed for situations in which a precise check between theory and analysis is required.

Subcritical Pulsed Neutron Data

Table 13 compares subcritical reactivities obtained from pulsed neutron measurements with those obtained by the poison tube substitution technique discussed previously: Also shown are subcritical reactivities for the 1.62-centimeter-pitch, water-reflected configuration calculated in a manner analogous to experimental measurement.

In the calculation, the fundamental mode decay constant α, which is the measured parameter in the experiment, is taken to be equal to the number density of a hypothetical isotope with a 1/v cross section, which must be removed to raise the core from the poisoned subcritical condition to prompt critical. The GAZE code search routine was used to determine α by uniform removal of the hypothetical 1/v isotope. Shutdown reactivity was then computed by a relation connecting shutdown reactivity, fundamental mode decay constant α, prompt neutron lifetime $\bar{l}$, and effective delayed neutron fraction β_{eff} (ref. 5, p. 6-58). This same relation was used to convert the measured values of α into values of the experimental shutdown reactivity.

Measured values of $\bar{l}/\beta_{eff}$ were used in the computation of the experimental shutdown reactivity. These values were obtained by pulsing each core at a known slightly subcritical reactivity and using the measured α and the known subcritical reactivity (measured by the poison tube technique) in the preceding relation to compute $\bar{l}/\beta_{eff}$. Since it is not very sensitive to the cadmium loading, the value of $\bar{l}/\beta_{eff}$ determined near critical for each core was then used to compute the shutdown reactivity from the measured values of α for all larger poison loadings.

It is seen in table 13 that the disparity between calculated and pulsed neutron measured values of the shutdown margin range from 1.44 dollars near prompt critical to 3.36 dollars at a shutdown reactivity of 9.00 dollars. The increasing discrepancy with shutdown between the value of the shutdown reactivity measured by pulsed neutrons and that predicted by calculation, using the uniform 1/v poison removal method, is not understood at present.

Comparison of values measured by the poison substitution technique and those measured by the pulsed neutron technique shows much closer correspondence, thus indicating that the disagreement probably arises from difficulties in the calculation.

Prompt Neutron Lifetime

Experimental values of the mean prompt neutron lifetime $\bar{l}$ were derived from the measured $\bar{l}/\beta_{eff}$ listed in table 17 using calculated values of β_{eff}. These values are compared in table 18 with the values of lifetime obtained from the one-dimensional GAZE calculations discussed in the section Subcritical Pulsed Neutron Measurements. The cal-

culated values range from 14 to 22 percent low for all cores with the exception of core III, which was a high-leakage core and contained no cadmium. The difficulty is not a result of errors in the cadmium cross section, since large changes in the disadvantage factors for cadmium have resulted in virtually no change in the calculated lifetime. The possibility that the leakage was not properly treated in the one-dimensional buckling iteration GAZE calculations was investigated in core VI by calculating $\bar{l}$ using two-dimensional GAMBLE calculations. It is seen in table 14 that the disagreement was not removed by the two-dimensional treatment. The reason for the discrepancy is unknown.

Isothermal Temperature Coefficient

The isothermal temperature coefficient was determined by measuring the change in reactivity of the 121-fuel-element poisoned core at a series of core temperatures from 27° to 80° C. Core temperature was elevated by heating the moderator water. Water temperature was uniform to within $\pm 0.25^{\circ}$ C after waiting 1/2 hour at a given temperature.

7.62-Centimeter-pitch, water-reflected core (core I). - Measured and calculated temperature coefficients for the core I configuration are compared in figure 8(a). The General Atomic design method was used for these calculations, however, with the exception that 18 thermal groups were used to represent the component of the temperature coefficient associated with the thermal utilization. Calculational results given in figure 8(a) are not altogether complete since changes in cell thermal disadvantage factors with temperature are not included in the calculations. The cell thermal disadvantage factors used were those calculated at 27° C. Calculated results, therefore, predict an overly large negative temperature coefficient for the upper temperature range. The effect of incorporating disadvantage factor change was investigated by recalculating reactivity at 100° C with the required disadvantage factor. Values of the temperature coefficient obtained with and without consideration of the change in disadvantage factor are compared with measured overall temperature coefficient extrapolated from 80° C in table 15. The tabular values indicate that the required change in thermal disadvantage factors will diminish the magnitude of temperature coefficient by about 32 percent, and incorporation of required disadvantage factors will probably bring calculated and measured temperature coefficients into good agreement in the temperature range of 50° to 80° C. The discrepancy in the 27° to 50° C region remains unexplained.

In the following sections considerably better agreement is shown between temperature coefficient measurement and calculation for the beryllium-reflected core experiments, which most closely approximated the geometry of the reference-design reactor and therefore are of the greatest interest in this study.

7.37-Centimeter-pitch, water-reflected core (core II). - Measured temperature coefficient data for the core II configuration are plotted in figure 8(b). As expected, the temperature coefficient for the 7.37-centimeter lattice is more negative than the temperature coefficient for the 7.62-centimeter lattice at elevated temperatures. Comparison of the data for the two cores reveals that the temperature coefficients are virtually identical in the temperature range of 27° to 40° C, which may be of significance in the problem (already noted for core I) of calculating the temperature coefficient near room temperature.

7.62-Centimeter-pitch, beryllium-reflected core (core IV). - Measured and calculated temperature coefficient data for this core are compared in figure 8(c). Calculations shown in the figure are based on constant thermal disadvantage factors evaluated at 27° C and the expanded thermal group structure as in core I. Good agreement is obtained between calculations and measurements. The inclusion of temperature-dependent thermal disadvantage factors will probably tend to improve agreement if, as noted in core I, their incorporation leads to a reduction in magnitude of the negative temperature coefficient.

7.62-Centimeter-pitch, beryllium-reflected, radially zoned core (core V). - The measured temperature coefficient data for this core are shown in figure 8(d).

7.62-Centimeter-pitch, beryllium-reflected, radially and axially zoned core (core VI). - The measured and calculated temperature coefficient data for this core are shown in figure 8(e). The General Atomic design method with the expanded thermal group structure and constant disadvantage factors evaluated 27° C was used for these calculations. Temperature-dependent disadvantage factors probably bring the measured and calculated results into close agreement.

Power Distribution Within Fuel Element

Power distribution within the center fuel element was measured by activating 0.635-centimeter circular tabs punched out of the 0.107-centimeter uranium-aluminum fuel alloy rings of the mockup fuel element. The tabs were located in their respective positions within fuel rings of the assembled fuel element during irradiation at about 10 watts. The tabs were removed after irradiation, and the integral gamma counting rate above 600 keV was measured relative to the activity of one tab that was repetitively counted to generate a standard decay curve.

Figure 9 compares measured power distribution through the center element with calculated power distributions. The calculated values result from one-dimensional P_1S_8 transport calculations in connection with the unpoisoned unit cell. As is evident from figure 9, results are in good agreement.

The reasonable agreement between calculation and experiment shows that a P_1S_8

transport calculation using updated cross-section data provides an adequate treatment of cell disadvantage factors, commensurate with the required precision of an analytical design method.

The accuracy of disadvantage factor calculation is improved by two-dimensional transport calculations that explicitly incorporate the 0.318-centimeter interstage gap. This improvement was discussed earlier in the section General Atomic Refined Analytical Method. Neutron streaming into this gap raises the thermal flux level within the fuel rings, the largest increase occurring at the ends of the fourth fuel ring from the center. This increase in flux level results in a 0.7-percent increase in reactivity of the core.

Gross Power Distributions

Axial power distributions were measured by copper and manganese foils taped to the exterior of the U^{238} ring and to the aluminum top and bottom spacer tubes of the center fuel element in the core. The foils were then irradiated, and the resultant gamma activity was counted. Standard corrections for weight deviation and background were made to data.

Radial power distributions were measured near the position of axial flux peak by activating removable circular tab punchouts described before in position within the fuel rings of the mockup fuel elements. Removable tabs were punched from each of the five fuel rings in some fuel elements, while in other fuel elements only the outermost ring contained removable tabs. The tabs were normalized to a constant amount of U^{235} prior to irradiation by normalization to counting rates obtained from U^{235} photopeaks in the range of 165 to 185 keV. The tabs were irradiated at 10 watts and then removed, and the integral gamma counting rate above 600 keV was recorded. The activity of one tab was repetitively counted during this interval to generate a decay curve.

The measured axial activation shape measured with copper foils is compared with that calculated for these copper foils in the 7.62-centimeter-pitch, water-reflected core (core I) in figure 10. The results of measurements made with manganese foils are also shown. It is apparent from figure 10 that good agreement is obtained between calculated and measured activation shaped for copper foils over the active core region, with the exception of points near the lower water reflector. These deviations result because the essentially infinite bottom water reflector is terminated at 25 centimeters in the calculational model. Since copper activation is a close parallel to the fission power distribution, this agreement lends confidence to the ability of the General Atomic analytical design method to predict axial power distributions in unzoned, water-reflected tungsten-water cores.

Measurements of the radial power distributions made with fuel tabs for the 7.62-

centimeter-pitch, water-reflected, 121-fuel-element core (core I) are shown in figure 11. Data obtained on a traverse from the center of the core to one corner of the core hexagon are shown; the overall power shape resulting from measurements made on the outer fuel ring is shown as a dashed line. Measurements were also made for several fuel elements with tabs from interior rings, and these are also shown in figure 11 as the fine structure within the fuel elements. The fine structure changes somewhat from the center fuel element to one located at the reflector. In the calculations, the fine structure or disadvantage factor is assumed to have the same shape everywhere as the central fuel element. A point-by-point comparison between calculated radial power distribution and measured power distribution cannot be made for these cores because the hexagonal core configuration is approximated by a cylinder of equal volume in the calculations. Figure 12 shows the radial power distribution calculated for the 7.62-centimeter-pitch, water-reflected core (core I).

Measurements of power distributions were not made with the 7.37-centimeter-pitch core (core II), but calculated radial and axial power distributions are given in figure 13.

Fairly extensive measurements of gross power distribution were made for the 7.62-centimeter-pitch, beryllium-reflected core (core IV). These data were obtained by counting the gamma activity of entire fuel rings by rotating them on an aluminum mandrel above a scintillation crystal. By this means, it is possible to average the variations in fuel density and also the azimuthal variations in the fission product activity of the fuel rings for elements at the core-reflector interface.

The axial power distributions shown in figure 14 were obtained by counting all the outer fuel rings of the stages of the fuel elements located at the three radial positions of the figure. The measured stage power was then normalized to the average of all the stages in that element. It is noted that the axial shape is independent of radial position.

The calculational results plotted in figure 14 were obtained by one-dimensional, 10-group, homogenized GAZE diffusion theory calculations. Excellent agreement is obtained everywhere except near the bottom beryllium reflector, where the calculated values are about 10 percent low.

The local to average radial power distributions in figure 15 were obtained by counting all the fuel rings near the midplane (stage 12) of fuel elements located in the indicated sector of the core. The average power was computed as the average of the local stage power in a fuel element weighted by the number of fuel elements in exactly symmetrical locations in the core. Because of the difference in counting geometry arising from differences in the diameters of the five sizes of fuel rings, it was not possible to interrelate the power densities directly. To obtain this relation, the five rings from stage 12 of the center fuel element were flattened, cut into equal areas, and then gamma-counted in the same geometry. These results were then used to interrelate the power density of the rings.

The radial calculations shown in figure 15 were obtained from an (R-Z) GAMBLE diffusion theory calculation in which the entire core and reflector were represented. Figure 16 shows the isopower plot obtained from this GAMBLE calculation.

For the radially zoned, beryllium-reflected core (core V), measurements made of the radial power distribution at a core height of 46 centimeters from the bottom of the core are compared with two-dimensional GAMBLE calculations in figure 17. The experimental data were normalized to average power measured in the inner 85 fuel elements. The normalization excluded the 36 outer fuel elements because of the poor fit between calculated and measured power near the core reflector interface. Good agreement was obtained between experiment and analysis on the radial power profile except for the elements that directly face the moderator. These fuel elements are represented by the four outermost points.

The two-dimensional isopower plot obtained from this same calculation is shown in figure 18. The power-flattening effect of the additional tungsten in the center zone is clearly seen when figure 18 is compared with figure 16, which is an isopower plot obtained from the GAMBLE calculation of the unzoned core.

The power distribution for the 7.62-centimeter-pitch, beryllium-reflected, radially and axially zoned core (core VI) was measured by counting the activity of the outer fuel ring of each fuel stage of the fuel elements in same 1/12 core sector of the core measured for the 7.62-centimeter-pitch beryllium-reflected core. For the zoned core, there were four different kinds of unit cells: cells with the normal amount of tungsten (regions 2 and 3 in fig. 19), cells with an additional 0.1270-centimeter tungsten ring (region 5), cells with an additional 0.0254-centimeter tungsten ring (region 1), and cells with both 0.0254- and 0.1270-centimeter rings (region 4). The relative power in each of these cells, normalized to a power of unity at the outer fuel ring of each cell, was calculated. The measured activity for each fuel stage was multiplied by the appropriate calculated relative cell power. The average stage power was then computed as a weighted average of the individual stage power multiplied by the number of stages in exact symmetrical locations in the core.

The measured radial traverses at various core heights are shown in figure 20. The various zoned regions can be identified in figure 19, and the calculated curves from a two-dimensional 10-group diffusion theory (R-Z) GAMBLE calculation are drawn in all three figures. The agreement between the calculated and measured radial power distributions is good considering the inadequacies of diffusion theory calculations in this complex core. The scatter of the experimental data is believed attributable to variation in the U^{235} content and distribution within the fuel rings. An estimate of the uncertainty involved in the measured points because of counting statistics and the nonuniformity of the U^{235} distribution is indicated by the error bars.

The measurements of the axial power distribution at various core radii are plotted

in figure 21. The various regions can again be identified in figure 19. The parallel results from the GAMBLE calculation are drawn in these three figures. It is noted that the diffusion theory calculation, as in the unzoned case, underestimates the power at the bottom beryllium reflector, but the agreement in the axial direction is somewhat better than that in the radial direction, at least in the traverses made with inner fuel elements.

The traverse made with element J-1, which is one of the outer elements, is compared in figure 21(c) with calculated values at 44.01- and 37.17-centimeter radii. A definitive comparison between the calculated and measured values cannot be made for this element because the actual hexagonal and the cylindrical boundary of the calculation do not coincide. As expected, the measured values lie within these calculated traverses. Figure 22 is the GAMBLE calculated isopower plot of the fully zoned core.

It is thus concluded that diffusion theory calculations are not entirely adequate in predicting the power shapes, especially the radial power shape in the fully zoned core. It is speculated that better agreement could be obtained with transport theory.

Reactivity Worth Measurements

To check the ability of the General Atomic analytical design method to calculate reactivity worth of core components at specific locations within the core, reactivity measurements were made with and without the component in place by using a calibrated regulating rod. Reactivity worth measurements were made of the fuel-element constituents at the center and at the outer two rows at the edge of the core. Measurements were also made comparing the worth of a $CdNO_3$-filled poison tube with that of a water-filled poison tube at a series of positions along the core radius. In addition, worths of various cadmium concentrations relative to water were measured in a central poison tube. The measurements were compared with calculations.

7.62-Centimeter-pitch, water-reflected core (core I). - The worth of fuel-element components were determined by measuring the change in core reactivity when the component under study was removed from all 24 stages of the fuel element. The worth of the entire mockup element relative to void was also measured.

Measured values of fuel-element components are compared with calculated values in table 16. The calculations were made by perturbation techniques in connection with radial diffusion theory calculations on the 121-fuel-element core by using the GAZE code and the 10-broad-group structure described for the General Atomic design method.

Perturbation analysis was in error in the calculation of the worth of uranium-aluminum constituents because of strong local peaking of thermal flux associated with the empty pressure tube. The calculated worth of uranium-aluminum constituents was obtained, therefore, by direct eigenvalue GAZE calculation in connection with center core

location, where the geometry and spectrum were azimuthally symmetrical. Geometric considerations precluded direct eigenvalue calculations to obtain uranium-aluminum constituent worth for locations other than the center of the core.

Worths calculated by the eigenvalue method are in fair agreement with experimental measurements in the center pressure tube location. This agreement indicates that the General Atomic analytical method adequately accounts for the major processes to thermal absorption, resonance capture, and fission.

The worth of various concentrations of cadmium was measured in a poison tube adjacent to the center fuel element. The cadmium disadvantage factors used in the analysis were extrapolated from the values obtained in the General Atomic design method (see section Poison tube disadvantage factors, p. 14). Procedures used in the General Atomic design method to obtain the disadvantage factor involved GAPLSN transport theory calculations in connection with a cylindrical cell centered around the poison tube and transformation of these results into the actual fuel-element - poison-tube geometry using two-dimensional diffusion theory GAMBLE calculations. Calculated data obtained by using disadvantage factors in GAZE perturbation calculations are indicated as circles in figure 23. Good agreement is obtained between calculation and experiment over the range of concentrations encompassed by the calculations. At the higher concentrations, however, the calculational method just described increasingly underestimated the poison worth. Worth of the higher poison concentrations was therefore calculated by using a two-dimensional approximation to the unit cell using the transport code 2DXY (ref. 26); the internal curved boundaries were represented in x-y geometry by a stepped approximation, and the calculation used five thermal groups. The results of these calculations are indicated in figure 23 as diamonds. The worst deviation is 8 percent over the range from 0. 122 to 0. 325 mole per liter. While correspondence is better than that obtained by using the previous method in the range, the results indicate a trend that might well lead to increasing the error above 0. 325 mole per liter. However, these poison concentrations are outside the poison concentration operating limits expected for the reference design.

The reactivity worth of a poison tube containing 0. 1255 mole of $CdNO_3$ per liter, compared with a tube filled with water, was measured at various tube locations along a radius of the core. Predicted worth as a function of radius was calculated by using the GAZE code. Comparison of experimental and calculated poison tube worths (fig. 24) shows good agreement for all but the outer two locations, which are affected by heterogeneities at the core-reflector interface. The agreement indicates that treatment of the poison tubes by GAPLSN-GAMBLE calculations just discussed is not seriously in error for poison solutions in this range of concentration.

7. 37-Centimeter-pitch, water-reflected core (core II). - Reactivity worth of several fuel components was measured in the center fuel element of this core. The component was entirely removed from the element in each case, and the resulting change in excess

reactivity was measured. Results are compared in table 17 with perturbation calculations identical to those performed for the 7.62-centimeter-pitch case just discussed.

The worth of a 0.0431 molar solution of $CdNO_3$ was measured in a poison tube adjacent to the center fuel element and calculated by using perturbation theory. The measured worth was 4.78 cents, and the calculated worth was 4.83 cents. The good agreement between calculated and measured values for fuel-element components and for poison worth in the 7.37- and 7.62-centimeter-pitch cores shows that the General Atomic design method is of sufficient generality to be valid over the range of lattice spacings and core sizes of interest for the TWMR concept.

7.62-Centimeter-pitch, beryllium-reflected core (core IV). - Fuel-element component worths were also measured for the central fuel element in the 7.62-centimeter-pitch, 121-fuel-element core. The component was entirely removed from the fuel element in each case, and the resulting change in reactivity was measured. Results of these measurements are shown in table 18.

The worths of a central poison tube containing a series of concentrations of $CdNO_3$ were measured, and these results are plotted in figure 25. The variation of cadmium poison solution worth as a function of radial position of the poison tube in the core was also measured, and these data are shown in figure 26. The values plotted indicate the difference of worth for a poison tube filled with a $CdNO_3$ solution of 0.2202 mole per liter and that of a similar tube filled with water.

7.62-Centimeter-pitch, beryllium reflected, radially zoned core (core V). - The worth of the 0.0254-centimeter tungsten rings used in the 19 central elements to zone core V radially was determined by successively removing these rings in turn from the center fuel element and from fuel elements in three other locations that have sixfold core symmetry and by measuring the increase in reactivity. The total worth of the 0.0254-centimeter tungsten was determined by multiplying the worth from the symmetrical elements by six and adding the worth from the center fuel element. The measured removal worth was 2.36. The removal worth determined by using two-dimensional GAMBLE calculations was 2.34 dollars. This good agreement indicates that the tungsten added for zoning purposes is properly included in the calculations.

Azimuthal Power Distributions

One area in the design and performance of thermal nuclear reactors that is not as yet amenable to calculations is the circumferential variation of power production around fuel elements closely spaced in repetitive arrays in the moderator. While Monte Carlo calculations based on statistical compilations of individual histories of large numbers of neutrons can be utilized to obtain calculated values, the cost in computer times generally

makes this approach prohibitive. Therefore, measurements of circumferential power distributions are reported herein without supporting analysis. Measured results indicate the magnitude of local power peaking factors that must be incorporated into reactor design to account for azimuthal power peaking.

Figure 27(a) displays results of azimuthal mapping measurements of thermal flux around the U^{238} ring of the tenth stage from the top of the 7.62-centimeter-pitch, water-reflected core (core I). The measurements were made in the center fuel element in the core and in the middle element on the hexagonal flat at the core reflector interface. It is apparent that the thermal flux is closely symmetrical about the center fuel element and that circumferential flux variation, caused by azimuthal variation in water thickness, is not pronounced. There is, however, significant peaking in a direction toward the water reflector for elements located at the core-reflector interface. This peaking is attributed to the net influx from the reflector of neutrons that are more thermal than neutrons in the core. This peaking must be taken into account as a local peaking factor in core design. The value of this factor, obtained from figure 27(a), is 1.6. The measured value of this factor for the beryllium-reflected core is shown in figure 27(b) for two water-gap spacings between the outer fuel element and the aluminum scallops adjacent to the beryllium reflector. The local maximum to average azimuthal for the center fuel element on the outer flat of the core was 1.15 for a 0.732-centimeter gap and 1.08 for a 0.411-centimeter gap. It is thus seen that the power peaking at the edge of the core is predicated on the water-gap thickness. Practically, this gap could be reduced still further to decrease the local peaking and still provide adequate cooling at the edge of the core.

COMPARISON OF ANALYTICAL DATA AND EXPERIMENTAL RESULTS IN GENERAL ELECTRIC TEST CONFIGURATION

Since the 37-fuel-element configuration is not of primary interest in establishing feasibility of the U^{235} fueled tungsten water-moderated concept, only a few supporting calculations have been completed. Therefore, in general, the experimental data are presented without parallel analytical results.

Measurements described in the following sections were made with all control rods withdrawn as a uniform bank. Excess reactivity of the poisoned and unpoisoned cores was evaluated from the measured critical rod bank position by reference to a curve relating the relative fraction of the total rod worth inserted in the core to the position of the banked rods. The shape of this curve, assumed to be independent of core criticality, was established by prior measurements in the subcritical core. This curve of fractional

worth was converted to true worth by calibration of a small portion of the curve by period measurements in the critical core.

Eigenvalue

The measured reactivity of the 37-fuel-element 7.87-centimeter-triangular-pitch core with 54 poison tubes was -0.382-percent $\Delta k/k$. The poison tubes contained a 0.0153 molar solution of $CdSO_4$ and were centered in the triflute water gaps between fuel elements. The core was reflected by 9.525-centimeter beryllium side reflectors backed by more than 7.62 centimeters of water. The reactivity calculated by using the LTWMR analytical method for this configuration was 1.283-percent $\Delta k/k$. A 7.62-centimeter water region backing the reflector was assumed in calculations. The calculated and experimental values are in reasonable agreement; the disparity is 1.67-percent $\Delta k/k$.

Excess Reactivity

The excess reactivity for the 37-fuel-element, 7.87-centimeter-pitch core with 9.525-centimeter beryllium side reflectors backed by more than 7.62 centimeters of water was measured to be 4.87±0.04 percent. Calculations of this configuration made by using the LTWMR method and a 7.62-centimeter layer of water backing the beryllium reflector resulted in a predicted excess of 5.93 (0.02, -0.0) percent. The difference between measurement and analysis is 1.06 percent in reactivity.

Since a rocket core of this design would not have a significant amount of water reflector exterior to the beryllium reflector, a second configuration was constructed in which a 0.635-centimeter boral sheet was placed directly behind the beryllium reflector to decouple thermally the water exterior to the reflector from the core. Excess reactivity measured for this core was 1.927±0.052 percent, while calculations resulted in a predicted excess of 1.77 percent. It is seen that agreement to within 0.16 percent was obtained when the water region beyond the beryllium reflector was decoupled by the boral sheet and that a large loss in reactivity (2.94 percent) resulted. The large worth obtained for the water region exterior to the beryllium suggests that the optimum reflector might be constructed by using a composite of beryllium and water.

Isothermal Temperature Coefficients

The temperature coefficient was measured in two core configurations, both with

elements spaced on a 7.87-centimeter-pitch. In the first configuration, the 37-fuel-element core contained 48 poison tubes filled with a 0.0153-molar solution of $CdSO_4$, which offset the major portion of the reactivity excess. The remaining 6 poison tube positions were used to accommodate control rods. Positions of these rods varied, but in all cases they were inserted only in the upper few inches of the core. The core was reflected by a 9.525-centimeter beryllium side reflector backed by water. In the second configuration, a 0.635-centimeter boral sheet was added external to the beryllium reflector to decouple thermally the beryllium-reflected core from the external water region. Excess reactivity of this core was offset by the 18 control rods, inserted as a bank at about 23.495 centimeters from the top of the active core.

Measured isothermal temperature coefficients for the two configurations are shown as the slopes of the curves plotted in figure 28. The temperature coefficients are substantially positive for both configurations. Calculations have not been completed to point out parameters responsible for the positive character of the isothermal temperature coefficient. It may be surmised, however, that the positive coefficient obtained with General Electric fuel elements, in contrast with the substantially negative coefficient obtained for the General Atomic fuel element, may be caused by the increased fuel loading of the test elements and the larger pitch of the array.

Power Distributions

Catcher foil techniques were used for all power distribution measurements. Aluminum tapes, 0.0254-centimeter thick, were circumferentially wrapped and irradiated at the desired locations around the 0.00254-centimeter-thick U^{235} sheets, which comprised the fuel of the General Electric elements. Subsequent to irradiation, 0.635-centimeter-diameter disks were punched from the tapes, and beta activity resulting from fission products embedded in each disk was then counted to determine circumferential power distribution. The average counts from these tapes were then used to construct plots of fine radial power distributions within the fuel elements as well as gross radial power distribution and gross axial power distribution.

Azimuthal (or circumferential) power distributions within fuel elements. - Measured azimuthal power is discussed first because certain aspects of these data are pertinent to evaluation of fine and gross radial and axial power distributions reported.

Azimuthal power distributions were measured around the middle stage of the center fuel element at 65.8° and 31.1° C. Catcher foil tapes were located at the outer surface of the element and at locations corresponding to 3, 6, 9, 13, 17, 20, and 25 wraps of fuel relative to the outside of the element. Figure 29 shows azimuthal power distributions measured at 65.8° C. Fluctuation of the power with azimuthal angle is negligible for the

central fuel element, and the small variance noted is essentially within the 3-percent error associated with the catcher foil technique. The azimuthal power distribution measurement was repeated at 31.1° C, and the same invariance of the power generation with azimuthal angle was again obtained.

Azimuthal power distributions were also measured for fuel elements situated in the outer two rows of the core. Figure 30 shows results of measurements made on the six fuel elements symmetrically located one element from the corner along the flat boundaries of the hexagonal core. It is noted that strong peaking in the power is evident in the direction normal to the beryllium reflector. The maximum to average value for this peaking is, in some instances, as large as 1.29. Azimuthal peaking measurements were also measured for a fuel element located at a core vertex, and the circumferential power distribution for this element is shown in figure 31. A somewhat flatter peak in the direction outward from the vertex of the hexagon is observed. The maximum to average value for this peak is 1.14.

Azimuthal power distribution measurements made with fuel elements on the second ring from the outside are plotted in figure 31. The circumferential power distribution measured by using fuel element 410, at the core vertex, shows some evidence of peaking in the direction toward the core vertex. The maximum to average power obtained for this element is about 1.10. A circumferential power distribution was also measured for fuel element 411, located one row in from fuel elements forming the outer flat of the core. This element shows a slight amount of peaking in a direction toward the core center, the largest value measured yielding a peak to average of about 1.06. The results show that it is important to include azimuthal power peaking factors for fuel elements situated on the outer row of beryllium-reflected cores that have the design features of the tungsten water-moderated concept. Whether azimuthal peaking factors should also be applied to fuel elements situated one row in from the reflector is not currently certain because of the paucity of data.

Radial power distribution within fuel elements. - Prior to construction of the critical 37-fuel-element core, which was discussed earlier, a 37-element subcritical test region was built in the center of General Electric 630-A reactor core (ref. 11). The purpose of this center zone of fuel elements was to establish a thermal spectrum similar to the TWMR reference design for experiments involving the center fuel element. The 37 fuel elements were constructed of U^{235}, U^{238}, and natural tungsten foil wrapped on the same nichrome and stainless-steel mandrels used for the critical General Electric test elements discussed in the section General Electric test fuel element (see fig. 5). The fuel and tungsten loading for these elements was set to match thermal neutron cross sections of the reference-design element. The fuel loading of these elements was about 70 percent of the loading required for criticality of the 37-element configuration by itself. The 630-A fuel-element outer region therefore served as a driver for the inner 37-fuel-element

General Electric insert. The 630-A core and insert were brought to critical, and measurements were made of power distribution between the concentric wraps of U^{235} of the middle fuel stage of the center fuel element.

Power distributions within the center fuel element were determined by calculating the average count rate for each catcher foil tape on the layers of fuel from the center to the outside of the fuel element. These average counts were then normalized to the outermost tape, and a plot was made of the normalized count against the related optical thickness $\Sigma_a r$ from the outside of the fuel element. The P_0S_4 calculations of power distribution within the center fuel elements were also made by using the transport theory TDSN code, and these results are compared with experiment in figure 32.

It is evident that good agreement between calculation and experiment is obtained everywhere but at the innermost fuel ring, where a 6-percent difference is noted. These results show that accurate values of the disadvantage factor for tungsten fuel elements can be obtained with the P_0S_4 transport theory calculational method incorporated in the LTWMR method.

In order to obtain a further check on the LTWMR method, power distribution data within the center fuel element of the more heavily loaded 37-test-fuel-element core were also measured in the same manner. Measurements made at 31.1° and 65.8° C are plotted in figure 33 and show that there is initially a slightly faster falloff in power generation at the lower temperature, which may be attributed to a somewhat softer incoming spectrum at the lower temperature.

Measured results are also compared with results of precritical calculations on the 37-fuel-element core in figure 33. Because the outer U^{238} ring was placed at a different position in the as-built General Electric test fuel element than was assumed when precritical calculations were made, the difference seen in this figure was not unexpected. However, because of the good agreement between calculation and experiment obtained for the more lightly loaded fuel element (fig. 32), it is expected that good agreement would also be obtained for the as-built element if a geometrically correct calculation were made.

Gross power distributions. - Axial power distribution was determined from the average count rate measurements obtained from catcher foil tapes irradiated in contact with the outer U^{235} fuel ring of alternate stages of the center fuel element. The average count rates for these tapes were then normalized to that of the middle stage, and the results were plotted in figure 34. Power distribution is unsymmetrical with somewhat more power being generated toward the bottom of the core because of the larger bottom water reflector.

Radial power distribution was evaluated by using measurements of the average count rate obtained from catcher foil tapes irradiated in contact with the innermost and outermost bare U^{235} fuel rings of the middle stage of fuel elements at each of the unique

lattice locations characteristic of the 37-element hexagonal lattice. The ratio of the average count rates on the innermost to the outermost catcher foil changed as a function of position across the diameter of the core. Figure 35 shows radial power distributions obtained with innermost and the outermost foil data. In each case, counts were normalized to the area-weighted average counts for the particular foils under consideration. As expected, the foils on the outermost fuel rings showed greater power generation than those on the innermost rings near the beryllium reflector. Thus, data taken with the outermost catcher foil probably give a more conservative estimate of the radial power peaking.

EXPERIMENTAL COMPARISON OF GENERAL ATOMIC MOCKUP FUEL STAGES WITH SPECIAL REFERENCE-DESIGN FUEL STAGES

In order to obtain experimental data on the precision of the analytical match of General Atomic mockup fuel elements to the TWMR reference-design fuel element, a series of intercomparison measurements were made in the 7.62-centimeter-pitch, beryllium-reflected critical assembly (core IV). For these measurements, five special fuel element stages were fabricated by using mixtures of calutron-separated tungsten isotopes, which bracketed the composition of the reference-design fuel element. These stages were substituted for an equal number of General Atomic mockup stages in the center of the critical assembly, and the reactor was used as a reactivity measuring device. Analysis was then performed to test the ability of the General Atomic design method to predict measured reactivity differences. The good agreement between experiment and measurement indicated that the treatment of the tungsten isotopes was correct in obtaining the neutronic match which established the design of the mockup fuel element and that the mockup fuel element is a good simulation of the reference-design fuel element.

Composition of Special Fuel Stages

Each special reference-design fuel stage consisted of up to 11 nested thin-walled tungsten cylinders fabricated by the vapor deposition process using separated isotopes. The special fuel stages were assembled by inserting the 4.128-centimeter-long isotopic tungsten cylinders between grooved circular zirconium or aluminum spacer plates that held the cylinders concentric and spaced the successive stages 0.318-centimeter apart. The outer diameter of the spacer plates was dimensioned to allow the plates to slip into standard aluminum pressure tubes of the mockup core. Thus, the five stacked special

reference-design stages could be directly substituted for the middle five General Atomic mockup element stages in the center pressure tube in the critical assembly.

Comparisons of mockup stages and special reference-design stages were made both with the stages unfueled and fueled with U^{235}. For some measurements, the mockup fuel stages were fueled with standard 0.10-centimeter uranium-aluminum alloy, and special reference-design stages were fueled with an essentially equal amount of U^{235} in the form of 0.0114-centimeter-thick U^{235} foil. In addition, for other measurements, both the special reference-design and mockup stages were fueled with standard 0.10-centimeter uranium-aluminum alloy. Sizes and the tungsten isotopic compositions of the cylinders are listed in table 19. It is noted that the rings approximate the dimensions of the reference element given in table 2.

The mixture of tungsten isotopes specified for the reference-design fuel element is predicated on the product obtainable by the gaseous diffusion process. Since the W^{183} and W^{184} isotopes used in fabrication of the special reference-design stages were not obtained from gaseous diffusion separations but from calutron separations, they contained a fractional concentration of W^{186} in excess of that specified for the reference-design mixture. Thus, it was not possible to match the reference-design isotopic tungsten mixture by combining various amounts of calutron-separated isotopes. Therefore, the composition of the reference-design stages was bracketed by varying the number of rings in the special reference element stages.

The 5-ring special reference stages (table 20) closely matched the composition of the reference stages in the resonance-absorbing isotopes W^{182}, W^{183}, and W^{186} but were deficient in the small-absorbing W^{184} isotope. The 11-ring special reference stages (table 20) closely matched the reference stages in W^{184} isotope but had an excess of other isotopes.

As postulated, the worth of the mockup stages was experimentally found to be bracketed by the worth of the 5- and the 11-ring special stages. Two intermediate special stage configurations were measured to find the configuration that more closely matched the worth mockup stages. These intermediate configurations are the 8- and the 9-ring special reference stages listed in table 20.

Measurements

The measurements were made in the 7.62-centimeter-pitch, beryllium-reflected reactor. The five stages below the core centerline in the center fuel element were replaced by special reference-design stages containing the amounts of isotopes listed in table 20. The reactivity change for each of these configurations relative to the mockup stages was measured by calibrated regulating rods. These measurements were also

made with the respective fuel components both in place and removed. Because there was some small difference between the fuel worth measurements made with the 0.10-centimeter uranium-aluminum alloy and the 0.0114-centimeter U^{235} foil, the results reported herein are for the worth of the nonfuel components of the stages measured with the fuel in place. This result is obtained as the difference between the fueled stage worth and the respective fuel worth and is unaffected by the small difference in worth between the mockup uranium-aluminum fuel and the special reference U^{235} foil fuel.

The difference in reactivity, measured with fuel in place, between the nonfuel components of the special reference-design stages and the mockup stages is plotted in figure 36. The mockup stage worth is bracketed by the worths of the 5- and the 11-ring special stages. Interpolation of these results showed that the best match to the unfueled mockup stages was the 8-ring special reference-design configuration. The mockup and the 8-ring special reference-design stage configuration were then compared when both were fueled with the same mockup element fuel rings. This result is shown in figure 36 by triangular symbols.

Analytical Results

A perturbation analysis to calculate the worth of the fueled 8-ring special reference-design element was then made by using the one-group GAZE diffusion theory code. The P_1S_4 disadvantage factors were obtained by using the GAPLSN transport code, and the 10-group structure is described in table 6. An average flux and adjoint flux were assigned to the axial direction, and the analysis was confined to the radial direction. The calculation predicted an increase of 0.42 cent in the core reactivity resulting from the replacement of the mockup stages by five 8-ring special reference-design stages. The result is shown as a square symbol in figure 36.

The calculated values for k_∞ are 1.1791 for the 8-ring special reference-design stages and 1.1694 for the mockup stages. The measured difference between the 8-ring special reference-design and mockup stages (0.08 cent) accounts for one-third of this discrepancy when converted to a full core value. The calculated values of k_∞ would agree within 0.5-percent $\Delta k/k$ if the mockup and special reference-design stages were exactly equal in worth.

A comparison of removal worths for each isotope as calculated is given in table 21. The part of the resonance absorption of the tungsten in the special reference-design element is offset by the U^{238} in the mockup element, as intended.

CONCLUSION - COMPARISON OF MOCKUP AND SPECIAL-REFERENCE STAGES

The worth of the mockup element falls between the 5-ring special reference-design element, which contains reference amounts of W^{182}, W^{183} and W^{186}, and the 11-ring special reference-design element, which contains about the reference amount of W^{184} but an excess of the other isotopes.

Specificially, the mockup fuel element composed of a natural tungsten-U^{238}-aluminum mixture has been shown experimentally to be a close match to the 8-ring special reference-design element that is constructed exclusively of separated tungsten isotopes. Supporting analyses have shown that, if these two fuel elements had exactly matched experimentally, the General Atomic calculational method would have overestimated the reactivity of a core built entirely of special reference-design elements by about 0.5 percent. It is evident that the General Atomic design calculational method does take the tungsten isotopes into proper account. Thus, the analytical match between the reference-design element and the mockup element, which involves substituting absorptions in U^{238} for absorptions in separated tungsten, is good, and the mockup element is a simulation of the reference-design element to within 0.5±0.2-percent $\Delta k/k$ core reactivity.

TWMR DESIGN STUDIES

One of the primary questions of neutronic feasibility is the amount of reactivity obtained when the maximum fuel loading is put into a reactor of a given size. For the TWMR, reactivity is required not only for criticality and for 10 hours of operational life but also for tailoring the power distribution to obtain more power and a higher specific impulse from the reference-sized reactor. The reactivity and reactivity control of the TWMR are discussed in the first part of the following section.

The initial design studies not only formed the basis for the unzoned core experiments but, among other things, were used as a basis for checking the accuracy of the temperature coefficient, the neutron lifetime, and the effective delayed neutron fraction calculations, discussed in the second part of this section.

Design studies were continued to investigate different methods of tailoring the power distribution. These studies formed the basis for the zoned core experiments and are reported in the third part of this section.

REACTIVITY AND REACTIVITY CONTROL

Reactivity Requirements

Reactivity requirements for the zoned reference-design rocket reactor are given in table 22 and in figures 37 and 38. Table 22 gives the percent $\Delta k/k$ required above that needed for clean core criticality at 27° C for various reactor requirements. The table includes all significant requirements except those for xenon and transient samarium. The effect of xenon poisoning buildup during a power run is shown in figure 37. The maximum length of a particular power run was assumed to be 1 hour at the end of which 0.4-percent reactivity is required for the steady-state xenon poisoning. A negligible xenon concentration is thus assumed at the beginning of the power run. The reactivity associated with samarium buildup after a power run will be less than the transient xenon requirement by about an order of magnitude. The peak value of transient samarium reactivity requirement will occur about 200 hours after shutdown from the power run.

Xenon curves were calculated with the assumption that no iodine 135 or xenon 135 fission products escape from the fuel elements. It appears, however, that this assumption is not true. Actually some gaseous fission products will diffuse through the clad. The amount is a function of clad thickness and temperature.

Reactivity requirements for 10 hours of full power life must be met by available reactivity. As shown in table 7, the excess reactivity available in the core with a 7.62-centimeter-pitch at 27° C is 17 percent. Since the total reactivity requirement, excluding xenon, is about 13 percent, only 4 percent is left for xenon override at the end of 10 hours of intermittent operation with the maximum duration of a single run being 1 hour. If the design and manufacturing tolerance were 1.5 percent rather than -1.5 percent, the xenon override allowance at the end of 10 hours of full-power operation would be about 5.5 percent. If it can be assumed that about 50 percent of the iodine and xenon atoms diffuse through the clad during both the run and shutdown times, then even at the end of design life the reactor would have full xenon override for power runs longer than an hour (see fig. 38). Without leakage through the clad, an enforced shutdown during the period from 4 to about 24 hours after a full-power run of 1-hour duration (fig. 39) would result near the end of reactor life.

There are several ways to improve peak xenon override capability if necessary. One way is to increase the radial reflector thickness, either by increasing beryllium thickness or by backing the beryllium with more water; the effect of this type of modification is shown in figure 40. Increasing the reflector effectiveness not only increases reactivity but also decreases the penalty incurred for obtaining a certain degree of gross radial power flattening. This, however, tends to increase local radial and circumferential power peaking at the core-reflector interface. Another way to improve the xenon override

capability might be to make the inlet-flow orifice plugs out of beryllium oxide rather than beryllium and incorporating uranium dioxide in them. Then the reactivity would be increased slightly, and the reactivity penalty incurred in axial power tailoring would be decreased significantly.

The reactivity limitation eases somewhat as the core is made larger with the same power density. Figure 41 shows this increase in the unzoned core reactivity. However, since this curve is for a constant fuel-element pitch of 7.87 centimeters, the water-temperature coefficient will tend to be less negative because of decreased leakage. This requirement might make a smaller lattice pitch mandatory for the larger cores, which would make the reactivity of the larger cores less than that shown in figure 41.

Reactivity Control Requirements

Only part of the reactivity requirements listed in table 22 need to be controlled by a reactivity control system. Reactivity penalties listed for power tailoring need not be controlled. If the design and manufacturing tolerance reactivity is positive, it can be made negative by the addition of a small percentage of heavy water (D_2O) to the moderating light water.

However, a reactivity control system must be able to shut down the reactor not only by a safe amount but by an amount sufficient to decrease flux, and hence prompt fission power, as rapidly as possible at the end of a power run. This is desirable from an operational standpoint. As shown by control requirements in table 23, 2-percent $\Delta k/k$ of reactivity control is set aside for this purpose. However, studies have not been made to determine the amount required for a suitable shutdown, and an amount in excess of 2 percent could be required.

As shown in table 23, the total required reactivity control is about 6 percent without that required for xenon. If no iodine or xenon atoms escape through the clad during the power run, as much as 0.4-percent $\Delta k/k$ could be required (fig. 37). However, this reactivity should be reduced by 12 percent because of xenon and iodine atoms escaping during the power run.

If, during shutdown, a total of 12 percent of these atoms escape through the clad, the total required control swing for full peak xenon override would be 11.7-percent $\Delta k/k$, based on an excess reactivity of 9.7 percent above the value for the cold, clean, critical reference-design core. The amount of required reactivity control would be larger if a faster shutdown were desired.

The total temperature defect is shown in table 23 to be about two orders of magnitude greater than propellant hydrogen reactivity. Thus, the fuel and water temperature defect will dominate fast control of the reactor. The variations of reactivity with water and fuel

temperature, shown in figures 42 and 43, were used for control analysis. The curve in figure 43 was originally calculated in reference 28 and later checked by ZUT-TUZ calculations. The water temperature reactivity curve is a close approximation to that measured by General Atomic in the beryllium-reflected mockup core with 7.62-centimeter pitch (fig. 8(c)). The fit to the 7.87-centimeter-pitch core will not be as good.

From the General Atomic critical experiments it was also found that radially zoning the core with natural tungsten support tubes adversely affects the magnitude of the negative water temperature reactivity. Instead it may be desirable, from a temperature coefficient standpoint, to zone the core by making the water thickness smaller in the center of the core. It should also be noted that the cadmium solution in the reference core will be at a lower temperature than the moderator, which should make the total water temperature reactivity coefficient more negative.

Figure 43 shows the calculated variation of reactivity with a change in fuel temperature. The shape of this curve ($a + b\sqrt{T}$) has been checked by the experiments reported in appendix B.

While these temperature reactivities will be capable of controlling power during fast transients, any change in reactivity will result in a change in average fuel and water temperature in the core. Since this change is not desirable during the power run, an external reactivity control system is required. External control is also needed to change the reactor condition from cold shutdown to hot critical, to take care of fission product poisons such as xenon, and to scram the reactor during certain accident situations. An estimate of the required rates of reactivity change is given in table 24. These rates were used to some extent in the control system feasibility studies. Better values will have to come from more detailed operations, neutronic calculations, and system kinetic studies.

Reactivity Control Methods

There are three general methods for controlling reactivity: controlling the number of parasitic neutron absorptions in the core, controlling neutron leakage from the core, and a combination of these methods.

Controlling reactivity by controlling the number of parasitic neutron absorptions in the core has significant advantages if the absorptions can be accomplished in a uniform manner. Since reactivity control has a first-order effect on power distribution in a reactor, the primary advantage accrues from being able to obtain a desirable power distribution throughout the core life rather than at only one control position and, hence, at only one point in the life of the core. Also, by uniformly distributing a neutron absorber over the whole core, a minimum amount is required because of the minimum amount of self-shielding associated with the dilute absorber concentration.

Because of the potential advantage of the uniform absorber system the feasibility of three types was considered. Primary emphasis was placed on determining the feasibility of an aqueous-cadmium-solution control system. As described in the section CRITICAL EXPERIMENTS, ANALYSES, AND EXPERIMENTS, the General Atomic critical experiment was designed to be a static model of this system. The dynamic and chemical aspects of feasibility were investigated by Westinghouse Atomic Products Division. This work is summarized in greater detail in reference 29. From these experiments, it was determined that about 2.0 grams of cadmium 113 per liter of solution will be required in the control tubes to hold down 10-percent reactivity.

Another aqueous solution control concept that is neutronically equivalent to the reference-design system is one in which the neutron-absorbing cadmium in the core is held in a solid ion exchange material. In this system, another ion exchanger is located outside the core, where the cadmium is stored when it is not needed in the core. The transfer of cadmium from in-core ion exchanger material to the external ion exchanger is controlled by electrical regulation of the pH of the solution. The major uncertainty affecting feasibility of this system is the stability under radiation of the required organic complexing agent and of the in-core ion exchange material. Basic research, including radiation experiments in the Lewis Plum Brook reactor, is being carried on to answer some of these questions.

The third type of uniform absorber control system investigated is one in which a multitude of control tubes (or comparatively homogeneously distributed spaces) are filled with a neutron-absorbing gas like helium 3, and reactivity is controlled by the gas pressure. The dominant characteristic of such a system is the extremely low inertia of the absorbing material. In comparison with a system in which a solid neutron absorber is moved by gas pressure, the all-gas system would have a high inherent speed of response, which is good from a control standpoint but unsatisfactory from a safety standpoint.

One method of slowing down the speed of response in an all-gas system is to substitute flow-area restrictions for inertia; orifices with flow area diameters of about 0.0254 centimeter placed in the main flowlines slow the response to reasonable rates. If desired, a sufficient number of orifices can be inserted throughout the system to slow the response to very low rates. In addition, the system inside the main flow orifices will be immersed in water that is under greater pressure than the absorbing gas system, so that a leak in the system will result in an inward water leak rather than an outward leak of absorber gas. Also, a sufficient number of control valves can be put in parallel in the feedline and in series in the exhaust line to attain the required system reliability.

Helium 3, obtained from the decay of tritium, costs about $100 per standard liter or about $750 per gram. If it is assumed that the helium is exhausted to space when an increase in reactivity is required from the reactor, about 8 grams are needed for 12-percent $\Delta k/k$ of reactivity control. If it is assumed that 12-percent control is sufficient,

the control cost would thus be about $6000. Figure 44, a typical control curve for the helium 3 system, shows the grams of helium in one tube (out of a total of 204 tubes) for a given amount of reactivity control.

Control stability may be a problem in the use of a gaseous control system. The portion of the system located in the center of the reactor will tend to be hottest, and the resultant expansion of absorber gas will remove poison from the most important flux region. The way in which this stability question was investigated is now discussed.

An initial multigroup transport theory calculation was performed in the axial direction, which had a uniform poison gas density distribution. The thermal group flux profile of this calculation was used to represent the internal heat generation profile in the helium 3 system. A heat-transfer analysis was performed to produce an axial density distribution in the gas, which was then inserted into another multigroup calculation. The process was repeated until a successive iteration produced no change in the calculated axial gas density profile. This technique converged very rapidly, and the change in reactivity in going from the calculation with the uniform distribution to the calculation with the converged distribution (i. e., the steady-state gas distribution at full power) was only about 1 cent.

The reason for this rapid convergence and the apparent stability is twofold. The gas temperature in this design was close to the container and surrounding water temperature, and the maximum gas temperature did not occur at the same axial point as the maximum power density. Thus, the positive reactivity feedback was not as large as expected.

With the stability problem apparently solved for the full-length gas tube, work proceeded on a reference control system, which included a distribution plenum. The placement of this distribution plenum at the outlet end of the core puts it in the least important flux region and allows the system to provide a negative reactivity power coefficient over a narrow range of design variables.

The only experimental work completed on this control system was verification of the calculated amount of flow through small orifices. While the feasibility of the overall system remains to be demonstrated, analytical results are encouraging. Some of the details of a helium 3 control system are described in references 30 and 31.

The usual method employed to control the reactor by the neutron leakage involves moving an absorber material within the reflector (e. g., control drums). In this case, the total amount of control available will be something less than the total reflector worth. Figure 45 shows total radial reflector worth for an essentially infinite beryllium-water reflector as a function of core radius.

For the reference-design core, with a radius of 45. 5 centimeters, the reflector worth is about 10. 5-percent $\Delta k/k$. For the reflector drum, however, controlled core design shown in figure 46 the total amount of control available from the control drums is calculated to be less than 4-percent $\Delta k/k$. If interstitial control rods (as shown in

fig. 46) are used to control shutdown reactivity and temperature defect, the control in the drums would allow meeting the full 1-hour steady-state xenon condition but only a small percentage of the transient xenon override. Thus, while it will be possible to use this control system on a marginal basis for the 121-fuel-element-assembly size core, it can be seen from the steep drop in the total reflector worth as core size is increased (fig. 45) that the use of this type of control for larger cores is impractical. From this curve it can also be seen that, for cores smaller than the reference-design size, it will be a feasible control method.

The usual form of the combination-type control system, in which both parasitic neutron absorption in the core and neutron leakage from the core are changed, is the axial control rod. If a sufficient number of highly absorptive rods are inserted into one end of the core, the control is primarily by changing neutron leakage (i. e., by changing effective core height). On the other hand, if only a few control rods only slightly more absorptive than the rest of the core are used to control the reactor, the control is primarily by parasitic neutron absorptions.

The type of rod control investigated for the reference-design core was one that replaced 19-fuel-element assemblies with water-cooled hafnium control rods, as shown in figure 47. The main reason for using 19 rods, rather than 13, was to simplify the analysis; for this number, the core was assumed to be composed of 17 supercells. The analysis showed that sufficient control for overriding xenon and meeting the one-stuck-out-rod condition can be obtained with the 19 control rods.

KINETIC PARAMETERS

Various kinetic parameters are needed to determine the dynamic behavior of a nuclear reactor system. The parameters considered herein are the isothermal temperature coefficient, cadmium poison solution temperature coefficient, mean prompt neutron lifetime $\bar{l}$, and effective delayed neutron fraction β_{eff}. These parameters are calculated periodically to incorporate design changes. Conversely, design changes may be effected to obtain a particular parameter behavior. Of particular interest are the sign and magnitude of the temperature coefficients. Desirable characteristics of stability and self-regulation, which afford greater flexibility and simplification in control and instrumentation design, result when the temperature coefficients are sufficiently negative.

The purpose of this section is to report calculational techniques used and results obtained and to evaluate the results by comparison with results of appropriate experiments. The basic calculational model has been described earlier in the section LTWMR Design Method. Only those parts of the model pertinent to this section are discussed.

A constant temperature is assumed throughout each cell, the core, and the reflector

(i. e., no axial or radial temperature gradient). In the actual design, however, the moderator, circulated through heat exchanger devices and separated physically from the fuel assemblies, is normally at a lower average temperature than fuel assemblies; for similar reasons, a temperature difference may exist between core and reflector. The effect of Doppler broadening is not specifically considered in these calculations for high-temperature operation of the fuel, although the temperature dependence for the temperature range considered is included in resonance calculations and in scattering kernels.

Separability of radial and axial flux distributions is assumed and, although a buckling iteration synthesis may be readily performed, it is not done here since axial leakage is small. A constant reflector-savings extrapolation distance is used. This assumption may affect the calculated temperature coefficient. Five reactor configurations are considered:

(1) TWMR 7. 62-centimeter Be. This 7. 62-centimeter-pitch, 6. 35-centimeter-thick (2. 5 in.) reflector is composed of 90 percent Be and 10 percent H_2O.

(2) TWMR 7. 62-centimeter Be-H_2O. This reactor is the same as the TWMR 7. 62-centimeter Be, except that it also includes an additional 3 centimeters of water reflector located about the Be-H_2O region of the core reflector.

(3) TWMR 7. 87-centimeter Be. This reactor has a pitch of 7. 87 centimeters and a 6. 35-centimeter-thick (2. 5 in.) reflector composed of 90 percent Be and 10 percent H_2O.

(4) GA-H_2O. This reactor is the General Atomic 7. 62-centimeter-pitch, water-reflected mockup (core I).

(5) GA-Be. This reflector is the General Atomic 7. 62-centimeter-pitch, beryllium-reflected mockup (core IV).

All cores are composed of 121 fuel assemblies, and temperature coefficients are calculated for five reactors; mean prompt neutron lifetime and effective delayed neutron fraction are calculated only for TWMR cores. A cadmium solution temperature coefficient is obtained for one TWMR reactor.

Moderator Temperature Coefficient

The isothermal temperature coefficient has been calculated for several TWMR core and reflector configurations. Similar calculations were done for two General Atomic mockup configurations and compared with experimental measurements. Results obtained by General Atomic for the GA-Be core are also reported. These calculations use the General Atomic design method.

Figures 48 and 49 show results of the calculations and experiments considered. Figure 48 includes two curves, the experimental values of reactivity as a function of temperature for the GA-Be core, and a curve of calculations for the TWMR 7. 62-

centimeter Be-H_2O core. The temperature coefficient of the two similar cores should be nearly the same. Calculated values obtained by General Atomic are given for the GA-Be core, and calculated values obtained by the LTWMR model are given for both cores. Comparison of LTWMR calculations with experimental results indicates a factor of about 2 in the temperature coefficients with the LTWMR model calculating more negative. Since the LTWMR calculation of both cores shows about the same temperature coefficient, it may be assumed that the TWMR 7.62-centimeter Be core behaves similarly to the GA-Be core with which it is compared. The General Atomic calculations of the mockup core show some scatter, and it is not clear which points are inconsistent. The General Atomic results are in better agreement with the experiment than the two points calculated by the LTWMR method.

Figure 49 shows results of additional calculations for different TWMR configurations and for the GA-H_2O core. The experimental core for the GA-H_2O core is shown in figure 27(a). The LTWMR calculations of the GA-H_2O core show a discrepancy similar to that observed with the GA-Be core (fig. 48).

A comparison of the two TWMR cores (fig. 49(b)), which differ only in reflector configuration, shows the effect of the extra 3 centimeters of water in the TWMR 7.62-centimeter Be-H_2O core. The decrease in leakage and the increase in thermal utilization with the extra water yield a slightly less negative temperature coefficient. A much larger effect is noted with more water within the core, as for the TWMR 7.87-centimeter Be core. The temperature coefficient of this core may well be positive at the colder temperatures, just as the water-reflected mockup is.

The same basic LTWMR model was used for all the temperature coefficient calculations given in figure 49. However, the scattering kernels for hydrogen differed for the TWMR cores and the General Atomic mockup cores. A consistent set of calculations was done for two temperatures to determine the effects of kernel differences on the temperature coefficients. The net effect of the kernel differences was to change the multiplication factor by about 1-percent $\Delta k/k$, with no effect on the temperature coefficient. An assumption that may be important to temperature coefficient calculations is that 10 thermal groups are adequate (i.e., with 10 thermal groups, the average cross sections are almost independent of the spectrum). The calculation of temperature coefficients requires very good spectral integrity. General Atomic uses 19 thermal groups for temperature coefficient calculations. Thus, at this time, the General Atomic method seems to be superior for these calculations.

One additional temperature coefficient has been calculated. The cadmium solution density decreases with increasing temperature, thus effectively withdrawing cadmium from the core. The worth of this density change is obtained by using a poison solution at 27° C in a core configuration that is otherwise at 82° C. The coefficient obtained is 0.58 cent per $^{\circ}$C for both of the TWMR 7.62-centimeter-pitch configurations. Thus, if

the 27° C solution is in the core, which is at 82° C, and the solution is allowed to warm up, reactivity is inserted at 0.58 cent per $^{\circ}$C.

Mean Prompt Neutron Lifetime

The calculational technique used for obtaining the mean prompt neutron lifetime is the "1/v addition" method. The reactivity change between two static multigroup full core calculations is required. The first calculation is for the unperturbed case. The second (perturbed) calculation is done the same way, except that a ficticious pure absorber material, whose cross section varies as 1/v, is added uniformly to the entire reactor. The amount of 1/v absorber material is chosen to give a significance of about 1-percent $\Delta k/k$. The lifetime is then computed as $\bar{l} = \Delta\rho/N\sigma_0 v_0$, where $\Delta\rho$ is the change in reactivity, N is the atom density of the absorber, and σ_0 is the absorption cross section at speed v_0. The cross section perturbation for one energy group and one material region is $\Sigma_a = N\sigma_0 v_0 < 1/v >$.

Calculations have been performed for the TWMR 7.62-centimeter Be-H_2O reactor at 52° and 82° C. The results of 26.6 and 26.2 microseconds, respectively, indicate that lifetime is not a strong function of temperature; a value of about 27 microseconds can be expected at 27° C. The TWMR 7.87-centimeter Be reactor at 27° C yields 30 microseconds; this higher value reflects the additional water within the core and the slightly larger size of the core. The General Atomic design method calculated value for the GA-Be core is 26.6 microseconds, while the measured value is 31.6 microseconds. The calculated value for the GA-H_2O core is 25.0 microseconds using the General Atomic design method, while the measured value is 28.9 microseconds. The method is quite similar to that used in the LTWMR model. The reason for this discrepancy is not well understood at present.

Effective Delayed Neutron Fraction

The calculation of β_{eff} is based on the "parallel group" method (ref. 32). This, like the lifetime calculation, is also a perturbation method, based on two static multigroup calculations. The linear nature of the equations solved allows them to be broken up into a prompt neutron set and a delayed neutron set. The solution proceeds in parallel, with the only common quantity being the fission source of neutrons. The prompt source is $1 - \beta$, and the delayed source is β. The source normalization is 1 neutron per cubic centimeter per second. The number of groups is double the number required for an ordinary eigenvalue calculation using the present energy structure. The second (perturbed) calculation is done in the same manner, but the delayed source is increased from β to 2β. The reactivity difference is then β_{eff}.

Macroscopic cross sections for the nonthermal groups are obtained from GAM II (ref. 19) by using the General Atomic method with self-shielding factors except for resonance groups. This procedure is considerably less cumbersome than using spatial flux-weighting procedures, since averages for both prompt and delayed neutrons must be obtained. It should be noted, however, that thermal group flux weighting is used. It is further assumed that self-shielding factors are the same for prompt and delayed neutrons. Calculated values for β_{eff} for the TWMR 7.62-centimeter Be-H_2O and 7.87-centimeter Be cores are 0.0070 and 0.0068, respectively. These values are quite similar to mockup core values obtained by General Atomic. Values of β_{eff} of 0.00702 and 0.00712 are obtained for the GA-Be core and the GA-H_2O core, respectively.

POWER DISTRIBUTIONS

Power Distribution Within Fuel Assembly

Radial. - A comparison of an experimental radial power distribution within an unzoned fuel assembly with that calculated by the TDSN program with cross sections from the GGC program (ref. 20) is given in the section CRITICAL EXPERIMENTS, ANALYSES, AND RESULTS. This same calculational procedure was used to determine the distribution of U^{235} within the reference-design fuel assembly that would give an approximately constant power density thoughout the assembly. Figure 50 shows results of this determination and the volume percent of UO_2 put into each fuel cylinder. The reactivity penalty caused by this zoning is about 1.5-percent $\Delta k/k$. This is about the same as a reduction in the average fuel loading of 2 volume percent UO_2.

The change in power density due to fuel loading tolerance was investigated by making two perturbations in the fuel distribution of figure 50. The first was to decrease the fuel loading in the outer (tenth) fuel cylinder by 0.5 volume percent. This decreased the power density in the outer fuel cylinder by about 3.0 percent, but increased the power density in the ninth fuel cylinder by 1 percent and increased the power density in all the rest of the fuel cylinders by a lesser amount. The second perturbation was to increase the fuel loading in the sixth fuel cylinder by 0.5 volume percent. This increased the power density in this ring by about 2.0 percent and decreased it slightly in all the rest of the fuel cylinders. Thus, the power sensitivity coefficient (i.e., the change in average power in a given ring of fuel per unit change in volume percent UO_2) for the tenth ring is about 6 percent, while this coefficient for the sixth ring is about 4 percent. If the fuel loading tolerance is ± 0.5 volume percent with a random distribution of uncertainties about the average loading, it is estimated that the variation in power density within the fuel assembly could be as much as ± 5.0 percent.

It should be noted in figure 50 that the calculation was made for a cell temperature of 27° C, whereas the actual average operating cell temperature (i.e., neutron moderator temperature) will be about 105° C. Thus, the fuel density for constant power density will be slightly different for the operating case. Fuel density in the outer rings will have to be raised somewhat, which will result in a slightly smaller loss in reactivity because of zoning.

In addition to the change in radial power density distribution with a change in moderator temperature, there will be a change with the amount of absorber in the control tubes. Putting 6.0×10^{19} atoms of natural cadmium per cubic centimeter in the control tubes increases the minimum power in the center of the assembly from 0.465 (relative to average) for the clean cell to about 0.488 for the cell with cadmium control tubes. Thus the final fuel zoning will have to take into account both the temperature factor and the factor for absorber in the control tubes.

Three-dimensional effects. - To determine the radial power density distribution within the fuel assembly as a function of axial length and particularly this distribution at the ends of the fuel assembly, a two-dimensional, 15-energy-group S_4 calculation was performed. Figure 51 shows these radial distributions at the middle of the core and at the two ends. Figure 52 shows how this distribution changes in the axial direction. From this it is seen that essentially the entire shift takes place within 5 centimeters at the ends of the fuel assemblies. Thus, these end fuel assemblies may require somewhat less radial zoning of the cylinders within the fuel assemblies than that required at the axial midplane.

Circumferential. - Experience to date has shown that a detailed two-dimensional, multigroup transport calculation is required to calculate circumferential power density distribution in the fuel assembly. This has not been done because of computer size and computer time limitations. However, this distribution was measured in the center fuel assembly of a simulated TWMR lattice in the General Electric 630-A critical assembly. In the clean lattice, the circumferential variation in power density was less than 3.0 percent, which is the estimated accuracy of the circumferential catcher foil measurements used to measure the distribution.

With 6.0×10^{19} atoms of natural cadmium in the control tubes, the maximum variation increased to 4.4 percent for the core with the 7.87 centimeter-pitch and to 3.7 percent for the core with the 7.62 centimeter-pitch. However, again the measured variation was unrelated to the hexagonal geometry and not cyclic as expected. Thus, it is assumed that the cyclical variation is less than ±3 percent.

Circumferential power distributions for several control rod configurations were also measured (ref. 33). The first set was for hafnium control tubes, which replaced fuel assemblies inside the pressure tubes. Wall thickness of the hafnium tubes varied from 0.254 to 0.635 centimeter, but the circumferential power density distributions in the ad-

jacent fuel assemblies were about the same regardless of hafnium thickness. A minimum value was found in the outer ring of each of the six surrounding fuel assemblies directly across the ligament from the control tube; the value of this minimum relative to the average was about 0.90. This caused a diametric peak of about 1.05.

The largest circumferential peaking occurs in the axial portion of the core from which the control rods have been removed in order to attain criticality. In this portion of the core, the unpoisoned water around the control rod pressure tube creates a thermal flux peak in the adjacent fuel assemblies. The resulting measured power peak was 1.23 relative to the average for the 7.87-centimeter-pitch case. If the control rods are assumed to be cooled with water, the space vacated by the withdrawn control rods fills with water, which causes additional power peaking in adjacent fuel assemblies. The measured value of the peak power density in the adjacent fuel assembly was 1.37 relative to average for a water ligament of 3.28 centimeters, which included the rod water.

Axial Power Distribution

At the high operating power densities of nuclear rocket reactors, a significant savings in core length can be obtained by tailoring axial power distribution so that as much of the core as possible is operating at the maximum allowable temperature. Reference 34 shows that an optimum-zoned TWMR can be 25 to 30 percent shorter than an unzoned core and can still produce the same outlet gas temperature for a given maximum fuel surface temperature. Optimum axial power density distribution shown in figure 53(a), has a peak to average value of about 1.82. The peak is located near the inlet rather than at the core center, as is obtained in the unzoned reference-design core.

There are several approaches for obtaining this distribution of power density. First, a good inlet end neutron reflector is desirable; this effect is shown in figure 53(b). In this case, part of the reflector is the beryllium top support structure for the core, and another part is the beryllium orifice plugs inside the pressure tubes. As seen in figure 53(b), the reflector makes the curve peak somewhat toward the inlet end of the core, but not nearly enough to obtain optimum distribution. Addition of the inlet end beryllium reflector increases the reactivity of the reference-design core by almost 1 percent. However, the power distribution shown in figure 53(c), which was obtained by having two isotopic mixtures of fuel material, caused a loss of about 4 percent in reactivity. From calculations, it appears that, to obtain the optimum distribution in figure 53(a) by this same zoning method of varying the isotopic mixture of tungsten, an additional loss of about 5 percent in reactivity is sustained. Since this amount of reactivity was not available in the reference-design core, the distribution of figure 53(c) was taken as the reference-design distribution. This distribution curve is not smooth but has irregularities at the end of the natural tungsten zone, which cause undesirable perturba-

tions in temperature distribution and should be smoothed out in an actual design. The smoothing can be done by local addition of a neutron absorber or by varying fuel loading.

The entire power tailoring can be done by varying the fuel density. This method, compared with the parasitic absorption method, results in a lower total fuel loading. The fuel zoning method, however, tends to create local power peaks at each zone boundary, because the neutron flux is continuous while the fuel density distribution is discontinuous. This zone interface peaking has to be accounted for if this method is to be used.

During normal full-power operating conditions, it appears that the chemical poison control tubes will not significantly perturb the tailored axial power distribution. As discussed in the section Reactivity Control Methods, however, there was some concern about the shift in power density caused by an axial shift in helium 3 density in the control tubes as the reactor is taken up to power. This shift was calculated as described in the reactivity control section and was found to be small. Results of this calculation are shown in table 25. This change in power distribution is kept small by designing the control system so that the temperature of the helium 3 is strongly controlled by the water temperature.

When reactivity is controlled by the axial control rods that enter the core from the inlet end, the axial power distribution is considerably different from the optimum shape. Since, in general, any deviation from optimum distribution requires that the core be made longer to obtain the same outlet gas temperature for a given surface temperature, the core controlled by axial control rods will be longer than one controlled by a strictly k_∞ type of reactivity control, which can maintain a power distribution close to optimum. The axial power distribution of an unzoned 147.3-centimeter core, which has about 6 percent in excess reactivity held down by the control rods, is shown in figure 54(a). This distribution can be improved somewhat by axially zoning the fuel density (or by varying the isotopic tungsten composition) within the limit of available reactivity. A distribution for a core which is axially zoned by fuel is shown in figure 54(b) but, even for this zoned distribution, the core length would have to be longer than 147.3 centimeters to satisfy the heat-transfer requirements.

An additional concern with all power distributions is the change in core reactivity. The k_∞ control systems minimize this change by removing a neutron absorber from the whole core. However, using relatively few moving absorbing rods to control the reactivity tends to maximize the change, since both the circumferential power distributions in local portions of the adjacent fuel assemblies and the axial power distribution change with a change in core reactivity. In the core controlled by reflector control drums, it is the circumferential power distributions in the outer ring of fuel assemblies and the gross radial power distribution across the core that change with a change in core reactivity.

Gross Radial Power Distributions

Figure 55 shows the gross radial power distribution of the reference-design core with 9.2 centimeters of 90 percent Be and 10 percent H_2O backed by 2.8 centimeters of H_2O for the radial reflector. This power density is for the unzoned core, that is, where all 121 hexagonal fuel cells are identical. The curve shows that there is a rapid increase in power density near the reflector. This increase occurs primarily in the outer half of the fuel assemblies next to the reflector and thus causes circumferential power distribution peaking in these assemblies. To investigate this local peaking at the outer edge of the core, a critical experiment was performed in which the thickness of the water channel between the core and the reflector was reduced from 0.508 to 0.254 centimeter. A reduction of power peaking to about 6 percent resulted, and it appears that this peak can be still further reduced by decreasing the amount of water in the triangular water gaps. In the radial zoning calculations described later, the reflector peaking is not as severe as in figure 55 because the beryllium is thinner and because it is not backed by 2.8 centimeters of water.

There are several methods for flattening the gross radial power distribution. One is to vary the spacing between the fuel assemblies so that there is less water and consequently more resonance absorption in the center of the core. Another method is to keep a constant lattice pitch but to vary the isotopic composition of the tungsten in the fuel assemblies in order to increase the resonance capture at the center of the core; a limited amount of this resonance absorption zoning was used to obtain the distribution shown in figure 56. This distribution was taken as the reference design rather than a flatter distribution because it can be obtained without excessive reactivity loss and without the excessive power peaking at the reflector-core interface that might be obtained if the reflector is too thick.

In order to determine the shift in the gross radial power distribution with a shift in cadmium concentration between the control tubes, a calculation was made in which 5 percent of the cadmium was removed from the center fuel cell. This increased the power in the center fuel assembly by 0.1 percent with an insignificant change in the power in the other fuel assemblies.

When reactivity of the core is controlled by movable absorbers in the radial reflector, the gross radial power distribution shifts with a change in control drum position. Also, the core controlled by reflector drums will require more radial power flattening because of the presence of the absorber in the reflector. Figure 46 shows the layout of a core that is controlled by reflector control drums. The control rods are used to shut down the reactor from the nominal operating condition to the cold shutdown condition. Figure 57 gives the gross radial power distribution of such an unzoned reactor with the control drums in the "poison-out" condition and with the control drums in the "poison-in"

condition. The change in circumferential power in the outer ring of fuel assemblies with a change in control drum position has not be investigated.

Figure 58, the result of a one-dimensional calculation, shows the comparison of gross radial power distributions of the reference-size core for an unzoned core and for a core zoned by using natural tungsten support tubes in 19 central fuel assemblies. Figure 59 shows similar results for the larger cores. The results of the larger core study are summarized in table 26.

RADIATION HEATING

Heat transferred to the hydrogen in the water-hydrogen heat exchanger is important in determing whether a topping cycle can supply part of or all the pumping power required by the tungsten water-moderated nuclear rocket without an additional heat source such as a fueled reflector. The heat-transfer rate in the heat exchanger is dependent, in part, on gamma heating rates in the water and water-cooled components in the reactor. Coolant requirements for the nozzle flange and other components that use hydrogen as the coolant are also dependent on gamma heating rates (neutron heating is another source of heat deposition in the water). It is necessary to know the spatial distribution of gamma heating in the aluminum structural members and in the water, in addition to determining the amount of energy available to the topping turbine, to define the cooling requirements for the structure.

The reactor core is a heterogeneous volume with gamma sources distributed in a complex manner throughout. In addition to the prompt and delayed gammas resulting from fission, there are several secondary gamma sources:

(1) Gamma rays from neutron captures in core structural materials

(2) Gamma rays from neutron resonance capture in tungsten

(3) Gamma rays from neutron inelastic scattering in tungsten

(4) Gamma rays from the decay of activation products

To provide a heat exchanger design that will ensure cooling of the structural members, that will not result in freezing the water in the heat exchanger over a wide range of reactor operation, and that will not waste pumping power, the spatial distribution of the heat deposited in the system must be known to a high level of confidence. For the heat deposited by gamma radiation, it is desirable that the calculated values lie within about ±10 percent of the values that would exist during reactor operation.

A digital computer program QAD IV, developed at Los Alamos Scientific Laboratory, which utilizes the point kernel technique, was used to calculate preliminary gamma heating rates. Because the TWMR is a heterogeneous core with fuel elements composed of materials of high atomic number and surrounded by water, it was not expected that the

point kernel method could yield heating rates better than ±20 percent of the values that would exist during reactor operation. Therefore, a computer program employing Monte Carlo techniques that can provide gamma heating values with the required accuracy was developed under contract with United Nuclear Corporation. The point kernel results were used for design purposes until the Monte Carlo results became available. The results of the point kernel and Monte Carlo calculations are presented in this report.

The validity and precision of the Monte Carlo program will be checked by comparison with the measured rate of gamma heat deposition and the rate of fission power generation throughout the 7.62-centimeter-pitch, beryllium-reflected core. The total spatial heat deposition caused by both gamma rays and neutrons were measured at General Atomic.

CALCULATIONAL STUDIES

Point Kernel Calculations

The digital computer program QAD IV was used for the gamma heating calculations by the point kernel method. Appendix C briefly outlines the calculational method used in this program.

Core representation. - The reactor core was represented as a cylinder of homogeneous composition with a length of 107.3 centimeters and a radius of 46.3 centimeters (equivalent to an average water ligament of 1.524 cm), as shown in figure 60. The compositions of the regions shown in the figure are given in table 27.

The final compositions of the reference core are slightly different from the values just given. However, because of the calculational inaccuracies introduced by a homogenized volume, a recalculation of the heating rates using the final values was not justified.

The reactivity control system was assumed to be a chemical poison control system. The poison solution concentration was assumed to be 3×10^{-3} gram of cadmium 113 per cubic centimeter of solution, with light water as the solvent. Because the concentration of the cadmium in the homogenized core is very low (the poison solution represents only 0.0298 volume fraction of the core), the poison solution was considered as pure water for gamma attenuation. However, the capture gammas resulting from neutron absorption in cadmium were included in the secondary gamma source term.

Source description. - The axial and radial power distributions used in these calculations are shown in figures 61(a) and (b), respectively. The gamma heating calculations were based on a heat-transfer rate of 1540 megawatts transferred to the hydrogen gas in the core. This heat-transfer rate is equivalent to a total fission rate of about 5.35×10^{19} fissions per second. Appendix D outlines the method used to relate the absolute fission rate to the core heat-transfer rate.

The gamma source was divided into 10 energy groups in increments of 1 MeV for the range 0 to 10 MeV. The gamma source energy in each increment is shown in table 28. The gamma source term in the core region includes

(1) Prompt fission gammas

(2) Delayed fission gammas that appear within 30 minutes of the fission process

(3) Capture gammas from thermal neutron capture in the following materials: tungsten, hydrogen in the water, aluminum, uranium (radiative capture), and cadmium 113 in the poison solution

Gamma rays resulting from inelastic scattering were not included. It is estimated that this term would increase the gamma source term by only 1 to 2 percent.

The thermal neutron capture in the core region was calculated by using the neutron flux values given in table 29. The thermal neutron capture rates were determined by using cross sections averaged over a Maxwellian energy distribution at the average moderator temperature of 96.1° C.

The buildup factors, linear attenuation coefficients, and mass absorption coefficients used in these calculations are shown in tables 30 to 32.

Results of point kernel calculations. - The calculated variation of the gamma heating rates with radius is shown in figure 62 for five axial locations in the core region. The heating rates are expressed in terms of watts per gram in an aluminum detector. The heating rates in tungsten and water can be estimated by multiplying the values shown in figure 62 by 1.575 and 1.133, respectively. These factors were obtained as illustrated in the following equation:

$$\text{Factor} = \frac{\text{Heating rate in tungsten, W/g}}{\text{Heating rate in aluminum, W/g}}$$

$$= \sum_{\text{All E}} \frac{\left[\frac{\mu_a(E)}{\delta}\right]_W}{\left[\frac{\mu_a(E)}{\delta}\right]_{Al}} \left(\frac{\text{Heating rate in aluminum at energy, E}}{\text{Total heating rate in aluminum}}\right)$$

The maximum and core average heating rates are 68.3 and 33.1 watts per gram of aluminum, respectively.

Monte Carlo Calculations

The digital computer program ATHENA (ref. 35) was used to calculate the detailed

gamma heating distribution in the TWMR. This computer program utilizes Monte Carlo techniques for radiation transport and heating calculations in complex geometry. A brief description of this computer program is given in appendix E.

Core representation. - For this calculation, the core was divided into three axial sections, as shown in figure 63. In addition, the option of specifying a 30° symmetrical sector with reflective boundaries at 0° and 30° was chosen. A cross section of the core at each axial section is shown in figure 64(a). The height of the axial section shown in figure 64(b) was chosen to be the length of one fuel stage, so that one fuel stage could be represented in detail to obtain the cylinder to cylinder gamma heating variation. A detailed representation is shown in figure 65. All other fuel assemblies were represented as homogenized cylinders that included the regions from the center plug to the inner diameter of the aluminum pressure tube. This representation separates the moderator and aluminum from the fuel and tungsten to provide a close approximation to the heterogeneous reactor.

Five sections of control tubes containing liquid poison solution were represented as cylinders of homogeneous composition of natural cadmium ions in water solution with aluminum as the tube material. These control tubes, each one stage in length in axial zone 2, were located in the vicinity of the fuel stage that is represented in detail in figure 64(b). Elsewhere in the core, the poison solution and control tubes were smeared in with the moderator.

The effectiveness of the cadmium poison solution is reduced when it is smeared with the moderator. Reference 11 describes the magnitude of this effect. Therefore, to obtain the same neutron absorption rate as in individual control tubes, the concentration of cadmium in the smeared case was increased by 1.926, as shown in reference 5.

The inlet end reflector location is shown in figure 63, and the side reflector location is shown in figures 63 and 64. The side reflector is composed of 90 volume percent Be and 10 volume percent H_2O.

The 19 central fuel assemblies were assumed to have natural tungsten support tubes. The tungsten fuel cylinders were assumed to be enriched in W^{184}, as shown in table 33.

Results of Monte Carlo calculations. - In the Monte Carlo calculation 3000 neutron histories were tracked. The neutron interactions produced 26 863 secondary gammas. This total includes "splitting" resulting from region and energy importance sampling. The secondary gammas were tracked, in turn, to yield the secondary gamma contribution to the total heating rate. To obtain the primary gamma heating contribution, 24 980 primary gammas were tracked.

The reactor was assumed to have operated at a power of 1540 megawatts for 30 minutes. The gross radial and axial power distributions are shown in figure 66 and table 34, respectively. The cylinder to cylinder power distribution within a stage is shown in

table 35. To describe the reactor, 144 tracking regions and 31 material compositions were used.

The calculated average heating rate in the water regions are plotted against radii in figure 67 for the three axial regions. The heating rates vary from 28 to 141 watts per cubic centimeter. The lengths of the bars in these figures represent the standard deviation for each of the calculated heating rates.

The calculated gamma heating rates are shown in table 36 for the fuel stage that is represented in detail. The heating rates in the fuel cylinders vary from 2221 watts per cubic centimeter in the innermost fuel cylinder to 3683 watts per cubic centimeter in cylinder 5. The heating rate in the tungsten support tube is 2725 watts per cubic centimeter and is comparable to the heating rates in the fuel cylinder.

The calculated gamma heating rates for the homogenized fuel assemblies are shown in table 37. The center plug, fuel cylinders, and support tube represent 21.3 percent of the homogenized volume. The other 78.7 percent represents hydrogen flow passages and the stagnant hydrogen gap between the support tube and pressure tube. These hydrogen-filled passages were treated as void. The heating rates in table 37 are expressed in watts per unit volume of homogenized volume. The fuel assemblies are numbered from 1 to 15 and can be identified by referring to figure 64(a). The calculated heating rates in the homogenized fuel assemblies vary from 230 to 781 watts per cubic centimeter of homogenized metal plus void. This value of 781 watts per cubic centimeter appears to be too high compared with the adjacent fuel assemblies. A more reasonable value appears to be approximately 700 watts per cubic centimeter.

One pressure tube was divided into 12 equal sectors to permit the calculation of the circumferential gamma heating variation. The flow divider is located near the side reflector, as shown in figure 64(b). The calculated circumferential variation is shown in figure 68 and varies from about 83 watts per cubic centimeter on the reflector side of the pressure tube to 258 watts per cubic centimeter on the side facing the center of the core.

The calculated heating rates in the inlet reflector and in the exit water plenum regions are 25 and 21 watts per cubic centimeter, respectively.

Comparison of Point Kernel and Monte Carlo Results

The straightforward comparison between the point kernel and Monte Carlo calculations indicates that the point kernel results are as much as 15 to 30 percent higher than the Monte Carlo results in the water regions. In the fuel regions, however, the Monte Carlo results are as much as 40 percent higher than the point kernel method. These results are consistent with the different representations of the reactor used by the two calculation methods. For the heterogeneous representation for the Monte Carlo calculation,

it is expected that a large fraction of the low-energy primary gammas would be absorbed in the tungsten and would not contribute significantly to the heating of the water regions. In the homogeneous representation used in point kernel calculations, this strong heterogeneous effect is not apparent, and the heating rate in the water is expected to be greater than in the Monte Carlo calculations.

It should be noted that the radial power shape used in the Monte Carlo calculations is slightly different from that used in the point kernel calculations, as can be seen by comparing figures 66 and 61(a). These differences are small, however, and should not significantly affect the comparisons between the two calculations.

GAMMA AND NEUTRON HEATING MEASUREMENTS

Description of Ionization Chambers

Ionization chambers used to measure the gamma and neutron dose consisted of small thimble condenser chambers, each being essentially a gas-filled condenser charged to a fixed voltage. When exposed to gamma or neutron flux, the gas in the tube ionizes and discharges the condenser in proportion to the exposure. The dose deposited is determined by measurement of the electrical charge remaining on the condenser.

Two types of ionization chambers, both of which were gas-filled and hermetrically sealed, were used to make the measurements. One type was constructed with graphite as the wall material and carbon dioxide as the filling gas at a pressure of about 1 atmosphere. This chamber was sensitive primarily to the energy deposition of gamma rays, but had a small inherent neutron sensitivity because of carbon recoils occurring primarily in the gas. The second type of chamber was constructed with polyethylene as the wall material and ethylene gas, at about 1-atmosphere pressure, as the filling gas. This chamber was sensitive to energy deposition from both gamma rays and neutrons.

The outside diameter of the chambers was limited to 1.245 centimeters so that they would fit into the center thin-wall aluminum tube of the mockup fuel-element support or into the poison tubes. In order to make gamma measurements, the gas-filled cavity of the chamber must be surrounded by an equilibrium thickness of solid medium so that all secondary particles crossing the cavity originate in the medium. The required thickness for electronic equilibrium is theoretically equal to the range of the maximum energy particle released in the medium although, in practice, path obliquity leads to approximate establishment of electronic equilibrium at a thickness considerably less than this maximum range.

Because of size restrictions on the outer diameter, the graphite wall thickness (area density) was 0.544 gram per square centimeter, which exceeds the range of a 1.25-MeV

electron and corresponds to a particle equilibrium for at least a 1.5-MeV photon. For the same reason, the wall thickness (area density) of the polyethylene was restricted to 0.385 gram per square centimeter. This thickness exceeded the range of the 1.0-MeV electrons and therefore provided an equilibrium thickness for gamma rays up to at least 1.25 MeV. During measurements, the chambers were surrounded by aluminum when located in the fuel elements and by both aluminum and water when located in the poison tubes. In effect, the wall thickness of the material surrounding the gas-filled cavities of the chambers was increased. It is estimated that, for fission gammas, the error in deposition dose in the wall material caused by nonequilibrium in the walls should not be more than 4 percent for the graphite - carbon dioxide and not more then 3 percent for the polyethylene - ethylene chambers.

Neutron dose measurements depend on ionization of the gas in the chamber cavity by atomic recoils; recoils from the walls of the cavity, however, contribute to the ionization. For the polyethylene - ethylene chamber, it can be shown that recoil losses from the gas are exactly balanced by recoils from the walls because the chamber is homogeneous in that its walls and gas content have the same atomic composition. In the case of the graphite - carbon dioxide chamber, the measured response to neutrons is some value between that in graphite and that in carbon dioxide. Since the recoil carbon atoms formed in the wall would be largely absorbed in the walls, however, the response is close to that for carbon dioxide.

The ionizable volume of the graphite - carbon dioxide chamber was 0.176 cubic centimeter and the length was 4.826 centimeters. The polyethylene - ethylene chamber had an ionizable volume of 0.040 cubic centimeter and was 4.699 centimeters long.

Calibration of Ionization Chambers

For chamber calibration, 16 carbon-dioxide-filled graphite chambers and 9 ethylene-filled polyethylene chambers were fabricated by the Landsverk Electrometer Company of Glendale, California. Chambers were initially standard calibrated using a cobalt 60 source and X-rays as radiation sources. The graphite - carbon dioxide chambers were then absolutely calibrated in terms of gamma energy deposition against a standard - a Victoreen Model 70-5 thimble chamber - by General Atomic.

The General Atomic linear accelerator (LINAC) was used to produce a 7-MeV beam of electrons that impinged on an 89-percent-tungsten, 7-percent-nickel, 4-percent-copper target to produce a bremsstrahlung spectrum with nearly a fission-source gamma distribution. Since the maximum energy gamma produced was below the (γ, n) threshold of the materials, no neutrons were produced; therefore, the chamber response was to gamma radiation only. Since the Victoreen thimble chamber standard was limited to

25 roentgens and the Landsverk chambers had a range of several thousand roentgens, a photodiode plastic fluor detector was first calibrated against the Victoreen standard chamber, and the fluor detector was then used to calibrate the Landsverk carbon-dioxide-filled graphite chambers. It is estimated that this absolute calibration gives the true absorbed gamma dose to within ±5 percent for the carbon-dioxide-filled graphite chambers over the range from 7 MeV to 20 keV. The ethylene-filled polyethylene chambers were calibrated with the same procedure.

A special calorimeter was built to determine the sensitivity of the Landsverk polyethylene chambers to neutron energy deposition and to obtain an absolute calibration of the chamber, in terms of the energy deposition in water, for the mixed neutron and gamma radiation fields in a reactor. Because the fluxes produced in the tungsten water-moderated critical assembly were insufficient to attain an appreciable rise rate in the water temperature, the calorimeter was designed to be used in the General Atomic TRIGA reactor, which could be operated at much higher power levels. The calorimeter was designed to be adiabatic; a thermistor was used as the temperature-measuring device within the water mass of the calorimeter. The thermistor was calibrated by raising the temperature of the known water mass in the calorimeter by addition of a measured amount of electrical energy with an internal electric heater. Measurement of the change of resistance of the thermistor for the calculated rise in water temperature permitted determination of the temperature coefficient of resistance for the thermistor.

The calibration of the Landsverk ethylene-filled polyethylene chambers was accomplished in two steps. First, the calorimeter was inserted into a tube in the TRIGA reactor core, and the reactor was operated at a steady-state power level of 10 kilowatts. A temperature rise rate of 0.0829° C per minute was observed with the calibrated thermistor. This temperature rise rate corresponded to a dose rate of 3.47×10^4 rads per minute. Then, the polyethylene chambers were placed in similar positions in the core, and the reactor was operated at 1.8 kilowatts to calibrate the chambers at a dose rate of 6250 rads per minute.

As a check on the linearity of the power level indication of the reactor, the reactor was operated at 20 kilowatts, and the expected doubling of the heating rate in the water mass (to 0.167° C/min) was observed. It is estimated that the absolute calibration procedure for the polyethylene chambers gives the true dose in water to within ±8 percent. Several of the graphite - carbon dioxide chambers were calibrated in the same manner as the polyethylene - ethylene chambers.

Measurement of Gamma and Neutron Heating

The hexagonal geometry of the General Atomic beryllium-reflected mockup core ex-

hibits a twelvefold symmetry. The 16 graphite - wall and the 9 polyethylene - wall chambers were positioned in the poison tubes or in the center thin-wall aluminum of the mockup fuel elements of one symmetrical segment of the core for the measurements, as shown in figure 69. Four runs, each at a power level of 84.2 watts, were required to complete the measurements.

The chambers were placed above and below the zirconium stud in the fuel elements by using 0.953-centimeter-diameter by 0.1524-centimeter-thick-wall aluminum tube spacers. In the poison tubes, 0.79-centimeter-diameter by 0.152-centimeter-thick-wall aluminum tube spacers were used, and the void between chambers was filled with $CdNO_3$. The relative power for all four runs was monitored by one graphite - wall chamber and one polyethylene - wall chamber placed in the same core location for each run. The relative power level varied by about 3 percent between runs.

Since comparison of the rate of gamma heat deposition calculated by the Monte Carlo code with the measured rate must consider the buildup (or decay) of fission and activation products during reactor operation, a gamma intensity profile had to be obtained for each of the four reactor runs. A gamma scintillation detector capable of discriminating against fast neutrons was used; this detector was positioned about 0.6 meter above the beryllium reflector at the edge of the core. The relative gamma intensity as a function of time for a typical run is shown in figure 70(a). Characteristic of each run was the initial exponential increase in power in 30 seconds and a leveling off at a steady 84.2 watts. Each run was continuous for approximately 40 minutes with the exception of run 1 (fig. 70(b)) in which a scram occurred during the run. An inspection of the curves confirms the expected buildup in intensity of the delayed gammas from fission during the run and the gradual decay after shutdown.

Measurement of Absolute Neutron Power

The comparison of the calculated and measured gamma heating rates is contingent on determination of the absolute core power for each run. Conversion factors were calculated relating the relative saturated subcadmium activity of gold and manganese-copper foils irradiated on the outside of the U^{238} ring of stage 12 of the center fuel element to the fission power in this stage. Absolute core power for a reactor run was then determined by dividing the measured absolute saturated subcadmium activity by the product of this conversion factor and the measured local to average core for stage 12 of the center fuel element. The local to average power was obtained by combining the measured axial and radial power distributions discussed for core IV in the section Gross Power Distribution.

The conversion factors relating saturated subcadmium activity per watt of power in

stage 12 of the gold and manganese-copper foils were evaluated by using GAMBLE-computed fluxes and transport-theory-determined disadvantage factors appropriate to the position of the foils adjacent to the U^{238} ring. The relative stage power was calculated by using a GAMBLE (R-Z) diffusion theory calculation (ref. 29) in which the entire core and reflector was represented. The accuracy of this GAMBLE calculation with respect to the power distribution at the stage 12 level in the core was checked by comparison with the relative radial power distributions measured at this height (see section Gross Power Distribution, p. 25). Agreement to within 4 percent everywhere, with the exception of the outer fuel elements, justified the use of calculated conversion factors.

Absolute saturated subcadmium activities were obtained from the measured disintegration rates by counting the gold and manganese-copper foils with an absolutely calibrated 7.62- by 7.62-centimeter crystal scintillation counter. This scintillation counter was calibrated by irradiating a series of the gold and manganese-copper foils in the high-flux TRIGA reactor to obtain high specific activity, counting these foils on the counter, and then dissolving the foils and counting their activity on a 4π beta counter to determine the absolute disintegration rate. The GAMBLE-calculated relative activity of the gold and manganese foil per unit of core power is given in table 38. The results of several measurements in which the gamma heating runs were repeated are given in table 39.

The wide spread in the manganese-copper data is attributed to possible uncertainties in the chemical analysis of the alloy or to nonhomogeneity of the alloy. Since the gold was in pure form, the average of the gold results (84.2 W) is considered to be the best estimate of the absolute power level of the reactor during the gamma heating measurements.

Dose Measurements in Core IV

The results of the axial measurements of the gamma and neutron absorbed doses in core IV are shown in figures 71 and 72. The lines are the best fit to the data; the tailed symbols indicate data from a possibly defective ionization chamber. Measurements were made at an average core power level of 84.2 watts, as discussed in the preceding section.

Since the polyethylene-wall chambers were calibrated against a water-filled calorimeter, the absorbed dose of these chambers is characteristic of water and not polyethylene. In addition, since these chambers were calibrated in the TRIGA reactor, the accuracy of the calibration is predicated on the gamma and neutron spectra of the TRIGA reactor and is very similar to that of the 7.62-centimeter-pitch beryllium-reflected core.

As discussed previously, the carbon-wall chambers have an inherent response to neutrons. This response was estimated by placing some of the carbon-wall chambers in the same positions as the water-filled calorimeter during the calibration runs.

Because of the short range of the carbon recoils resulting from collisions with fast

neutrons, virtually all the ionization is due to particles originating in the carbon dioxide gas. The response of the carbon-dioxide-filled carbon-wall chambers to neutrons has been calculated to be 15 percent, on the basis that all the recoils occurred in the carbon dioxide gas.

CONCLUSIONS

The series of critical experiments and calculational programs have generally demonstrated the neutronic feasibility of the tungsten water-moderated reactor (TWMR) concept. The following specific conclusions in the various study areas are discussed.

1. The General Atomic mockup fuel element composed of natural tungsten, aluminum, and U^{238} is an accurate simulation of the reference-fuel-element design, which uses the reference mixture enriched in W^{184}. Therefore, valid data in connection with reactivity, temperature behavior, and other design margins of the reference design can be obtained from experiments by using these mockup fuel elements.

2. The 7.62-centimeter-pitch, beryllium-reflected core (core IV), considered the mockup of the unzoned reference-design reactor, has a 14.4-percent $\Delta k/k$ available reactivity margin.

3. The 7.62-centimeter-pitch, beryllium-reflected, fully zoned core (core VI) has a 10.0-percent $\Delta k/k$ available reactivity margin. The core is considered a mockup of the zoned reference-design core.

4. The maximum required reactivity for the zoned reference reactor is 6.3 percent, but this does not include the amount required for xenon override. Since the measured amount of reactivity in fully zoned core VI was 10 percent, 3.7 percent of reactivity would be available for xenon override at the end of 10 hours of operation. Without any leakage of iodine or xenon atoms through the tungsten clad, this would make the reactor inoperable for a period of about 28 hours after the end of a 1-hour full-power run near the end of 10 hours of operational life. Experiments have shown, however, that about 12 percent of the xenon and iodine atoms diffuse through the clad during the power operation. Since the fuel elements will continue to be hot after the reactor is shut down, the xenon and iodine atoms will continue to diffuse out. Thus, the actual enforced shutdown caused by transient xenon would be considerably less than 28 hours.

5. Criticality data for the 121-fuel-element configurations can be consistently predicted as a function of lattice pitch, reflector composition, and poison tube loading by calculations using the General Atomic refined analytical method. The design method of the Lewis tungsten water-moderated reactor (LTWMR), which is similar to the General Atomic method in major calculational features but differs in computer codes employed, similarly can be used to predict the eigenvalue of mockup cores to the desired precision.

[redacted]

6. Criticality data for the 37-fuel-element tungsten water-moderated mockup cores measured by General Electric are predicted accurately by the LTWMR design method.

7. The reference-design reactor can be adequately controlled, from the viewpoint of static shutdown characteristics, by cadmium-solution-filled control tubes located at the midpoints of the water triflutes between the fuel elements, and the reactivity swing can be accurately calculated.

8. Of the three reactivity control systems investigated, the uniform poison control system (with either 204 control tubes containing cadmium solution or helium 3 control tubes) will allow the highest specific impulse and the most power to be taken out of the reference-size reactor. Reflector control drums tend to distort the radial power distribution and offer an inadequate amount of control for the longer reactors. However, reflector control drums will be adequate for TWMR cores made up of 19 to 37 fuel assemblies. Control rods inserted from the inlet end severely distort the axial power distribution and would make the core considerably longer if the same specific impulse were to be obtained.

9. The gaseous helium 3 control system was calculated to have satisfactory stability characteristics in the TWMR.

10. The 7.62-centimeter-pitch, beryllium-reflected core (core IV) has a negative temperature coefficient of about -1.4 cents per ^{o}C over the proposed operating range of the reactor. The measured temperature coefficient was reasonably predicted by the General Atomic analytical method over a range from room temperature to 100^{o} C.

11. The 7.62-centimeter-pitch, beryllium-reflected, fully zoned core (core VI) has a negative temperature coefficient of about -1.4 cents per ^{o}C over the proposed operating range of the reactor. The temperature coefficient was reasonably predicted by the General Atomic analytical design method with constant disadvantage factors. The indications are that better agreement would be obtained if temperature-dependent disadvantage factors were used.

12. The measured prompt neutron lifetimes were 31.6 microseconds for the unzoned mockup of the reference design reactor (core IV) and 35.9 microseconds for core VI, the zoned mockup. The value calculated for core IV by the LTWMR design method is 26.6 microseconds. This value is the same as that calculated by the General Atomic design method. The value calculated for core VI by the General Atomic design method was 27.9 microseconds.

13. The calculated value of the effective delayed neutron fraction for was 0.00702 for core IV and 0.00703 for core VI.

14. Power distributions from ring to ring within the central General Atomic mockup fuel element can be accurately predicted by the General Atomic analytical design method, while the power distribution from ring to ring with the central General Electric test fuel element can be accurately predicted by the LTWMR design method. Therefore, these

[redacted]

methods can be used to zone the fuel composition radially (within the reference-design fuel element) to flatten the power.

15. Gross power distributions are accurately calculated by the General Atomic design method for water-reflected cores. An underestimation approaching 10 percent in calculated power near the beryllium reflector is obtained when the General Atomic design method is applied to beryllium-reflected cores. This discrepancy must be taken into account in engineering calculations of power generation.

16. The overall maximum to average power (radial maximum to average axial maximum to average) for the 7.62-centimeter-pitch, beryllium-reflected core (core IV) was 1.62. The value of this factor calculated by the General Atomic refined method was 1.68. The 10-centimeter axial beryllium reflector shifted the axial peak about 7 centimeters toward the inlet.

17. Radial zoning by the addition of natural tungsten sleeves to the 19 center fuel elements (core V) resulted in a measured radial maximum to average power factor of 1.14. A reactivity of 1.5 percent was required for radial zoning. The measured 1.14 factor was an improvement over the 1.2 factor used in the heat-transfer and system design calculations. This margin will ensure that the reference-design power can be obtained.

18. The axial zoning of core VI shifted the axial power an additional 10 centimeters closer to the inlet end and gave a measured overall maximum to average power factor of 1.58. The comparable calculated value for this factor obtained by the refined General Atomic analytical method was 1.62. A reactivity of 4.5 percent was required for the combined axial and radial zoning.

19. The calculated maximum and core average gamma heating rates obtained from the point kernel computer program (QAD IV) are 68.3 and 33.1 watts per gram of aluminum, respectively.

20. The calculated gamma heating rates obtained from the Monte Carlo computer program ATHENA in various regions of the core are as follows:

(a) The rates vary from 28 to 141 watts per cubic centimeter in the water regions.

(b) The rates vary from 2221 to 3683 watts per cubic centimeter among the cylinders in a fuel stage.

(c) The circumferential heating variation in a pressure tube located near the side reflector varied from 83 to 258 watts per cubic centimeter.

21. A comparison between the point kernel and Monte Carlo calculations indicated that the point kernel results are as much as 15 to 30 percent higher than the Monte Carlo results in the water regions. In the fuel regions, however, the Monte Carlo results are as much as 40 percent higher than the point kernel results.

22. The measurements of the radiation heating in the TWMR mockup are estimated to have a probable error of ±9 percent for the polyethylene ionization chambers and ±6 percent for the graphite ionization chambers. The absolute neutron power level calibration

is accurate to a probable error of ±7 percent. These results indicate that a meaningful comparison between ATHENA-calculated an in-core-measured radiation heating can be made.

In summary, therefore, it is concluded that reactivity margin is available in the reference design for power tailoring, temperature defect, and burnup within metallurgically imposed limits on loading of the fuel elements, that adequate shutdown margins can be obtained by using the distributed poison control system, and that the temperature coefficient is sufficiently large to be relied on as an inherent control mechanism in the reactor. It is also concluded that analytical methods have been validated in connection with the experimental program and that they are of sufficient generality and have sufficient physical basis to permit extrapolation to higher temperatures over a considerable range of TWMR core sizes and power densities.

Lewis Research Center,
National Aeronautics and Space Administration,
Cleveland, Ohio, March 16, 1967,
122-28-03-05-22.

APPENDIX A

SYMBOLS

$B(\vec{r}, \vec{r}_T, E)$, $B(\vec{r}, \vec{r}_T)$	energy-dependent and energy-independent build-up factor
d_i	distance from source to target in i^{th} material
E	energy, MeV
f	thermal utilization
I	$a + b\sqrt{T}$
I(r, z)	fission rate associated with source region at r and z, fissions/sec
ΔI	resonance integral, b
I_{eff}	effective resonance integral
k_{eff}	effective multiplication factor
k_∞	infinite multiplication factor
$\Delta k/k$	reactivity, percent
$\bar{l}$	mean prompt neutron lifetime
N	atom density of absorber
N(E)dE	number of neutrons in dE at E
P	local power density
$\bar{P}$	core average power density
P_A	local axial power density
$\bar{P}_A$	average axial power density
P_E	local power density within fuel element
$\bar{P}_E$	average power density within fuel element
P_R	local radial power density
$\bar{P}_R$	core average radial power density
P_Φ	local azimuthal power density
$\bar{P}_\Phi$	average azimuthal power density
R/R_o	ratio of radius to core radius
$\vec{r}, \vec{r}_T$	vector location of source and target, respectively
$S(E, \vec{r})$	source strength, photons per unit energy range per unit volume per second
S/M	surface to mass ratio
$\mathcal{S}$	source term in energy interval, MeV/fission
V	volume, V
v_o	velocity, m/sec
$\bar{v}$	average velocity, m/sec
x/L	ratio of distance from inlet x to axial core length L
α	fundamental mode decay constant

β	delayed source
β_{eff}	effective delayed neutron fraction
δ	density
η	number of fission neutrons per neutron absorbed in fuel
$\mu_a(E), \mu_a$	energy-dependent and energy-independent linear absorption coefficient, cm^{-1}
$\mu(\vec{r}, E), \mu_i$	attenuation coefficient, cm^{-1}
ν	number of fission neutrons emitted per fission
ρ	reactivity
$\Delta\rho$	change in reactivity
Σ_a	absorption cross section, cm^{-1}
$\Sigma_a r$	optical thickness
Σ_c	capture cross section, cm^{-1}
Σ_f	fission cross section, cm^{-1}
$\Sigma_R(f \rightarrow th)$	removal cross section, fast to thermal group, cm^{-1}
Σ_s	scattering cross section, cm^{-1}
Σ_t	total cross section, cm^{-1}
Σ_{tr}	transport cross section, cm^{-1}
σ_0	absorption cross section, b
τ	Fermi age (2.38 eV), cm^2
φ	azimuthal angle, deg

APPENDIX B

DOPPLER EFFECT IN SEPARATED ISOTOPES OF TUNGSTEN

One of the more important aspects of the tungsten water-moderated reactor is the manner in which its reactivity varies with fuel temperature. Two of the three primary effects comprising the total change in reactivity, the change in density and the change because of shifting of the thermal spectrum, can be analyzed by techniques that are presently available. The third, the Doppler effect, is difficult to predict accurately because of lack of sufficiently accurate cross sections and the inherent difficulty in analytically solving the complex spatial and energy-dependent problem.

In order to study the Doppler coefficient or reactivity for a reference-design fuel cell, a contract was awarded for experimental measurements of the temperature coefficient of reactivity of samples of separated tungsten isotopes. These experiments, by the Atomics International Division of North American Aviation Corporation, are to be used both as a check on available cross-section data and to predict directly effective resonance integrals of the reference-design fuel cell. Analysis of the experiments, both at the Lewis Research Center and at Atomics International, will serve as a check on existing resonance parameters and will provide a means for predicting the temperature coefficient of the reference-design reactor. The current status of experiments and analyses is presented in the following section.

EXPERIMENTS

The effective resonance integral, which is related to the temperature coefficient of reactivity, is known to be basically a function of the surface to mass ratio S/M for a specimen at a specific temperature. The primary objective of experiments at Atomics International is to obtain curve plots of the effective resonance integral for surface to mass ratios equal to those in the reference-design fuel cell over the temperature range that will exist in the tungsten water-moderated reactor. To make these measurements possible, Lewis provided test specimens of separated tungsten isotopes with a wide variety of surface to mass ratios, including those existing in the reference-design fuel cell.

In the Atomics International experiment, measurements are made in a central graphite island of the Sodium Graphite Reactor - Critical Assembly (SGR-CA) (refs. 36 to 38). The radius of this region and the spacing of surrounding fuel elements have been analytically selected to produce a nearly 1/E flux spectrum and a flat adjoint flux spectrum.

The reactivity worth of tungsten samples at various temperatures is determined from a continuous digital recording of the power level of the SGR-CA as the specimen is alternately inserted into and removed from the reactor. Dynamic reactivities are computed from these data by a computer program based on reactor kinetics equations. "Sample-out" data are used to follow any drift in power or instrumentation while "sample-in" data are used to measure the change in reactivity of the sample as its temperature is varied. Total sample worth is obtained by removing the sample and, in effect, returning the reactor to its unperturbed configuration.

The system is calibrated in terms of the resonance integral of a gold standard whose reactivity is determined in the same way as the tungsten samples, but whose resonance integral is well known. Tungsten values are then obtained by comparison with the standard.

All samples are sintered-metal cylinders, 10.16 centimeters long and 1.11 centimeters in diameter. These cylinders are placed in evacuated ovens consisting basically of an inner cylinder of high-temperature ceramic, a double helical winding of heater wire, a molybdenum reflector, and an outer stainless-steel shell. The entire oven assembly is then oscillated within a cadmium-shielded cavity within the reactor to remove the thermal flux component.

Initial measurements have been made of samples with several isotopic compositions up to approximately 1127° C; subsequent values will be determined for samples at higher temperatures. As each tungsten sample contains a certain amount of the four naturally occurring isotopes, each single measurement returns an effective resonance integral value for four surface to mass ratios. For W^{186}, the only tungsten isotope with an appreciable activation cross section, reactivity results will be checked by an activation analysis.

Corrections will also be made experimentally and analytically for such perturbing effects as flux and importance gradients, cadmium thickness, expansion, and oven heating. Preliminary experimental results for the Doppler effect are shown in figure 73.

ANALYSIS

While the experimental measurements just described may be used directly (e.g., by requiring that multigroup cross sections used in a fuel cell calculation conform to the measured effective resonance integral for a corresponding surface to mass ratio), the most desirable procedure is to use the experimental results as a check of the analysis. The contribution of individual isotopes to the overall effective resonance integral is calculated and used as a check of cross-section data. If correct cross-section data are available, the effective resonance integral may then be obtained analytically for an geo-

metrical configuration and isotopic enrichment. This approach is more difficult, however, since the complex space- and energy-dependent problem must be solved concurrently. Several approximations to solution of the problem together with their limitations are described briefly:

(1) The energy-dependent part of the problem may be solved by treating the material basically as an infinite medium and assuming that the neutron flux distribution recovers between each resonance. The basic assumption in this approach is that the change in flux occasioned by neighboring resonances in the same isotope and overlapping resonances in other isotopes is neglected.

(2) The energy-dependent problem may be solved with the effect of overlapping and neighboring resonances taken into account. The flux distribution is then more accurate, but its spatial dependence is still not treated accurately.

(3) The complete space-energy problem may be solved by using point cross sections (many energy groups) in combination with fine spatial detail and by solving the resulting transport equation. The main limitation on this method is the amount of computer memory and time involved.

(4) The complete problem may be solved by Monte Carlo techniques. These techniques are equivalent to performing the experiment analytically and would seem to require the least amount of machine time of any complete solution.

Of these methods, the first has been used most extensively in this investigation. Real and adjoint fluxes of the SGR-CA are calculated by using the 15-group diffusion theory. Multigroup cross sections were generated by a nuclear data tape averaged over a fission-plus-1/E spectrum. Resonance parameter data, including recent experiments (ref. 39), were analyzed to obtain cross-section libraries for the individual isotopes. A machine program, that uses approximations outlined in approximation (1), was employed to obtain multigroup values which were used in conjunction with a perturbation theory program to calculate worths and reactivity coefficients of natural and separated tungsten isotopes. Some results are given in the comparison with experiment demonstrated in figure 73.

Because of the lack of accuracy incurred by the approximations mentioned for method (1), an attempt is now being made at Lewis to apply Monte Carlo techniques to the problem in order to determine more precisely the contribution of individual isotopes to the total effective resonance integral.

APPENDIX C

DESCRIPTION OF POINT KERNEL COMPUTER PROGRAM

The computer program QAD IV calculates the heating effect of gamma radiation from a volume distributed source. The method involves dividing the source region into as many as 8000 point isotropic sources (effectively 16 000 for a symmetric cylindrical core) and computing the distance, with associated attenuation and buildup, through all regions intercepted by the line of sight from the source point to the receiver point.

The gamma heating rate (energy per unit volume) at a point whose position vector is $\vec{r}_T$ can be expressed for point sources as

$$\int_{\text{Energy}} \int_{\text{Space}} S(E, \vec{r})\mu_a(E)\, E \frac{B(\vec{r}, \vec{r}_T, E) \exp\left(- \int_{\vec{r}}^{\vec{r}_T} \right) \mu(\vec{r}', E)\, d\vec{r}}{4\pi |\vec{r} - \vec{r}_T|^2} dE\, dV$$

This equation is expressed in the following form for numerical integration for each energy interval:

$$\sum_{r=0}^{R} \sum_{z=0}^{Z} \sum_{\varphi=0}^{\varphi} \mathcal{S}\mu_a \frac{B(\vec{r}, \vec{r}_T) \exp\left(- \sum_i \mu_i d_i \right)}{4\pi |\vec{r} - \vec{r}_T|^2} I(r, z)$$

The term $I(r, z)$ represents the fission rate associated with each division of the source and is normalized to the total fission rate. The power distribution is considered to vary with r and z (in cylindrical geometry) but is assumed to be constant with respect to the azimuthal angle I. The term $\mathcal{S}$, in this case, represents the photon energy per fission in each energy interval.

It has been estimated that the QAD IV gamma heating program can yield results within about 20 percent of actual values. Comparison of a calculated gamma heating rate in HT-1 test facility hole in the NASA Plum Brook Reactor Facility with an experimentally measured value supports this estimate. In this investigation, however, no comparison was made of experimentally measured gamma heating rates and rates calculated by QAD IV in the fueled region of a reactor.

APPENDIX D

CALCULATION OF TOTAL FISSION RATE

The fission rate was calculated by using the following considerations:

(1) Average power transferred to gas per fuel assembly (from heat-transfer calculations) = 12.72 MW (total reactor power = 1540 MW).

(2) Gamma heating:

$$\text{Tungsten: } \frac{22.05 \text{ lb}}{\text{Assembly}} \times \frac{454 \text{ g}}{\text{lb}} \times \frac{52.2 \text{ W}}{\text{g}} \text{ (est.)} = 5.22 \times 10^{5} \text{ W}$$

$$UO_2\text{: } \frac{2.02 \text{ lb}}{\text{Assembly}} \times \frac{454 \text{ g}}{\text{lb}} \times \frac{42.8 \text{ W}}{\text{g}} \text{ (est.)} = 3.93 \times 10^{4} \text{ W}$$

(3) Beta emission rate at 30 minutes operation = $7.26 \frac{\text{MeV}}{\text{fission}}$

(4) Fission fragment kinetic energy = $165 \frac{\text{MeV}}{\text{fission}}$

(5) $$\frac{\text{Fission rate}}{\text{Assembly}} = \frac{(12.72 \text{ MW} - 0.56 \text{ MW})}{(165 + 7.26) \frac{\text{MeV}}{\text{fission}}} \times \frac{1 \text{ MeV}}{1.603 \times 10^{-13} \text{ W-sec}} \times \frac{10^{6} \text{ W}}{\text{MW}} = 4.4 \times 10^{17} \frac{\text{fissions}}{\text{sec}}$$

(6) Total fission rate = $4.4 \times 10^{17} \frac{\text{fissions}}{(\text{sec})(\text{assembly})} \times 121 \text{ assemblies} = 5.35 \times 10^{19} \frac{\text{fissions}}{\text{sec}}$

APPENDIX E

DESCRIPTION OF ATHENA-A MONTE CARLO DIGITAL COMPUTER PROGRAM

The digital computer program ATHENA permits the solution of radiation transport and heating problems in a three-dimensional reactor configuration. Neutron and gamma fluxes can also be obtained. In addition, a statistical estimator is included that permits heating rates to be calculated at points either inside or outside of the fueled region.

The main segments of ATHENA included

(1) Source generator (VANGEN)
(2) Geometry organizer (EZGEOM)
(3) Cross-section data organizer (DATORG)
(4) Problem-dependent input program (INPUTD)
(5) Monte Carlo program (ATHENA)
(6) Secondary-gamma source program (GASP)
(7) Editing program (STATC)

VANGEN

The source-generator program is designed to provide neutron and gamma source tapes for the Monte Carlo calculation. The following functions are some of those performed by its component subroutines:

(1) Integrate over an arbitrary reactor power history to find delayed fission-gamma intensity and spectrum at a specifed final instant and time-integral of power.

(2) Compute fission fractions in several neutron energy bins.

(3) Generate modified gamma and/or neutron spectra for the source tapes based on the results of (1) and (2) and input-specified energy weights.

(4) Select source-particle locations within a reactor core at random from a detailed spatial distribution.

(5) Perform splitting or Russian roulette or the source particles to reflect region-dependent weighing in the tracking program.

Neutrons are selected from a portion of the fission spectrum as approximated by Cranberg, in which

$$N(E)dE = 0.453 \exp\left(-\frac{E}{0.965}\right) \sinh \sqrt{2.29\ E}\ dE$$

where E is the energy in MeV and N(E)dE is the number of neutrons in dE at E.

VANGEN computes the instantaneous gamma spectrum corresponding to an instant following an arbitrary reactor operating history. The data describing delayed-gamma emission rates following U^{235} fissioning are embodied in tables as functions of time and gamma energy. The present data cover 78 postfission times from 10^{-16} second to 10 hours, and 13 gamma energies representing the fission-gamma source from 0.02 to 7.5 MeV.

EZGEOM

The EZGEOM program processes the geometry input that consists of the description of the desired configuration and stores the information into tables for rapid data access in subsequent Monte Carlo programs. The geometric forms that can be handled are non-intersecting rectangular parallelepipeds, right cylinders, spheres, and right wedges.

DATORG

The DATORG program reads the neutron or gamma cross-section data tape and stores all information concerning the nuclides called for in the various compositions specified in the input. It computes the total macroscopic cross sections of each composition at each energy by using the concentration data supplied as input. There were 81 neutron energy groups used in the program that ranged from 0.037 eV to 18.02 MeV in constant lethargy increments of 0.25.

For gamma problems, there is, in addition, a computation of composition-dependent gamma-heating response functions that are used to estimate heat deposition corresponding to computed gamma track lengths.

For both neutron and gamma problems, DATORG stores the microscopic total, elastic scattering, and absorption cross sections for each nuclide and at each energy, and the data describing inelastic and anisotropic elastic scattering.

INPUTD

Program INPUTD reads in a variety of data needed to complete the problem specification. The data include energy and region importance sampling data, composition number for each region, identification of sectored cylinder and flux regions, and specification of number of histories per statistical group.

ATHENA

The program ATHENA performs the Monte Carlo calculation. This calculation is the analog of an actual experiment, the stochastic behavior of the actual particles and the relative probabilities of competing events being simulated for a large number of computed histories. The total accumulated scores (fluxes, heating, etc.) tend to approximate the corresponding physical results more closely as the number of histories increases.

GASP

The GASP program generates secondary-gamma sources by using a neutron interaction tape and gamma-production data for the pertinent nuclides. The output of this program is a secondary-gamma source tape that can be used as the source for a Monte Carlo calculation.

STATC

The STATC program edits the answers computed by ATHENA during the Monte Carlo calculation. It computes the region volumes and standard deviations of the flux and heating scores.

REFERENCES

1. Cohen, S. C.; Joanou, G. D.; Moore, R. A.; and Peak, J. C.: Neutronic Simulation of the Tungsten Water Moderated Nuclear Rocket Reactor. Rep. No. GA-6141 (NASA CR-54293), General Atomic Division, General Dynamics Corp., Feb. 22, 1965.

2. Peak, J. C.; Cohen, S. C.; Merrill, M. H.; and Lovallo, J. M.: Criticality Calculations for the 3-Inch Pitch As-Built Core. Rep. No. GA-6484 (NASA CR-54431), General Atomic Division, General Dynamics Corp., June 18, 1965.

3. Peak, J. C.; and Lovallo, J. M.: Precritical Calculations for the 2.9 Inch Pitch, TWMR Critical Assembly. Rep. No. GA-6633 (NASA CR-54644), General Atomic Division, General Dynamics Corp., Aug. 1, 1965.

4. Peak, J. C.; and Lovallo, J. M.: Precritical Calculations for the 3.0 Inch Pitch, Beryllium Reflected, TWMR Critical Assembly. Rep. No. GA-6807 (NASA CR-54786), General Atomic Division, General Dynamics Corp., Nov. 8, 1965.

5. Bardes, R. G.; et al.: Tungsten Nuclear Rocket. Phase I. Final Report, Part 1. Rep. No. GA-6890 (NASA CR-54909), General Atomic Division, General Dynamics Corp., Apr. 22, 1966.

6. Bardes, R. G.; Cohen, S. C.; Joanou, G. D.; Peak, J. C.; and Moore, R. A.: Tungsten Nuclear Rocket. Phase I. Final Report, Part 2. Rep. No. GA-6890 (NASA CR-54909), General Atomic Division, General Dynamics Corp., Apr. 22, 1966.

7. Bardes, R. G.; Bohren, C. F.; Cohen, S. C.; Gillette, E. M.; Hoover, G. F.; Joanou, G. D.; Lavigne, L. O.; Lovallo, J. M.; Peak, J. C.; Smith, N.; and Stewart, L.: Tungsten Nuclear Rocket. Phase II, part 1. Rep. No. GA-7190 (NASA CR-54986), General Atomic Division, General Dynamics Corp., June 15, 1966.

8. Bohren, C. F.; Lovallo, J. M.; Peak, J. C.; Smith, N.; and Stewart, L.: Tungsten Nuclear Rocket. Phase II, part 2. Rep. No. GA-7190 (NASA CR-54986), General Atomic Division, General Dynamics Corp., June 15, 1966.

9. Pincock, G. D.; and Jacoby, M. A.: A Tungsten Water Moderated Nuclear Rocket Reactor Critical Experiment with 37 Fuel Elements. General Electric Co., Nuclear Materials and Propulsion Operations (NASA CR-54453), July 21, 1965.

10. Pincock, G. D.: A Tungsten Water Moderated Nuclear Rocket Reactor Critical Experiment. Addendum No. 1. General Electric Co., Nuclear Materials and Propulsion Operation (NASA CR-54655), Aug. 26, 1965.

11. Pincock, G. D.; and Jacoby, M. A.: Test Program and Procedures for the Mockup 630A Critical Experiment. Rep. No. TM 62-10-701, General Electric Co., Nuclear Materials and Propulsion Operation, Oct. 17, 1962.

12. Joanou, G. D.; and Stevens, C. A.: Neutron Cross Sections for Aluminum. Rep. No. GA-5884 (NASA CR-54260), General Atomic Division, General Dynamics Corp., Nov. 13, 1964.

13. Joanou, G. D.; and Stevens, C. A.: Neutron Cross Sections for Tungsten Isotopes. Rep. No. GA-5885 (NASA CR-54261), General Atomic Division, General Dynamics Corp., Nov. 13, 1964.

14. Friesenhahn, S. J.; Haddad, E.; Fröhner, F. H.; and Lopez, W. M.: The Energy Dependence of the Neutron Capture Cross Section of the Tungsten Isotopes From 0.01 to 10 eV. Rep. No. GA-6832 (NASA CR-54860), General Atomic Division, General Dynamics Corp., 1965.

15. Joanou, G. D.; and Stevens, C. A.: Neutron Cross Sections for Beryllium. Rep. No. GA-5905 (NASA CR-54262), General Atomic Division, General Dynamics Corp. Nov. 13, 1964.

16. Drake, M. K.: Neutron Cross Sections for Cadmium Isotopes. Rep. No. GA-6997 (NASA CR-54933), General Atomic Division, General Dynamics Corp., Mar. 25, 1966.

17. Joanou, G. D.; and Drake, M. K.: Neutron Cross Sections for U^{235}. Rep. No. GA-5944 (NASA CR-54263), General Atomic Division, General Dynamics Corp., Dec. 10, 1964.

18. Joanou, G. D.; and Stevens, C. A.: Neutron Cross Sections for U^{238}. Rep. No. GA-6087, rev. (NASA CR-54290, rev.), General Atomic Division, General Dynamics Corp., Apr. 16, 1965.

19. Joanou, G. D.; and Dudek, J. S.: GAM II - A B_3 Code for the Calculation of Fast-Neutron Spectra and Associated Multigroup Constants. Rep. No. GA-4265, General Atomic Division, General Dynamics Corp., Sept. 16, 1963.

20. Smith, C. V.; and Vieweg, H. A.: GGC-II. A Program for Using the GAM-II and GATHER-II Spectrum Codes in Preparing Multigroup Cross-Section Input on Punched Cards for the GAZE, GAZED, DSN, GAPLSN, 2DXY, TDC, GAMBLE, FEVER, and GAD Codes. Rep. No. GA-4436, General Atomic Division, General Dynamics Corp., Dec. 17, 1963.

21. Joanou, G. D.; Smith, C. V.; and Vieweg, H. A.: GATHER-II - An IBM-7090 FORTRAN-II Program for the Computation of Thermal-Neutron Spectra and Associated Multigroup Cross Sections. Rep. No. GA-4132, General Atomic Division, General Dynamics Corp., July 8, 1963.

22. Alexander, J. H.; Hinman, G. W.; and Triplett, J. R.: GAPLSN - A Modified DSN Program for the Solution of the One-Dimensional Anisotropic Transport Equation. Rep. No. GA-4972, General Atomic Division, General Dynamics Corp., Mar. 16, 1964.

23. Cyl-Champlin, C.; Dorsey, J. P.; and Kaestner, P. C.: GAMBLE - A Program for the Solution of the Multigroup Neutron-Diffusion Equations in Two Dimensions, with Arbitrary Group Scattering, for the IBM-7090 FORTRAN II System. Rep. No. GA-4246, General Atomic Division, General Dynamics Corp., June 15, 1963.

24. Lenihan, S. R.: GAZE-2, A One-Dimensional, Multigroup, Neutron Diffusion Theory Code for the IBM-7090. Rep. No. GA-3152, General Atomic Division, General Dynamics Corp., Aug. 3, 1962.

25. Barber, Clayton E.: A FORTRAN IV Two-Dimensional Discrete Angular Segmentation Transport Program. NASA TN D-3573, 1966.

26. Bengston, J.; Perkins, S. T.; Sheheen, T. W.; and Thompson, D. W.: 2DXY - Two Dimensional, Cartesian Coordinate S_n Transport Calculation. Rep. No. AGN-TM-392, Aerojet-General Nucleonics, June 1961.

27. Stevens, C. A.; and Smith, C. V.: GAROL - A Computer Program for Evaluating Resonance Absorption Including Resonance Overlap. Rep. No. GA-6637, General Atomic Division, General Dynamics Corp., Aug. 24, 1965.

28. Bevilacqua, F.; Harding, R. S.; and Valerino, M. F.: Study of Reactivity Control Methods. Rep. No. GNEC-325, General Nuclear Engineering Corp., Jan. 1964.

29. Eanes, W. F.; Fultonberg, D. N.; Rosal, E. R.; Fletcher, W. D.; and Loving, J. J.: Feasibility of a Chemical Poison Loop System. Rep. No. WCAP-2993 (NASA CR-72105), Westinghouse Electric Corp., Sept. 1966.

30. Davison, H. W.; and Heath, C. A.: The Control of a Nuclear Reactor Using Helium-3 Gas Control Elements. Am. Nucl. Soc. Trans., vol. 9, no. 2, Nov. 1966, pp. 574-575.

31. Davison, Harry W.; Heath, Colin A.; and Lowen, W.: Control of a Nuclear Reactor with a Gaseous Control System. NASA TN D-4093, 1967.

32. Kaplan, S.; and Henry, A. F.: An Experiment to Measure Effective Delayed Neutron Fractions. Rep. No. WAPD-TM-209, Bettis Atomic Power Lab., Westinghouse Electric Corp., Feb. 1960.

33. Archibald, G. R.; Jacoby, M. A.; and Pincock, G. D.: Control Absorber and Fuel Element Mockup Experiment for the Tungsten, Water Moderated Nuclear Rocket Reactor. Rep. No. GEMP-350 (NASA CR-54335), General Electric Co., Mar. 26, 1965.

34. Lantz, Edward: Axial-Power-Distribution Optimization in the Tungsten Water-Moderated Reactor. NASA TM X-1239, 1966.

35. Spielberg, D.: ATHENA - A System of FORTRAN Programs for Radiation Transport and Heating Calculations in Complex Reactor Geometries. Rep. No. UNC-5148 (NASA CR-54905), United Nuclear Corp., Mar. 1966.

36. Carpenter, S. G.; Otter, J. M.; Paschall, R. K.; and Royden, H. N.: Tungsten Resonance Integrals and Doppler Coefficients. Rep. No. AI-65-225 (NASA CR-54769), Atomics International, Oct. 29, 1965.

37. Carpenter, S. G.; Otter, J. M.; Paschall, R. K.; and Royden, H. N.: Tungsten Resonance Integrals and Doppler Coefficients. Rep. No. AI-66-16 (NASA CR-54888), Atomics International, Feb. 11, 1966.

38. Carpenter, S. G.; Levitt, L. B.; Otter, J. M.; Paschall, R. K.; and Royden, H. N.: Tungsten Resonance Integrals and Doppler Coefficients. Rep. No. AI-66-85 (NASA CR-54954), Atomics International, May 13, 1966.

39. Stehn, J. R.: Tentative Tabulation of Resonance Parameters for Tungsten. Rep. No. BNL-325, 2nd ed., Suppl. 2, Vol. 2, Aug. 1967.

40. Way, K., comp.: Revised A-Chains: A = 182 (Hf, Ta, W, Re, Os, Ir, and Pt). Nuclear Data Sheet 1:B1. 1-36, National Academy of Sciences, Feb. 1966.

41. Artna, A., comp.: Revised A-Chains: A = 183 (Hf, Ta, W, Re, Os, Ir, Pt, and Au). Nuclear Data Sheet 1:B1. 37-62, National Academy of Sciences, Feb. 1966.

42. Martin, M. J., comp.: Revised A-Chains: A = 184 (Ta, W, Re, Os, Ir, and Pt). Nuclear Data Sheet 1:B1. 63-81, National Academy of Sciences, Feb. 1966.

43. Sen Gupta, A. K., comp.: Revised A-Chains: A = 185 (Ta, W, Re, Os, Ir, Pt, Au, and Hg). Nuclear Data Sheet 1:B1. 83-103, National Academy of Sciences, Feb. 1966.

44. Treado, P. A.; and Chagnon, P. R.: Neutron-Capture Gamma-Ray Spectra of the Tungsten Isotopes. Nuclear Phys., vol. 34, 1962, pp. 623-627.

TABLE 1. - TEN-RING REFERENCE-DESIGN

CELL GEOMETRY

Cell component	Material	Radius, cm	
		Inside	Outside
Support	W	0.490	0.516
First fuel ring	W + $U^{235}O_2$	.633	.686
Second fuel ring	W + $U^{235}O_2$	.813	.866
Third fuel ring	W + $U^{235}O_2$	.993	1.047
Fourth fuel ring	W + $U^{235}O_2$	1.173	1.227
Fifth fuel ring	W + $U^{235}O_2$	1.359	1.412
Sixth fuel ring	W + $U^{235}O_2$	1.557	1.610
Seventh fuel ring	W + $U^{235}O_2$	1.765	1.819
Eighth fuel ring	W + $U^{235}O_2$	1.989	2.042
Ninth fuel ring	W + $U^{235}O_2$	2.223	2.281
Tenth fuel ring	W + $U^{235}O_2$	2.464	2.517
Support	W	2.669	2.695
Radiation shield	W	2.847	2.860
Pressure tube	Al	3.012	3.165
Moderator	H_2O	3.165	3.379
Flow divider tube	Al	3.379	3.481
Moderator	Al + ^aD_2O + H_2O	3.481	4.209

[a] D_2O to be used for reactivity shimming in the "as-built" core.

TABLE 2. - CRITICAL CONFIGURATIONS BUILT AT GENERAL ATOMIC

[Core height, 106.36 cm.]

Core	Description		Diameter across hexagonal flats of active core, cm	Reflectors, cm		
	Configuration	Number of elements		Side	Top	Bottom
I	7.62-cm pitch	[a]121	85.79	Infinite water	[b]15.24 water and structure	[b]15.24 water and structure
II	7.37-cm pitch	[a]121	82.93	Infinite water	[b]15.24 water and structure	[b]15.24 water and structure
III	7.37-cm pitch	[c,d]85	70.17	Infinite water	[b]15.24 water and structure	[b]15.24 water and structure
IV	7.62-cm pitch	[a]121	85.79	7.30 Be + 0.635 boral sheet	[b]5.08 water and structure	10.16 Be
V	7.62-cm pitch radially zoned	[e]121	85.79	7.30 Be + 0.635 boral sheet	[b]5.08 water and structure	10.16 Be
VI	7.62-cm pitch radially and axially zoned	[e]121	85.79	7.30 Be + 0.635 boral sheet	[b]5.08 water and structure	10.16 Be

[a]Six rings plus center element; six corner elements omitted.

[b]Same water volume fraction as core.

[c]Five rings plus center element; six corner elements omitted.

[d]No poison tubes in core.

[e]With parasitic tungsten.

TABLE 3. - DIMENSIONS OF MOCKUP UNIT CELL

Component	Radius, cm	
	Inside	Outside
Al center post	0.635	0.969
Tungsten	0.984	0.997
Fuel	.997	1.104
Al tube	1.276	1.365
Tungsten	1.381	1.393
Fuel	1.393	1.500
Al tube	1.673	1.762
Tungsten	1.777	1.789
Fuel	1.789	1.896
Al tube	2.069	2.158
Tungsten	2.173	2.186
Fuel	2.186	2.292
Al tube	2.465	2.554
Tungsten	2.569	2.582
Fuel	2.582	2.689
Tungsten	2.706	2.714
U^{238} ring	2.714	2.816
Pressure tube	3.089	3.254
Moderator	3.254	4.209

TABLE 4. - NEUTRONIC COMPARISON OF REFERENCE-DESIGN CELL WITH MOCKUP CELL

Neutronic parameter	Reference design	Mockup	Deviation, percent
Fast group			
Absorption cross section, Σ_a, cm^{-1}	0.00652	0.00649	-0.5
Capture cross section, Σ_c, cm^{-1}	0.00420	0.00401	-4.5
$\nu\Sigma_f$, cm^{-1}	0.00569	0.00614	7.9
Transport cross section, Σ_{tr}, cm^{-1}	0.1635	0.1729	5.7
Total cross section, Σ_t, cm^{-1}	0.4217	0.4210	-.2
Scattering cross section, Σ_s, cm^{-1}	0.4076	0.4094	.4
Removal cross section (fast to thermal group), $\Sigma_R(f \rightarrow th)$, cm^{-1}	0.01549	0.01531	-1.2
Fermi age, τ(2.38 eV), cm^2	95.16	90.56	-5.1
Thermal group			
Absorption cross section, Σ_a, cm^{-1}	0.07068	0.07562	7.0
Capture cross section, Σ_c, cm^{-1}	0.0236	0.0255	8.1
$\nu\Sigma_f$, cm^{-1}	0.1144	0.1218	6.5
Transport cross section, Σ_{tr}, cm^{-1}	0.6332	0.6373	.6
$(\Sigma_a)_{fuel}$, cm^{-1}	0.0555	0.0591	6.5
Thermal utilization, f	0.7857	0.7820	-.5
Number of fission neutrons per neutron absorbed in fuel, η	2.0604	2.0600	0
Total cross section, Σ_t, cm^{-1}	1.5286	1.5971	4.5
Scattering cross section, Σ_s, cm^{-1}	1.4579	1.5215	4.4
Average velocity, $\bar{v}$, m/sec	3613	3701	2.4
Infinite multiplication factor, k_∞	1.398	1.413	1.1

TABLE 5. - COMPARISON OF THERMAL AND EPITHERMAL MACROSCOPIC CAPTURE CROSS SECTIONS BY NUCLIDE FOR REFERENCE-DESIGN AND MOCKUP CORES

Nuclide	Capture cross section, Σ_c, cm^{-1}		Deviation, percent
	Reference design	Mockup	
Epithermal			
W^{182}	0.000334	0.000436	-8.8
W^{183}	.001390	.000504	
W^{184}	.000537	.000055	
W^{186}	.000268	.000456	
Total W	.002529	.001451	
U^{238}	0.000111	0.000975	
Total W + U^{238}	.002640	.002426	
Thermal			
W^{182}	0.000558	0.001372	12.5
W^{183}	.001600	.000341	
W^{184}	.002869	.000149	
W^{186}	.001044	.003138	
Total W	.006071	.005000	
U^{238}	0.000018	0.001848	
Total W + U^{238}	.006089	.006848	

TABLE 6. - TEN-GROUP STRUCTURE FOR GENERAL ATOMIC EIGENVALUE CALCULATIONS

Group	Energy interval	Lethargy interval
1	2.73 to 14.9 MeV	1.3 to -4.0
2	0.498 to 2.73 MeV	3.0 to 1.3
3	0.0674 to 0.498 MeV	5.0 to 3.0
4	0.0614 to 67.4 keV	12.0 to 5.0
5	2.38 to 61.4 eV	15.2 to 12.0
6	0.414 to 2.38 eV	----------
7	0.09 to 0.414 eV	----------
8	0.05 to 0.09 eV	----------
9	0.03 to 0.05 eV	----------
10	0 to 0.03 eV	----------

TABLE 7. - EIGENVALUES OF REFERENCE-DESIGN AND MOCKUP CORES

Core	Method	Effective multiplication factor, k_{eff}	Reactivity, $\Delta k/k$, percent
Reference design	Buckling iteration	1.196±0.0005	16.4
Mockup	Buckling iteration	1.211±0.001	17.4
	Two dimensional	1.210±0.003	17.4

TABLE 8. - COMPARISON OF NEUTRON BALANCE OF REFERENCE-DESIGN AND MOCKUP CORES

Nuclide	Reference design	Mockup
Absorptions per source neutron		
H	0.07072	0.06894
O	.00175	.00159
Al	.01060	.01378
U^{235} (capture)	0.12624	0.12599
U^{235} (fission)	.49116	.48977
W^{182}	0.01735	0.02757
W^{183}	.06572	.02185
W^{184}	.04404	.00324
W^{186}	.01903	.04251
W (total capture)	.14614	.09517
U^{238} (capture)	0.00431	0.05152
U^{238} (fission)	.00013	.00680
W + U^{238} (total capture)	.15045	.14669
H reflector	0.02412	0.02343
O reflector	.00005	.00004
Be reflector	[a]-.00802	-.00758
Leakage per source neutron		
Axial	0.04376	0.04216
Radial	.07664	.07533

[a]Negative sign indicates a net gain from (n, 2n) reaction.

TABLE 9. - ATOM DENSITIES

(a) Reference core zone

Material	Homogenized atom densities, atoms/(b-cm)			
	Zone			
	1	2	3	4
H	260.9×10^{-4}	260.9×10^{-4}	260.9×10^{-4}	260.9×10^{-4}
O	137.6	137.6	137.6	137.6
Al	65.8	65.8	65.8	65.8
W^{182}	4.086×10^{-4}	5.806×10^{-4}	2.545×10^{-4}	0.825×10^{-4}
W^{183}	5.739	6.048	5.463	5.153
W^{184}	37.44	33.54	40.93	44.84
W^{186}	4.274	6.148	2.596	0.721
U^{235}	3.361×10^{-4}	3.361×10^{-4}	3.361×10^{-4}	3.361×10^{-4}
U^{238}	.242	.242	.242	.242

(b) Mockup core zone

H	260.9×10^{-4}	260.9×10^{-4}	260.9×10^{-4}	260.9×10^{-4}
O	130.4	130.4	130.4	130.4
Al	166.8	166.8	166.8	166.8
W^{182}	4.731×10^{-4}	5.951×10^{-4}	3.431×10^{-4}	2.217×10^{-4}
W^{183}	2.584	3.251	1.873	1.209
W^{184}	5.483	6.897	3.975	2.569
W^{186}	5.092	6.405	3.961	2.385
U^{235}	3.361×10^{-4}	3.361×10^{-4}	3.361×10^{-4}	3.361×10^{-4}
U^{238}	13.98	13.98	13.98	13.98

TABLE 10. - NEUTRONIC PARAMETER COMPARISON

(a) Zone 1 (axially zoned)

Neutronic parameter	Reference design	Mockup	Deviation, percent
Fast group			
Absorption cross section, Σ_a, cm^{-1}	0.00723	0.00754	4.3
Capture cross section, Σ_c, cm^{-1}	0.00495	0.00511	3.2
$\nu\Sigma_f$, cm^{-1}	0.00559	0.00602	7.7
Transport cross section, Σ_{tr}, cm^{-1}	0.1666	0.1841	10.5
Total cross section, Σ_t, cm^{-1}	0.4525	0.4551	.6
Scattering cross section, Σ_s, cm^{-1}	0.4376	0.4413	.8
Removal cross section (fast to thermal group), $\Sigma_R(f \rightarrow th)$, cm^{-1}	0.01495	0.01481	-.9
Fermi age, τ(2.38 eV), cm^2	92.3	82.7	-10.4
Thermal group			
Absorption cross section, Σ_a, cm^{-1}	0.07300	0.7768	6.4
Capture cross section, Σ_c, cm^{-1}	0.02888	0.02893	.2
$\nu\Sigma_f$, cm^{-1}	0.1072	0.1185	10.5
Transport cross section, Σ_{tr}, cm^{-1}	0.655	0.662	1.1
$(\Sigma_a)_{fuel}$, cm^{-1}	0.05204	0.05752	10.5
Thermal utilization, f	0.7129	0.7405	3.9
Number of fission neutrons per neutron absorbed in fuel, η	2.0596	2.0595	~0
Total cross section, Σ_t, cm^{-1}	1.5519	1.6052	3.4
Scattering cross section, Σ_s, cm^{-1}	1.4789	1.5275	3.3
Average velocity, $\bar{v}$, m/sec	3655	3745	2.5

TABLE 10. - Continued. NEUTRONIC

PARAMETER COMPARISON

(b) Zone 4 (unzoned)

Neutronic parameter	Reference design	Mockup	Deviation, percent
Fast group			
Absorption cross section, Σ_a, cm^{-1}	0.006527	0.006743	3.3
Capture cross section, Σ_c, cm^{-1}	0.004201	0.004288	2.1
$\nu\Sigma_f$, cm^{-1}	0.005704	0.006078	6.6
Transport cross section, Σ_{tr}, cm^{-1}	0.1660	0.1747	5.2
Total cross section, Σ_t, cm^{-1}	0.4305	0.4242	-1.5
Scattering cross section, Σ_s, cm^{-1}	0.4163	0.4124	-.9
Removal cross section (fast to thermal group), $\Sigma_R(f \rightarrow th)$, cm^{-1}	0.01553	0.01513	-2.6
Fermi age, τ(2.38 eV), cm^2	93.1	88.8	-4.6
Thermal group			
Absorption cross section, Σ_a, cm^{-1}	0.07068	0.07562	7.0
Capture cross section, Σ_c, cm^{-1}	0.0236	0.0255	8.0
$\nu\Sigma_f$, cm^{-1}	0.1144	0.1218	6.5
Transport cross section, Σ_{tr}, cm^{-1}	0.6332	0.6373	.6
$(\Sigma_a)_{fuel}$, cm^{-1}	0.0555	0.0591	6.5
Thermal utilization, f	0.7857	0.7820	-.5
Number of fission neutrons per neutral absorbed in fuel, η	2.0604	2.0600	-.02
Total cross section, Σ_t, cm^{-1}	1.5386	1.5971	4.5
Scattering cross section, Σ_s, cm^{-1}	1.4579	1.5215	4.4
Average velocity, $\bar{v}$, m/sec	3613	3701	2.4

TABLE 10. - Continued. NEUTRONIC

PARAMETER COMPARISON

(c) Zone 3 (radially zoned)

Neutronic parameter	Reference design	Mockup	Deviation, percent
Fast group			
Absorption cross section, Σ_a, cm^{-1}	0.00696	0.00712	2.3
Capture cross section, Σ_c, cm^{-1}	0.00466	0.00470	.9
$\nu\Sigma_f$, cm^{-1}	0.00564	0.00599	6.2
Transport cross section, Σ_{tr}, cm^{-1}	0.1665	0.1773	6.5
Total cross section, Σ_t, cm^{-1}	0.4437	0.4358	-1.8
Scattering cross section, Σ_s, cm^{-1}	0.4291	0.4231	-1.4
Removal cross section (fast to thermal group), $\Sigma_R(f \rightarrow th)$, cm^{-1}	0.01518	0.01478	-2.6
Fermi age, τ(2.38 eV), cm^2	93.1	87.4	-6.1
Thermal group			
Absorption cross section, Σ_a, cm^{-1}	0.07321	0.07765	6.1
Capture cross section, Σ_c, cm^{-1}	0.02862	0.02943	2.8
$\nu\Sigma_f$, cm^{-1}	0.1083	0.1172	8.2
Transport cross section, Σ_{tr}, cm^{-1}	0.646	0.611	-5.4
$(\Sigma_a)_{fuel}$, cm^{-1}	0.0526	0.0569	8.2
Thermal utilization, f	0.7185	0.7331	2.0
Number of fission neutrons per neutron absorbed in fuel, η	2.0595	2.0583	-.1
Total cross section, Σ_t, cm^{-1}	1.5478	1.5493	-.2
Scattering cross section, Σ_s, cm^{-1}	1.4746	1.4717	.1
Average velocity, $\bar{v}$, m/sec	3679	3847	4.6

TABLE 10. - Concluded. NEUTRONIC

PARAMETER COMPARISON

(d) Zone 2 (axially and radially zoned)

Neutronic parameter	Reference design	Mockup	Deviation, percent
Fast group			
Absorption cross section, Σ_a, cm^{-1}	0.00773	0.00784	1.4
Capture cross section, Σ_c, cm^{-1}	0.00548	0.00543	-.9
$\nu\Sigma_f$, cm^{-1}	0.00553	0.00596	7.8
Transport cross section, Σ_{tr}, cm^{-1}	0.1667	0.1868	12.1
Total cross section, Σ_t, cm^{-1}	0.4600	0.4651	1.1
Scattering cross section, Σ_s, cm^{-1}	0.4446	0.4505	1.3
Removal cross section (fast to thermal group), $\Sigma_R(f \rightarrow th)$, cm^{-1}	0.01453	0.01453	~0
Fermi age, τ(2.38 eV), cm^2	92.0	81.4	-11.5
Thermal group			
Absorption cross section, Σ_a, cm^{-1}	0.07636	0.08012	4.9
Capture cross section, Σ_c, cm^{-1}	0.03387	0.03293	-2.8
$\nu\Sigma_f$, cm^{-1}	0.1033	0.1147	11.0
Transport cross section, Σ_{tr}, cm^{-1}	0.653	0.626	-4.1
$(\Sigma_a)_{fuel}$, cm^{-1}	0.05016	0.05573	11.0
Thermal utilization, f	0.6568	0.6955	5.9
Number of fission neutrons per neutron absorbed in fuel, η	2.0589	2.0581	~0
Total cross section, Σ_t, cm^{-1}	1.5596	1.5632	.2
Scattering cross section, Σ_s, cm^{-1}	1.4832	1.4831	~0
Average velocity, $\bar{v}$, m/sec	3703	3859	4.2

TABLE 11. - FIFTEEN-GROUP STRUCTURE

FOR LEWIS TWMR EIGENVALUE

CALCULATIONS

Group	Energy interval	Lethargy interval
1	0.821 to 14.9 MeV	-4.00 to 2.50
2	5.531 to 0.821 keV	2.50 to 7.50
3	0.454 to 5.531 keV	7.50 to 10.00
4	2.382 to 0.454 eV	10.00 to 15.25
5	0.532 to 2.382 eV	15.25 to 16.75
6	0.30 to 0.532 eV	----------
7	0.22 to 0.30 eV	----------
8	0.16 to 0.22 eV	----------
9	0.10 to 0.16 eV	----------
10	0.08 to 0.10 eV	----------
11	0.06 to 0.08 eV	----------
12	0.04 to 0.06 eV	----------
13	0.0253 to 0.04 eV	----------
14	0.015 to 0.0253 eV	----------
15	0 to 0.015 eV	----------

TABLE 12. - COMPARISON OF CALCULATED AND MEASURED MULTIPLICATION FACTORS

Core	Description			$CdNO_3$ poison concentration, moles/liter	Effective multiplication factor, k_{eff}		Deviation, $\Delta k/k_1 k_2$
	Configuration	Number of elements	Number of tubes		Measured	Calculated	
General Atomic design method calculation							
I	7.62-cm pitch, water reflected	121 121	207 ---	0.0953 Unpoisoned	1.021 1.114	1.000 1.090	-0.0205 -.0198
II	7.37-cm pitch, water reflected	121 121	204 ---	0.0431 Unpoisoned	1.008 1.050	0.986 1.025	-0.0221 -.0232
III	7.37-cm pitch, water reflected	85	None	Unpoisoned	1.006	0.990	-0.0160
IV	7.62-cm pitch, beryllium reflected	121 121	204 ---	0.2202 Unpoisoned	1.002 1.169	0.986 1.143	-0.0162 -.0194
General Atomic refined method calculation							
I	7.62-cm pitch, water reflected	121 121	204 204	0.1255 .1255	1.001 [a]1.001	[b]0.999 [c]1.0056±0.001	-0.0020 0.0045±0.001
IV	7.62-cm pitch, beryllium reflected	121	---	Unpoisoned	1.169	1.162	-0.0046
V	7.62-cm pitch, beryllium reflected, radially zoned	121 121	204 ---	0.1704 Unpoisoned	1.009 1.151	1.001 1.140	-0.008 -.008
VI	7.62-cm pitch, beryllium reflected, radially and axially zoned	121 121	204 ---	0.1278 Unpoisoned	1.001 1.111	1.001 1.108	------- -0.0021

[a]Additional 10 in. of upper water reflector included.

[b]One-dimensional synthesis.

[c]Two dimensional.

TABLE 13. - COMPARISON OF SUBCRITICAL REACTIVITY OBTAINED BY POISON-TUBE SUBSTITUTION, PULSED NEUTRONS, AND CALCULATION

Core	Description		$CdNO_3$ poison concentration in 204 tubes, moles/liter	Reactivity, $			Ratio of mean prompt neutron lifetime to effective delayed neutron fraction (measured), $\bar{l}/\beta_{eff}$, sec
	Configuration	Number of elements		Measured by poison substitution	Measured by pulsed neutrons	Calculated analogous to pulsed neutron technique	
I	7.62-cm pitch, water reflected	121	0.1255 .1677 .2899	-0.38 -3.24 -9.37	[a]-0.38 -2.91 -9.01	-1.82 -5.49 -12.37	4.06×10^{-3}
II	7.37-cm pitch, water reflected	121	0.04309 .1255	-0.305 -6.32	[a]-0.305 -5.73	------ ------	4.12×10^{-3}
III	7.37-cm pitch, water reflected	85	0	-0.14	[a]-0.14	------	4.00×10^{-3}
IV	7.62-cm pitch, beryllium reflected	121	0.2202 .2899 .4045	-0.38 -2.89 -7.04	[a]-0.38 -2.77 -6.06	------ ------ ------	4.51×10^{-3}
VI	7.62-cm pitch, beryllium reflected, radially and axially zoned	121	0.1278 .1704	-0.37 -2.65	[a]-0.37 -2.56	------ ------	5.10×10^{-3}

[a]Measured value of $\bar{l}/\beta_{eff}$ obtained by pulsing at this calibrated subcritical reactivity was used to compute the shutdown reactivity from the measured α's for the other cores having the same pitch and reflectors but increased $CdNO_3$ loadings.

TABLE 14. - COMPARISON OF MEASURED AND CALCULATED

VALUES OF PROMPT NEUTRON LIFETIME

Core	Description		Effective delayed neutron fraction, β_{eff}	Lifetime, μsec		
	Configuration	Number of elements		Measured	Calculated	
					One dimensional	Two dimensional
I	7.62-cm pitch, water reflected	121	0.00712	28.9	25.0	----
II	7.37-cm pitch, water reflected	121	0.00724	29.9	25.0	----
III	7.37-cm pitch, water reflected	85	0.00724	28.9	28.8	----
IV	7.62-cm pitch, beryllium reflected	121	0.00702	31.6	26.6	----
VI	7.62-cm pitch, beryllium reflected, radially and axially zoned	121	0.00703	35.9	----	27.9

TABLE 15. - CALCULATED AND MEASURED

TEMPERATURE COEFFICIENTS

Temperature, ^{o}C	Effective multiplication factor, k_{eff}	Overall temperature coefficient over range of 27^{o} to 100^{o} C, ¢/C^{o}	
		Calculated	Measured
27	0.971037	-----	------
[a]100	.967306	-0.76	[c]-0.63
[b]100	.968215	-.58	[c]-.63

[a]Change in thermal disadvantage factors neglected.

[b]Change in thermal disadvantage factors incorporated.

[c]Extrapolated from 80^{o} C.

TABLE 16. - COMPARISON OF MEASURED AND CALCULATED COMPONENT WORTH (CORE I)

Material	Worth, $		
	Measured	Calculated	
		Eigenvalue calculation	Perturbation analysis
Center pressure tube			
U-Al rings and Al structure	1.082	1.011	0.665
W rings	-.352	-.329	-.313
U^{238} ring	-.113	-.115	-.114
Total	0.617	0.567	0.238
Element measured directly	.619	-----	-----
Pressure tube in row next to outer row			
U-Al rings and Al structure	0.366	-----	0.207
W rings	-.101	-----	-.099
U^{238} ring	-.027	-----	-.036
Total	0.238	-----	0.072
Element measured directly	.240	-----	-----
Pressure tube in outer row			
U-Al rings and Al structure	0.358	-----	0.192
W rings	-.071	-----	-.071
U^{238} ring	-.019	-----	-.025
Total	0.268	-----	0.096
Element measured directly	.270	-----	-----

TABLE 17. - COMPARISON OF MEASURED AND CALCULATED REACTIVITY WORTH FOR 7.37-CENTIMETER-PITCH, WATER-REFLECTED CORE (CORE II)

Material	Worth, $	
	Measured	Calculated from perturbation analysis
Outermost U-Al fuel ring	0.157	------
U-Al fuel ring next to outermost ring	.108	------
W rings	-.326	-0.331
U^{238} ring	-.110	-.120

TABLE 18. - CENTRAL FUEL ELEMENT COMPONENT WORTHS FOR 7.62-CENTIMETER-PITCH, BERYLLIUM-REFLECTED CORE

Material	Worth, $
W	-0.281
U^{238} ring	-.102
U^{235}/Al rings and Al structure	.957
Fuel element against void	.574

TABLE 19. - NOMINAL DIMENSIONS OF 4.13-CENTIMETER ENRICHED TUNGSTEN CYLINDERS FOR SPECIAL FUEL STAGES

Number	Inside diameter, cm	Wall thickness, cm	Material	Weight percent
1	1.255	0.0533		
2	1.666	.0381		
3	2.088	.0381	W^{180}	0.0025
4	2.525	.0533	W^{182}	2.0139
5	2.936	.0381	W^{183}	1.5752
6	3.358	.0381	W^{184}	93.9112
7	3.795	.0508	W^{186}	2.4972
8	4.206	.0381		
9	4.628	.0356		
10	5.060	.0533		
11	5.436	.0325	W^{180}	.010
			W^{182}	6.174
			W^{183}	81.892
			W^{184}	8.704
			W^{186}	3.220

TABLE 20. - COMPARISON OF COMPOSITION AND RESONANCE ABSORPTION OF FIVE REFERENCE-DESIGN AND FIVE SPECIAL REFERENCE FUEL STAGES

Isotopic contribution	W^{182}	W^{183}	W^{184}	W^{186}	Total
Reference-design fuel stages					
Mass, g	30.8900	194.1150	1698.0500	27.6200	1950.65
Surface to mass ratio, S/M, cm^2/g	11.49	1.829	0.209	12.85	
$\sqrt{S/M}$, $cm/g^{1/2}$	3.39	1.35	0.457	3.58	
Effective resonance integral, I_{eff}, b	140	60	2.2	128	
$M \times I_{eff}$, (g)(b)	4330	11 600	3730	3530	23 190
Weight percent	1.583	9.951	87.05	1.416	
5-Ring special reference stages; rings 1, 4, 7, 10, 11					
20 Enriched W^{184} cylinders, g	17.0444	13.2853	791.4390	21.0191	842.83
5 Enriched W^{183} cylinders, g	13.7405	181.2766	19.3679	7.1428	221.55
Total mass, g	30.7849	194.5619	810.8069	28.1619	1064.38
Surface to mass ratio, S/M, cm^2/g	11.61	1.837	0.4407	12.69	
$\sqrt{S/M}$, $cm/g^{1/2}$	3.41	1.36	0.664	3.56	
Effective resonance integral, I_{eff}, b	135	60	2.8	126	
$M \times I_{eff}$, (g)(b)	4160	11 700	2270	3550	21 680
Weight percent[a]	1.578	9.974	41.56	1.444	
8-Ring special reference stages; rings 1, 2, 4, 6, 7, 9, 10, 11					
35 Enriched W^{184} cylinders, g	25.7616	20.1499	1201.9388	31.9554	
5 Enriched W^{183} cylinders, g	13.7405	181.2766	19.3679	7.1428	
Total mass, g	39.5021	201.4265	1221.3067	39.0982	1501.42
Surface to mass ratio, S/M, cm^2/g	9.046	1.774	0.2926	9.140	
$\sqrt{S/M}$, $cm/g^{1/2}$	3.01	1.32	0.541	3.02	
Effective resonance integral, I_{eff}, b	120	59	2.40	110	
$M \times I_{eff}$, (g)(b)	4740	11 900	2930	4300	23 870

[a]Based on total five-reference-stage mass.

TABLE 20. - Concluded. COMPARISON OF COMPOSITION AND RESONANCE ABSORPTION OF FIVE REFERENCE-DESIGN AND FIVE SPECIAL REFERENCE FUEL STAGES

Isotopic contribution	W^{182}	W^{183}	W^{184}	W^{186}	Total
9-Ring special reference stages; rings 1, 2, 3, 4, 6, 7, 9, 10, 11					
40 Enriched W^{184} cylinders, g	27.9985	21.9142	1306.8273	34.7630	
5 Enriched W^{183} cylinders, g	13.7405	181.2766	19.3679	7.1428	
Total mass, g	41.7390	203.1908	1326.1952	41.9058	1613.12
Surface to mass ratio, S/M, cm^2/g	8.561	1.760	0.2695	8.527	
$\sqrt{S/M}$, $cm/g^{1/2}$	2.93	1.33	0.519	2.92	
Effective resonance integral, I_{eff}, b	118	59	2.37	107	
$M \times I_{eff}$, (g)(b)	4930	12 000	3140	4480	24 500
11-Ring special reference stages					
50 Enriched W^{184} cylinders, g	35.1830	27.5188	1640.6568	43.6265	1747.07
5 Enriched W^{183} cylinders, g	13.7405	181.2766	19.3679	7.1[illegible]	221.55
Total mass, g	48.9235	208.7954	1660.0247	50.7693	1968.62
Surface to mass ratio, S/M, cm^2/g	7.304	1.712	0.2153	7.039	
$\sqrt{S/M}$, $cm/g^{1/2}$	270	1.30	0.462	2.64	
Effective resonance integral, I_{eff}, b	110	58	2.2	97	
$M \times I_{eff}$, (g)(b)	5380	12 100	3650	4930	26 060
Weight percent[a]	2.508	10.704	85.101	2.603	

[a]Based on total five-reference-stage mass.

TABLE 21. - REMOVAL WORTH OF NUCLIDES IN MOCKUP AND 8-RING SPECIAL REFERENCE ELEMENT

Nuclide	Mockup element	Special reference element
Removal worth of parasitic capture, ¢		
H	1.88	1.86
O	.06	.06
Al	.63	.72
W^{182}	1.62	1.04
W^{183}	1.32	3.62
W^{184}	.20	1.56
W^{186}	2.24	1.21
U^{235}	6.17	6.19
U^{238}	2.92	.23
Removal worth of fission capture, ¢		
U^{235}	21.97	22.14
U^{238}	.30	.01
Removal worth of fission production, ¢		
U^{235}	-41.19	-41.49
U^{238}	-.88	-.02
Removal worth of scattering, ¢		
H	-9.10	-9.21
O	-.19	-.20
Al	-.41	-.41
W^{182}	-0.02	-0.01
W^{183}	-.02	-.07
W^{184}	-.03	-.35
W^{186}	-.03	-.01
U^{235}	-0.02	-0.02
U^{238}	-.15	~0
Total removal worth, ¢	-12.73	-13.15

TABLE 22. - REACTIVITY REQUIREMENTS FOR ZONED REFERENCE-DESIGN ROCKET REACTOR EXCLUDING XENON AND TRANSIENT SAMARIUM

Temperature defect:	
Fuel, 21^{o} to 50^{o} C	-1.5 to -2.5
H_2O, 21^{o} to 102^{o} C	-1.0 to -2.5
Propellant hydrogen	0.03
Fuel loss, 1 percent of fuel diffusing through clad	-.19
Fuel transmutation (burnup)	-.32
Long lived fission product poisoning (including steady-state Sm but excluding Xe and transient Sm)	-.80
Penalty incurred by gross power distribution tailoring (axial and radial)	-6.4
Penalty incurred by fuel zoning within fuel elements	-1.0
Design and manufacturing tolerance	±1.5
Total reactivity requirements (excluding Xe or transient Sm), $\Delta k/k$, percent	-12.68

TABLE 23. - REACTIVITY REQUIREMENTS FOR CONTROL SYSTEM EXCLUDING XENON

Ensured shutdown	-2.0
Temperature defect:	
Fuel, 21^{o} to 2507^{o} C	-1.5 to -2.5
H_2O, 21^{o} to 102^{o} C	-1.0 to -2.5
Propellant hydrogen	0.03
Fuel loss, 1 percent of fuel diffusing through the clad	-.19
Fuel transmutation (burnup in 10 full-power hr)	-.32
Long-lived fission product poisoning (10 full-power hr)	-.80
Total reactivity excluding xenon requirements, $\Delta k/k$, percent	-5.78

TABLE 24. - REACTIVITY CONTROL RATE REQUIREMENTS

Item	Type control	Approximate reactivity, Δk/k, percent	Maximum delay time, sec	Approximate required reactivity rate, ¢/sec	Total time
Cold shutdown - hot critical	External system	0.045	----	8 (av)	75 sec
Xenon override	External system	.08	----	2 (av)	9 min
Power control	Temperature defect	.025	----	Fast inherent control	------
Bulk moderator temperature control during power run	External system	.02	----	----------	------
Regular control	----------	-----	----	±0.5	------
Fast drive down	----------	-----	----	-8	------
Scram	Auxiliary external system	-.15	0.30	-800	------
Scram recovery	----------	-----	----	8 (av)	Several hours

TABLE 25. - LOW-POWER AND FULL-POWER AXIAL-POWER DENSITY DISTRIBUTIONS WITH HELIUM 3 CONTROL OF UNZONED REFERENCE CORE

Core length, fraction from inlet	Relative power densities at -	
	Low reactor power[a]	Full reactor power[a]
At inlet	0.764	0.752
0.1	.867	.855
.2	1.066	1.056
.3	1.210	1.205
.4	1.288	1.288
.5	1.295	1.300
.6	1.231	1.238
.7	1.098	1.106
.8	.904	.911
.9	.660	.664
1.0	.457	.460

[a]Relative to core average.

TABLE 26. - RESULTS OF LARGER CORE STUDY FOR EFFECTIVE MULTIPLICATION FACTOR AND RADIAL MAXIMUM TO AVERAGE POWER

Number of fuel assemblies	Number of central fuel assemblies with natural tungsten support tube	Effective multiplication factor, k_{eff}		Reactivity required for zoning, $\Delta k/k$, percent	Radial maximum to average power, $\hat{P}_R/\bar{P}_R$	
		Unzoned	Zoned		Unzoned	Zoned
121	19	1.206	1.178	2.32	1.501	1.280
325	91	1.296	1.248	3.7	1.712	1.245
811	397	1.333	1.259	5.54	1.862	1.156
1255	721	1.343	1.261	6.09	1.892	1.124

TABLE 27. - COMPOSITION OF CORE FOR POINT KERNEL CALCULATIONS

Region	Composition, volume fraction					
	UO_2	W	Al	H_2O	Be	Void[a]
1	0.0183	0.0915	0.1233	0.3628	------	0.4041
2	------	------	------	.1	0.9	------
3	------	------	.0710	.9290	------	------
4	------	.0067	.0840	.4030	------	.5063
5	------	.0118	.1233	.3628	------	.5021
6	------	.0046	.0951	.1377	.4973	.2653

[a]Hydrogen gas was treated as a void with respect to gamma ray attenuation because of its low density compared with the other materials.

TABLE 28. - GAMMA SOURCE DESCRIPTION

[These values for W are for natural W and include gammas resulting from resonance capture. Thermal neutron capture gamma spectra are taken from refs. 47 to 51. Unresolved capture gammas were arbitrarily distributed among the energy intervals.]

Energy interval, MeV	Gamma source, MeV/fission								
	U^{235} fission and radiative capture	W^{182}	W^{183}	W^{184}	W^{186}	Al	H_2O	Cd	Total
0 to 1	4.25	1.326×10^{-1}	2.83×10^{-1}	1.163×10^{-1}	1.042×10^{-1}	1.56×10^{-2}	---	1.029×10^{-1}	5.005
1 to 2	4.26	1.326	2.83	1.163	1.042	4.79	---	1.222	5.067
2 to 3	2.13	1.326	2.83	1.163	1.042	1.57	2.46×10^{-1}	2.125	3.240
3 to 4	8.68×10^{-1}	1.326	2.83	1.163	1.042	1.47	---	1.538	1.673
4 to 5	2.99	1.326	6.54	1.163	1.042	2.54	---	1.050	.549
5 to 6	1.16	5.69×10^{-2}	2.92	4.93×10^{-2}	---	1.11	---	6.29×10^{-2}	.588
6 to 7	3.96×10^{-2}	1.370×10^{-1}	9.69×10^{-2}	---	---	8.13×10^{-3}	---	2.75	.309
7 to 8	1.33	---	4.91	---	---	3.36×10^{-2}	---	9.5×10^{-3}	.106
8 to 9	3.73×10^{-3}	---	---	---	---	---	---	3.0	.007
9 to 10	1.40	---	---	---	---	---	---	1.6	.003
Total gamma source per fission from 0 to 10 MeV									16.547

TABLE 29. - THERMAL FLUX IN CORE

Material	Thermal flux, neutrons/(cm^2)(sec)
W	4.64×10^{14}
Al	9.28×10^{14}
H_2O	1.16×10^{15}
Cadmium 113 (poison solution)	9.28×10^{14}

TABLE 30. - ENERGY ABSORPTION BUILDUP FACTORS

[$B(r, r_T) = \beta_0 + \beta_1 d + \beta_2 d^2 + \beta_3 d^3$, where d is attenuation length.]

Energy interval, MeV	Buildup factors			
	β_0	β_1	β_2	β_3
0 to 1	1.0245	0.45096	-4.1100×10^{-2}	1.4830×10^{-3}
1 to 2	1.0059	.68561	-1.8974	5.6287×10^{-4}
2 to 3	1.0034	.44940	-2.5837×10^{-4}	3.6300
3 to 4	1.0023	.28179	8.1351×10^{-3}	4.4817
4 to 5	1.0005	.20187	7.3063	9.5400
5 to 6	.99683	.17135	4.2784×10^{-4}	1.6490×10^{-3}
6 to 7	.99395	.14702	-4.9832×10^{-3}	2.1292
7 to 8	.99184	.12888	-8.9268	2.3947
8 to 9	.99049	.11693	-1.1403×10^{-2}	2.4454
9 to 10	.98991	.11116	-1.2412	2.2814

TABLE 31. - LINEAR ATTENUATION COEFFICIENTS

Energy interval, MeV	Attenuation coefficient, μ, cm^{-1}				
	UO_2	W	Al	H_2O	Be
0 to 1	1.785	2.41	0.227	0.0962	0.1416
1 to 2	.588	.948	.135	.0575	.0846
2 to 3	.484	.801	.104	.0435	.0644
3 to 4	.4615	.0774	.0882	.0361	.0526
4 to 5	.457	.782	.0791	.0316	.0456
5 to 6	.461	.799	.0734	.0286	.0407
6 to 7	.470	.818	.0694	.0264	.0372
7 to 8	.479	.840	.0661	.0247	.0344
8 to 9	.492	.862	.0642	.0235	.0322
9 to 10	.501	.888	.0626	.0224	.0304

TABLE 32. - LINEAR ENERGY ABSORPTION COEFFICIENTS

Energy interval, MeV	Absorption coefficient, μ_a, cm^{-1}		
	Al	W	H_2O
0 to 1	0.0774	1.525	0.0330
1 to 2	.0664	.544	.0283
2 to 3	.0575	.534	.0241
3 to 4	.0524	.581	.0214
4 to 5	.0497	.635	.0196
5 to 6	.0475	.679	.0184
6 to 7	.0464	.718	.0175
7 to 8	.0459	.756	.0167
8 to 9	.0454	.791	.0161
9 to 10	.0454	.824	.0156

TABLE 33. - ISOTOPE COMPOSITION OF TUNGSTEN FUEL CYLINDERS

Isotope	Volume percent
W^{182}	1.6
W^{183}	10.0
W^{184}	87.0
W^{186}	1.4

TABLE 34. - 30° GEOMETRY AXIAL POWER DISTRIBUTION

Axial location, Z, cm	Ratio of local to average power, $P_A/\bar{P}_A$	Axial location, Z, cm	Ratio of local to average power, $P_A/\bar{P}_A$
0	0.315	75	1.398
10	.478	76	1.399
20	.636	77	1.400
30	.793	78	1.398
40	.947	80	1.396
50	1.090	82	1.387
60	1.230	87	1.348
65	1.300	92	1.281
70	1.360	97	1.180
72	1.379	102	1.010
74	1.392	107	.760

TABLE 35. - CYLINDER TO CYLINDER POWER DISTRIBUTION

Cylinder	Relative number of fissions
[a]1	0.0403
2	.0536
3	.0669
4	.0802
5	.0935
6	.1067
7	.1200
8	.1333
9	.1465
[b]10	.1590

[a]Innermost fuel cylinder.
[b]Outermost fuel cylinder.

TABLE 36. - GAMMA HEATING RATES IN FUEL STAGE

Fuel cylinders	Gamma heating rate, W/cc	Standard deviation
[a]1	2221	328
2	2896	479
3	2917	363
4	2894	340
5	3683	468
6	3160	424
7	2914	323
8	2770	295
9	2840	270
10	2781	247
W support tube	2725	284
Al pressure tube	242	20
H_2O, high-velocity region	109	9
Al flow divider	257	28

[a]Innermost fuel cylinder.

TABLE 37. - GAMMA HEATING IN HOMOGENIZED FUEL ASSEMBLIES

Fuel assembly vertex number (fig. 7(a))	Gamma heating rates, W/cc homogenized metal plus void[a]					
	Axial region 1	Standard deviation	Axial region 2	Standard deviation	Axial region 3	Standard deviation
1	548	62	465	101	389	34
2	562	34	658	55	425	18
3	509	26	719	56	406	16
4	561	24	---	--	423	13
5	519	30	653	69	400	14
6	520	21	576	34	399	12
7	490	26	594	64	354	14
8	485	18	662	57	365	10
9	490	24	781	81	387	13
10	386	24	501	66	284	13
11	409	17	505	31	311	9
12	419	19	583	40	336	10
13	305	15	348	26	230	8
14	339	13	442	27	250	7
15	380	26	426	42	261	12

[a]Center plug, fuel cylinders, and W support tube represent 21.3 vol % of the homogenized volume.

TABLE 38. - GAMBLE CALCULATED RELATIVE

ACTIVITY OF FOILS

Nuclide	Weight percent	Activation cross section at 2200 m/sec	Subcadmium activity, $(dis)(sec^{-1})(mg^{-1})(W^{-1})$
Gold	100	98.8±0.2	135.5±0.2
Manganese	80	13.2±0.1	51.9±0.4

TABLE 39. - GAMMA HEATING

MEASUREMENTS

Foil	Thickness, cm	Power, W		
		Run 1	Run 2	Run 3
Gold	0.00508	82.6	85.2	84.7
Manganese	.00508	80.7	----	----
Manganese	.01270	----	72.8	70.4

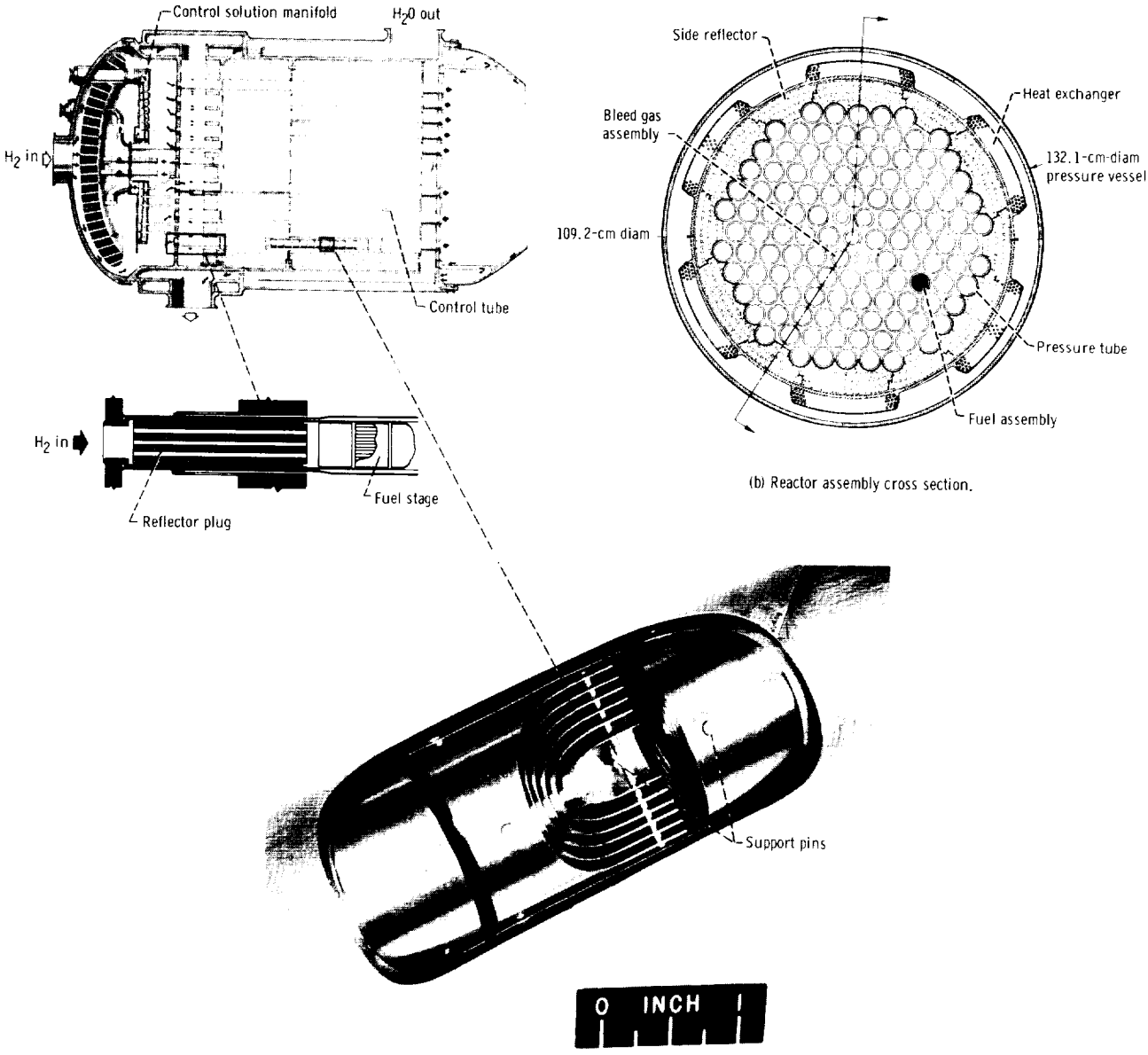

(b) Reactor assembly cross section.

(a) Reactor assembly axial section.

Figure 1. - TWMR reference-design reactor and fuel-element detail.

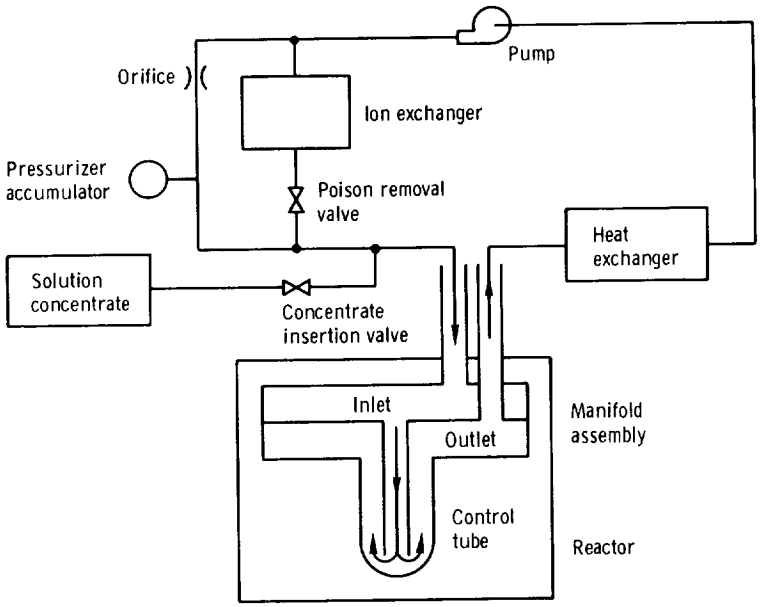

Figure 2. - Schematic diagram of reactivity control solution system.

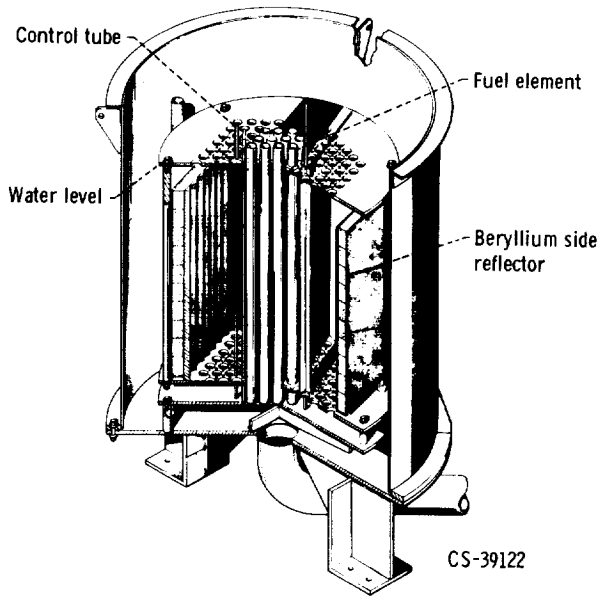

(a) Reactor assembly

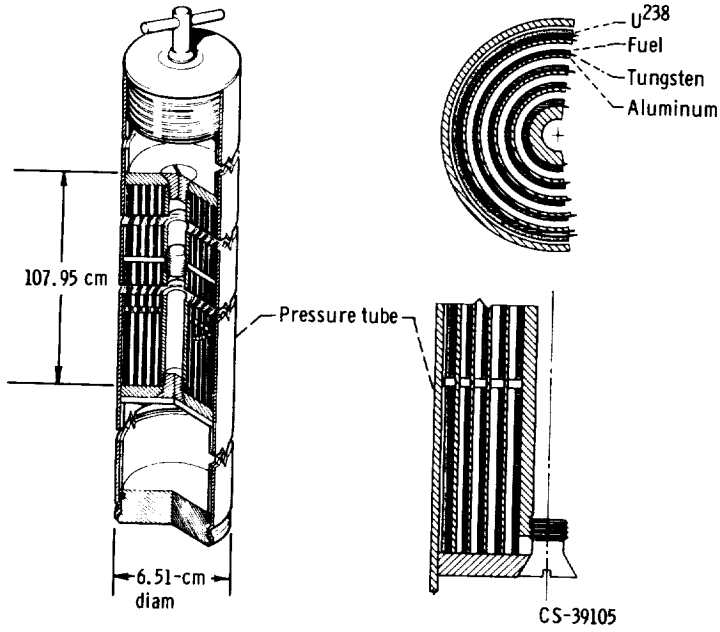

(b) Fuel-element assembly.

Figure 3. - General Atomic reactor and fuel-element assembly.

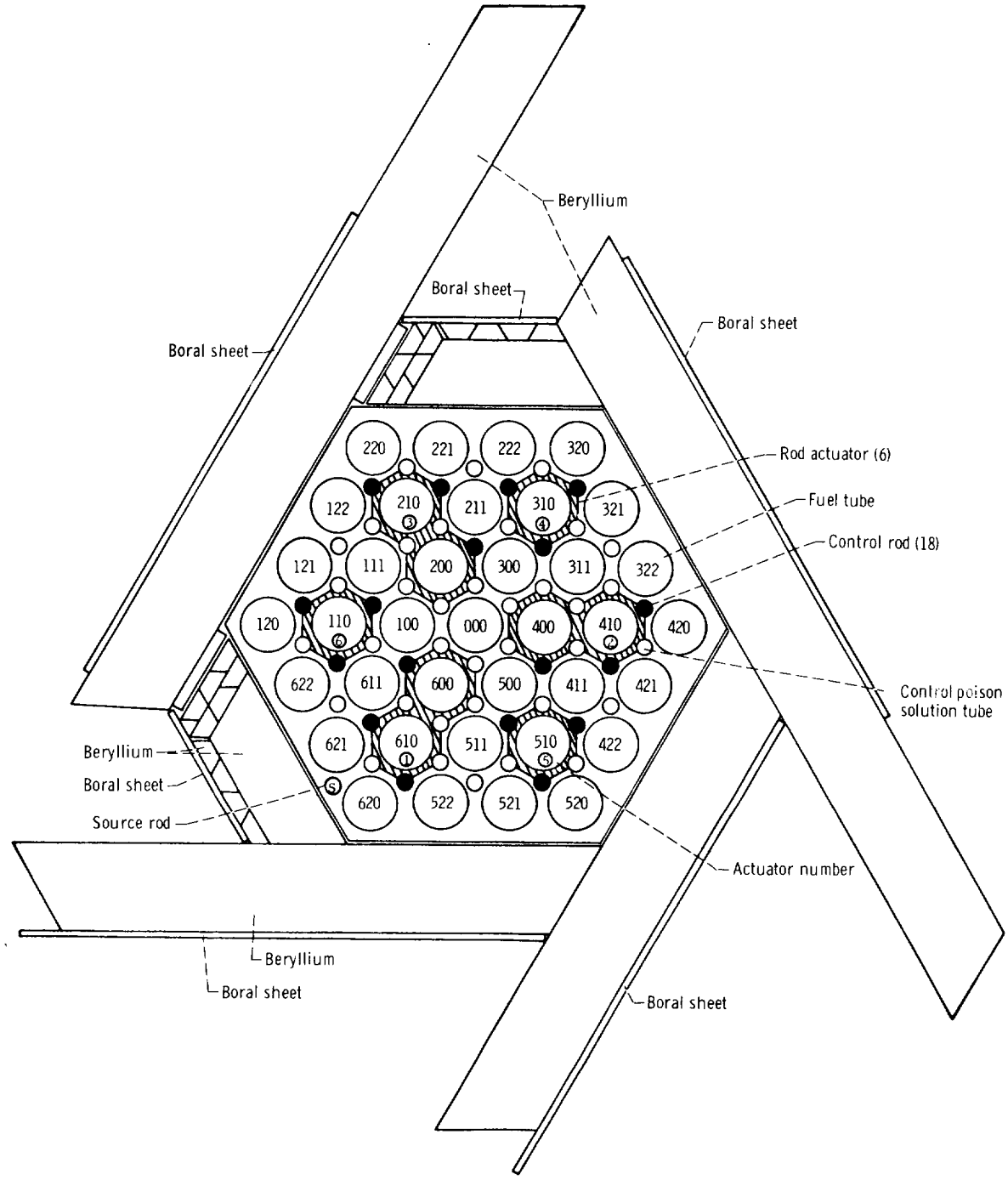

Figure 4. - General Electric critical configuration.

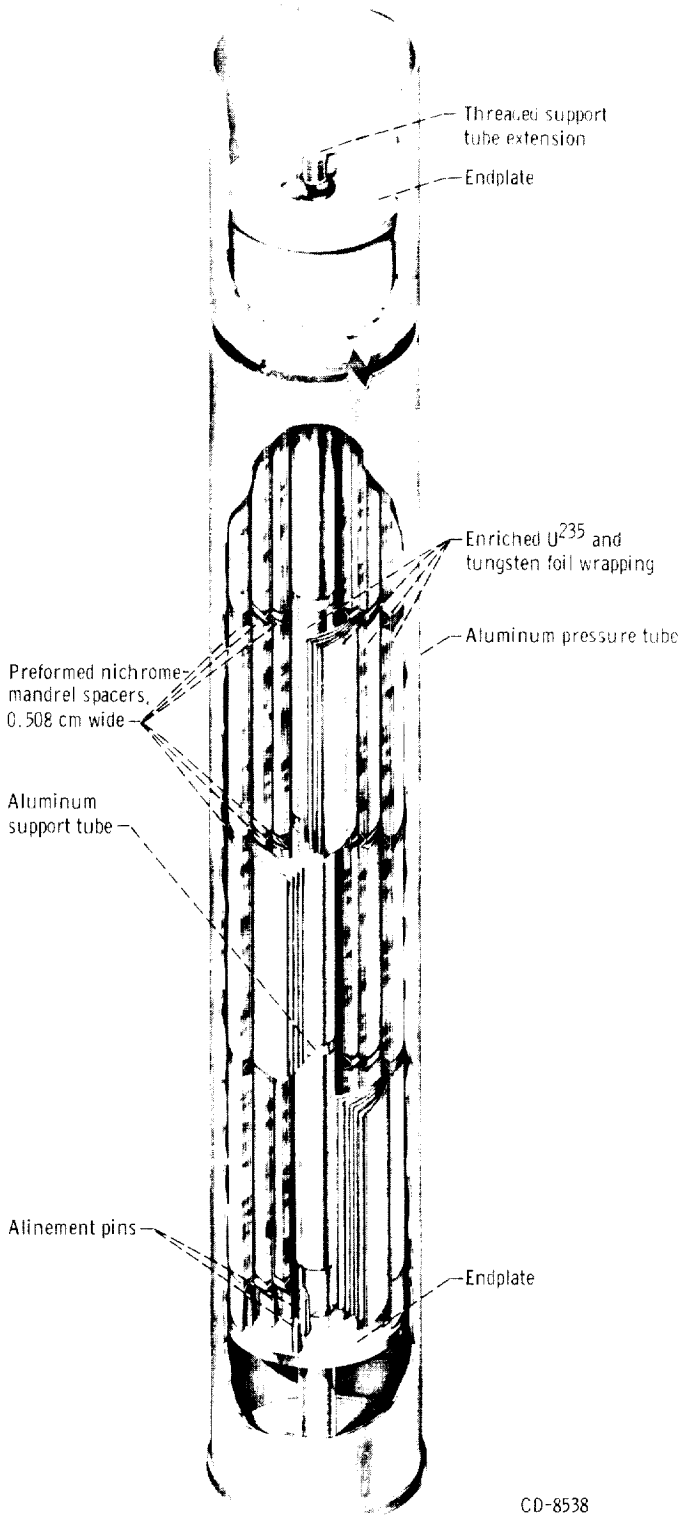

Figure 5. - General Electric fuel-element assembly.

Reflector region	Homogenized atom density		
	Hydrogen	Oxygen	Beryllium
I	0.000334	0.00117	0.1169
II	.0668	.0334	0
III	.005804	.002902	.06365
IV	.005804	.002902	0

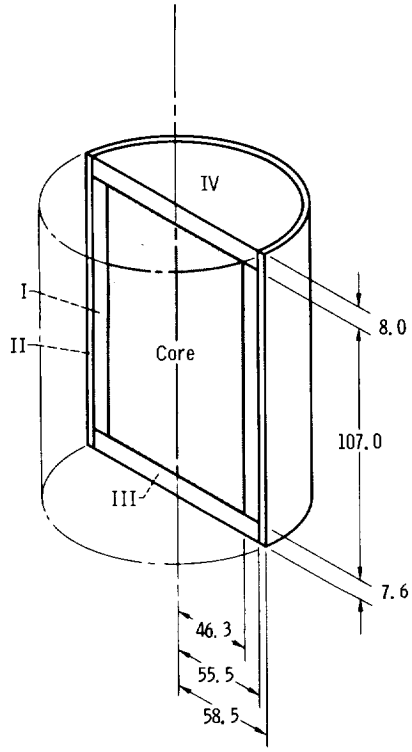

Figure 6. - Geometry for eigenvalue calculations for reference-design and mockup cores. (All dimensions are in centimeters.)

Schedule of tungsten composition			
Zone	Fuel rings, percent	Outer support tube	All other tungsten components
1	70 Natural 30 Enriched	Enriched	Enriched
2	70 Natural 30 Enriched	Natural	↓
3	100 Enriched	Natural	↓
4	100 Enriched	Enriched	↓

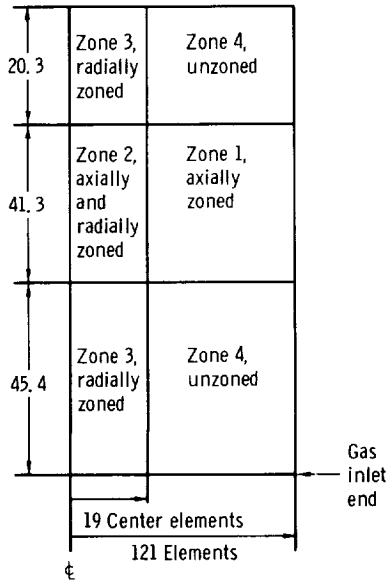

Figure 7. - Zoning scheme for reference core. (All dimensions are in centimeters.)

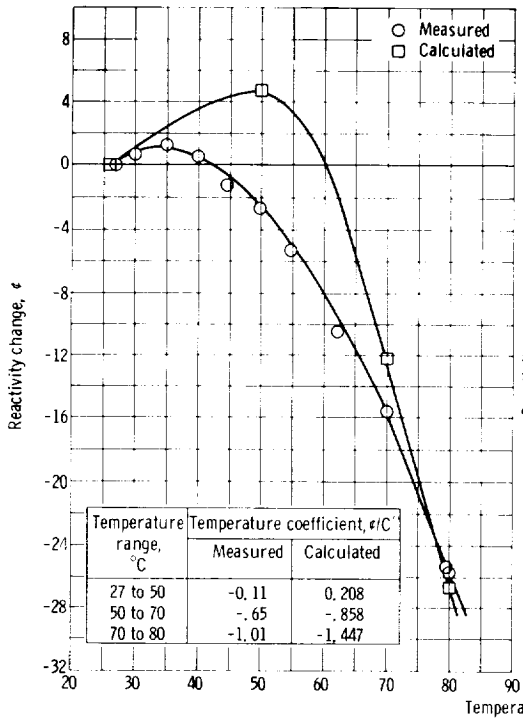

(a) 7.62-Centimeter-pitch, fully water-reflected core (core I); poison tubes contain 0.1255 mole per liter $CdNO_3$.

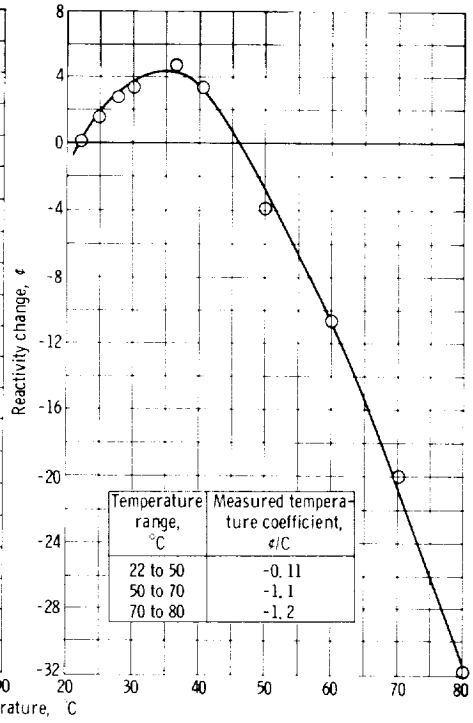

(b) 7.37-Centimeter-pitch, fully water-reflected core (core II); poison tubes contain 0.043 mole per liter $CdNO_3$.

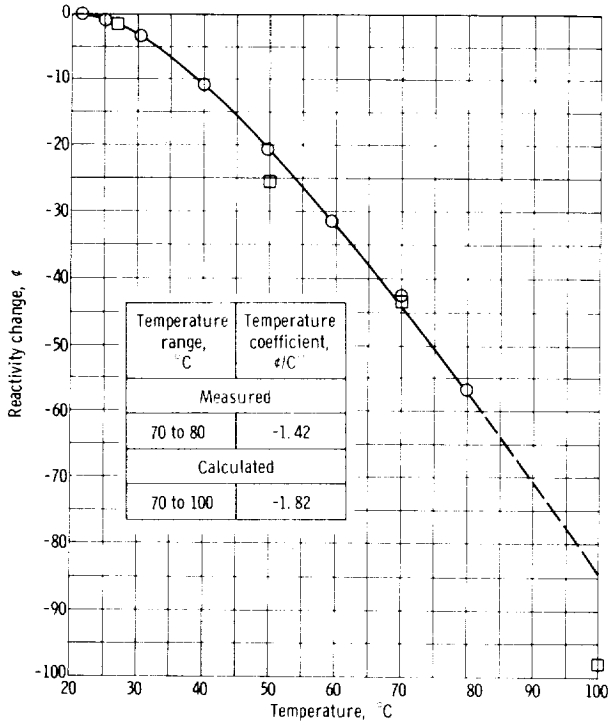

(c) 7.62-Centimeter-pitch, beryllium-reflected, unzoned core (core IV); poison tubes contain 0.2202 mole per liter $CDNO_3$.

Figure 8. - Isothermal temperature defect.

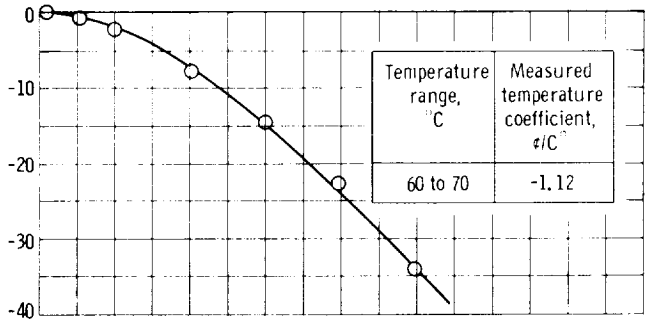

(d) 7.62-Centimeter-pitch, beryllium-reflected, radially zoned, core (core V); poison tubes contain 0.1704 mole per liter $CdNO_3$.

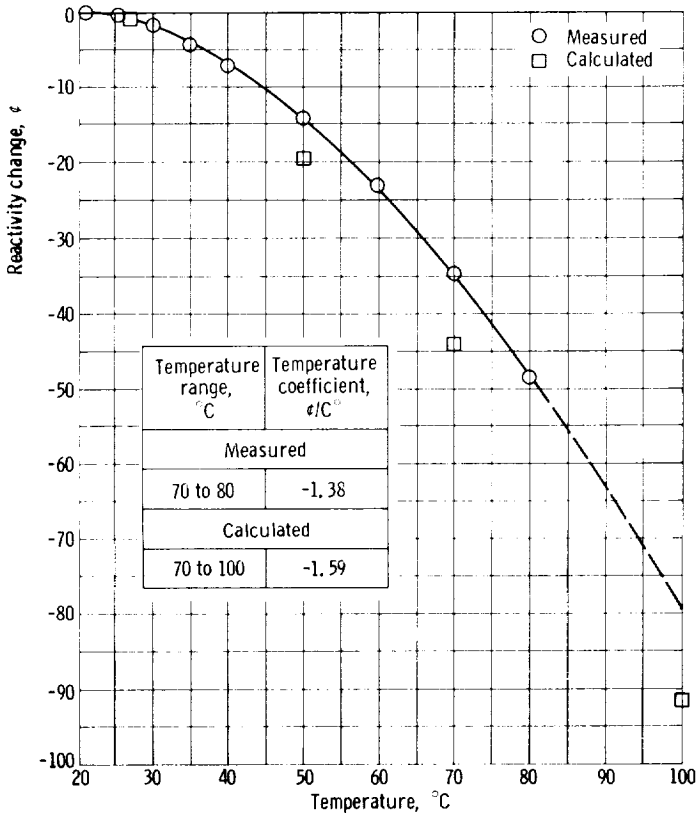

(e) 7.62-Centimeter-pitch, beryllium-reflected, fully zoned core (core VI); poison tubes contain 0.1278 mole per liter $CdNO_3$.

Figure 8. - Concluded.

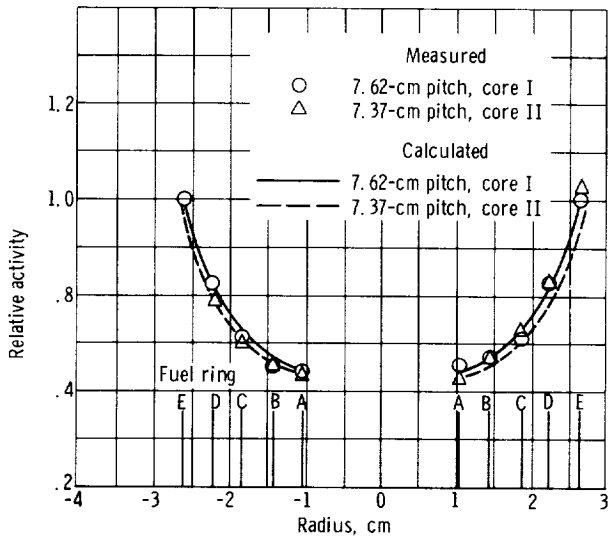

Figure 9. - Power distribution in central mockup fuel element of indicated lattice.

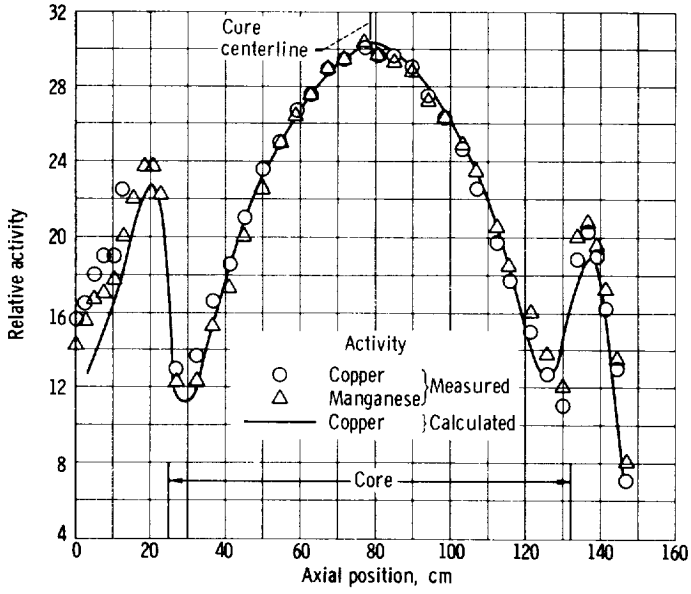

Figure 10. - Comparison of measured and calculated copper activation in axial direction in 121-mockup-element, 7.62-centimeter-pitch, water-reflected core (core I).

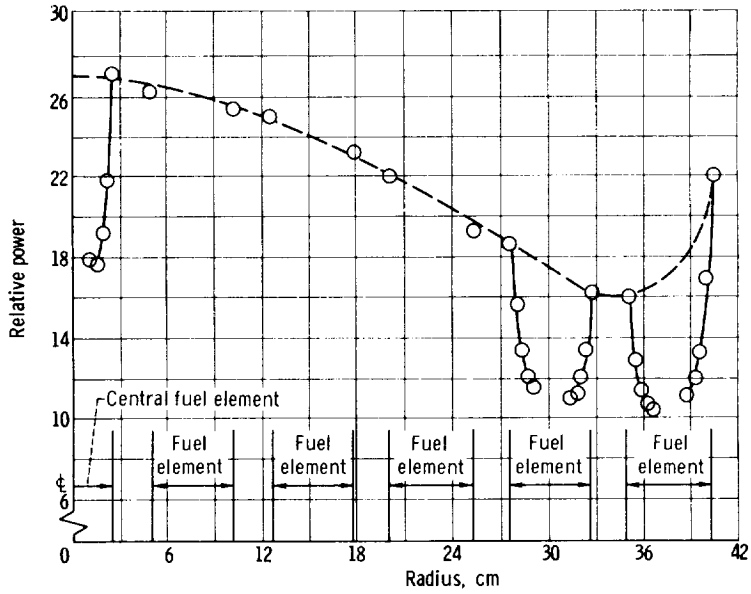

Figure 11. - Measured radial power distribution for 7.62-centimeter-pitch, 121-fuel-element, water-reflected core (core I).

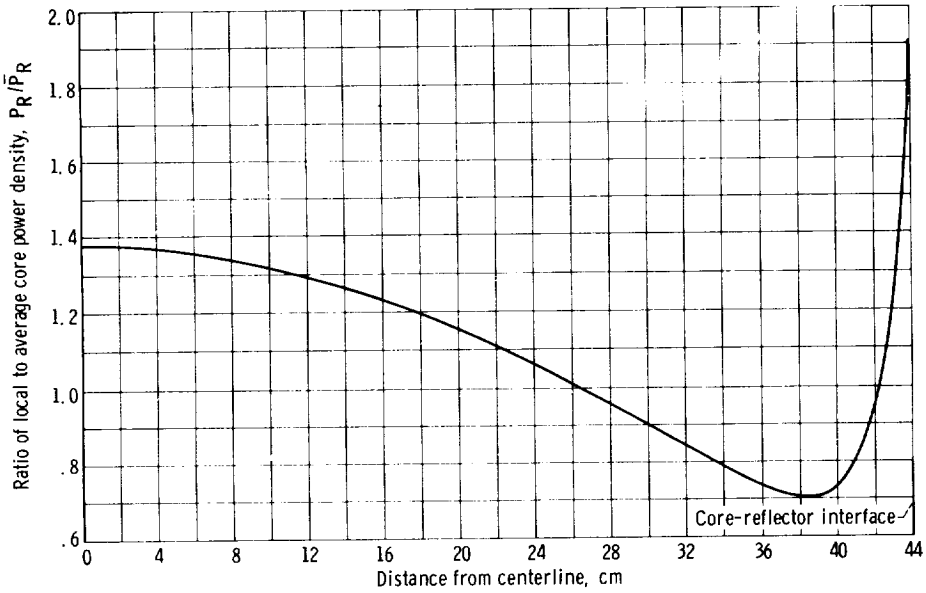

Figure 12. - Calculated one-dimensional radial power traverse for 7.62-centimeter-pitch, water-reflected core.

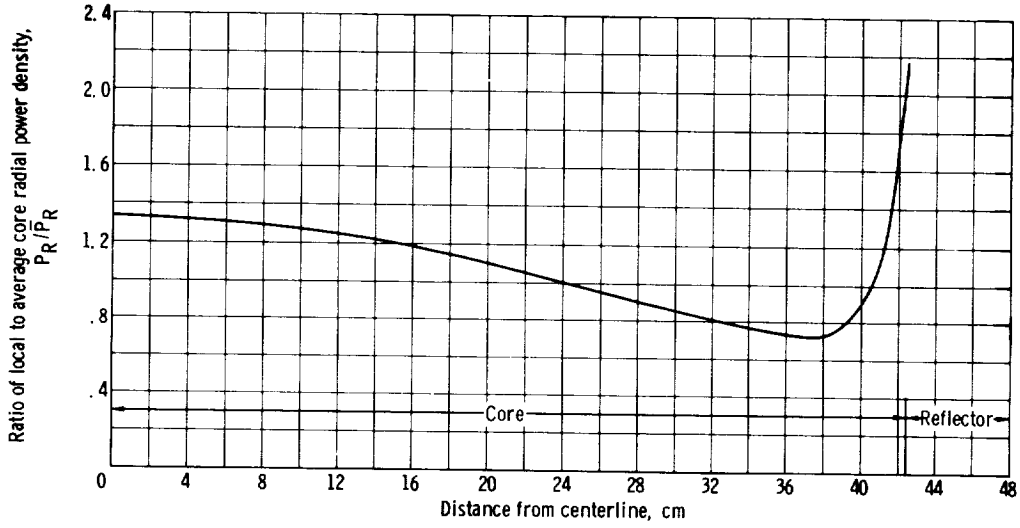

(a) Radial power distribution.

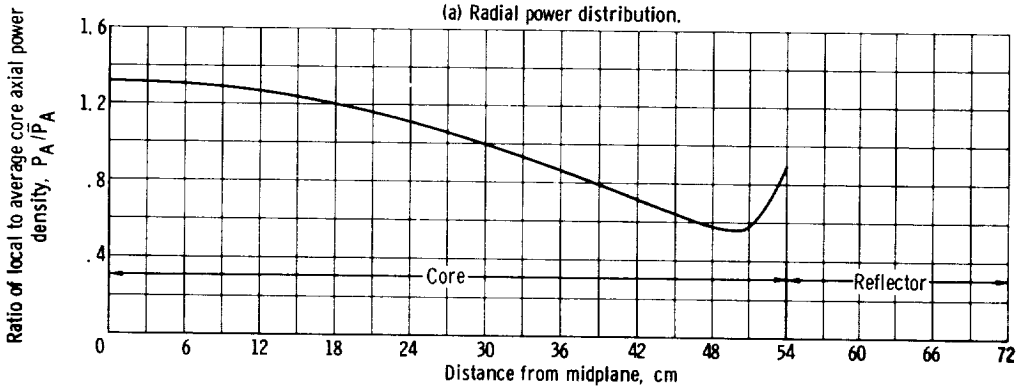

(b) Axial power distribution.

Figure 13. - Calculated power distribution for 7.37-centimeter-pitch core (core II).

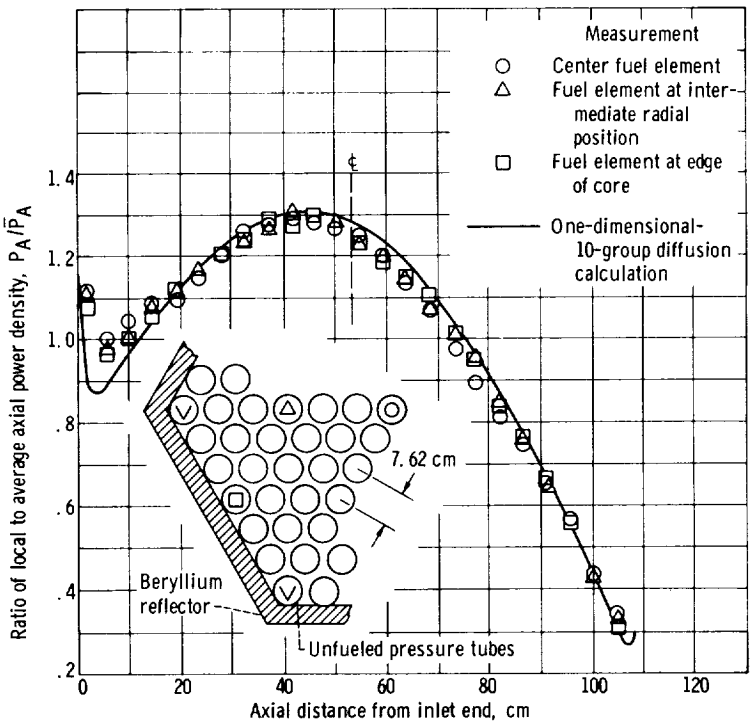

Figure 14. - Comparison of measured and calculated axial power distribution in 7.62-centimeter-pitch, beryllium-reflected core (core IV).

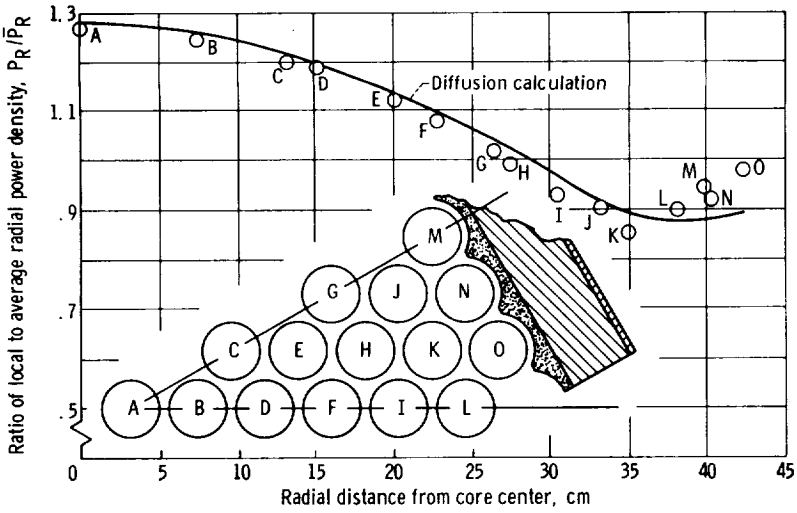

Figure 15. - Calculated and measured radial power distributions compared near midplane (stage 12) in 7.62-centimeter-pitch, beryllium-reflected core (core IV).

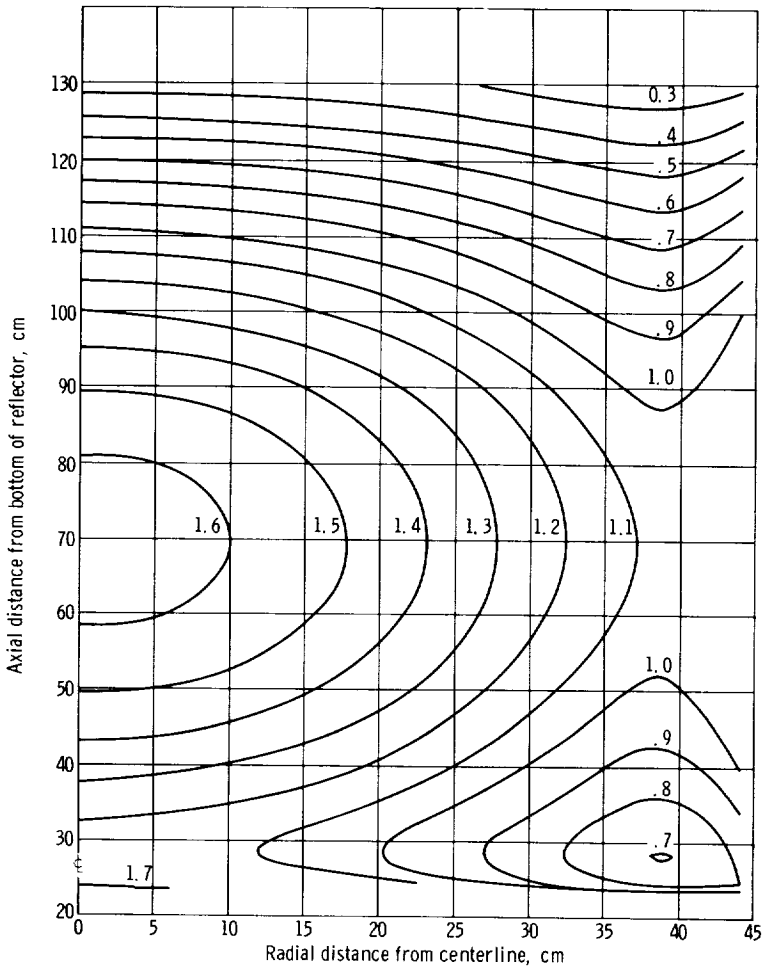

Figure 16. - Calculated ratio of local to core average isopower plot of 7.62-centimeter-pitch, beryllium-reflected core (core IV) using GAMBLE code (0.2202 mole/liter $CdNO_3$).

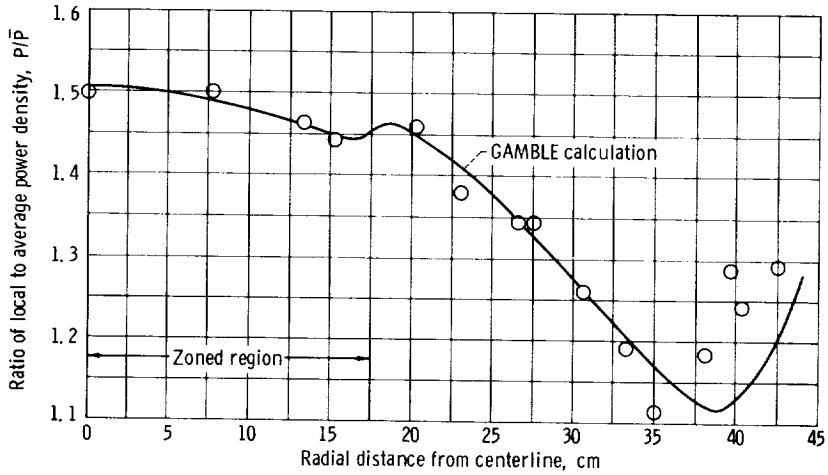

Figure 17. - Radial power traverse at core height of 46 centimeters. Comparison of experimental results with analysis for 7.62-centimeter-pitch, beryllium-reflected, radially zoned core (core V).

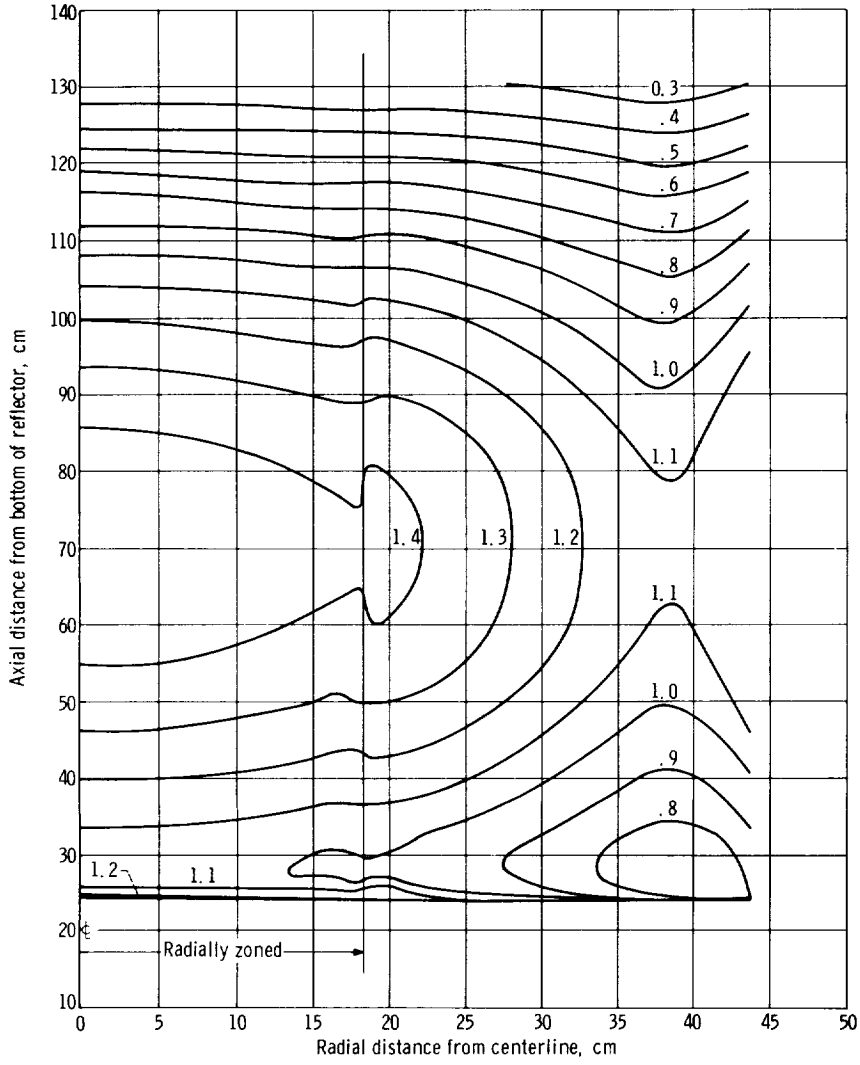

Figure 18. - Calculated local to core average isopower plot of 7.62-centimeter-pitch, radially zoned, beryllium-reflected core (core V) using GAMBLE code (0.1704 mole/liter $CdNO_3$).

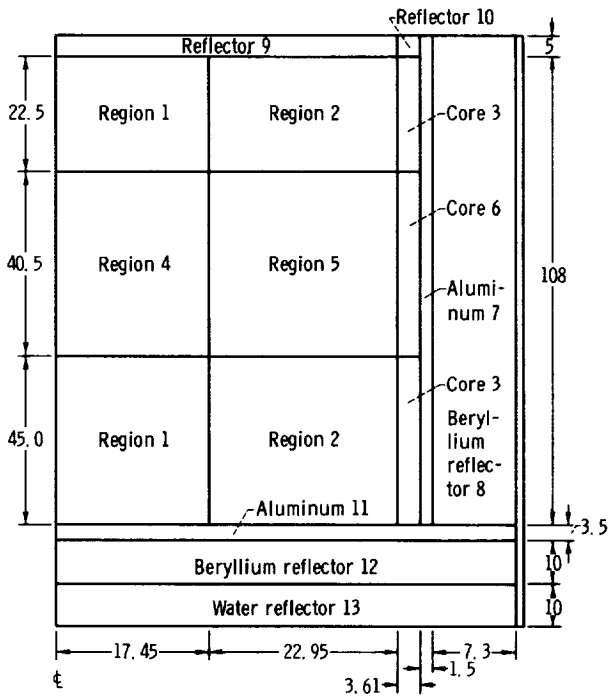

Figure 19. - Fully zoned 7.62-centimeter-pitch assembly. (All dimensions are in centimeters.)

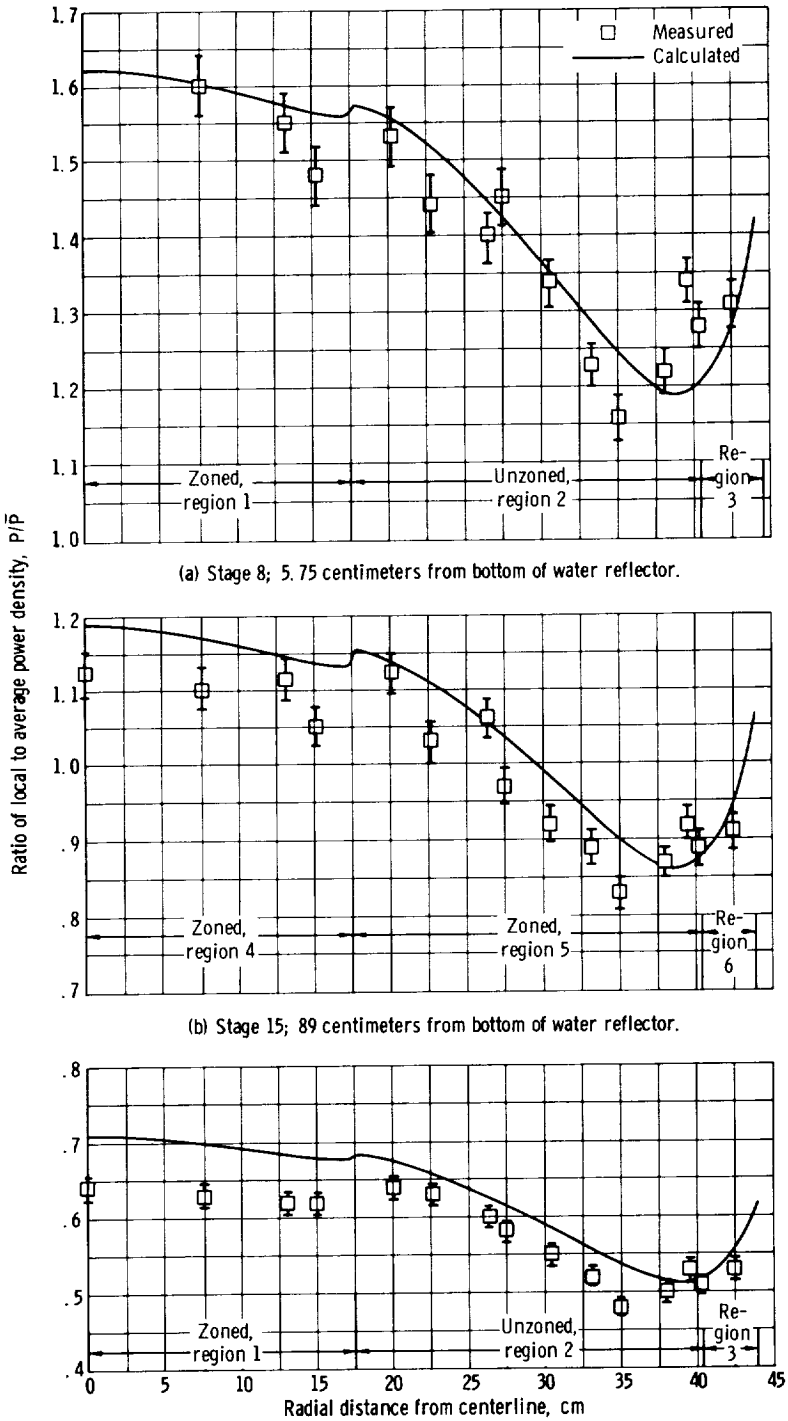

(a) Stage 8; 5.75 centimeters from bottom of water reflector.

(b) Stage 15; 89 centimeters from bottom of water reflector.

(c) Stage 21; 116 centimeters from bottom of water reflector.

Figure 20. - Radial power traverse. Comparison of measured results with calculation for 7.62-centimeter-pitch, beryllium-reflected, fully zoned core (core VI).

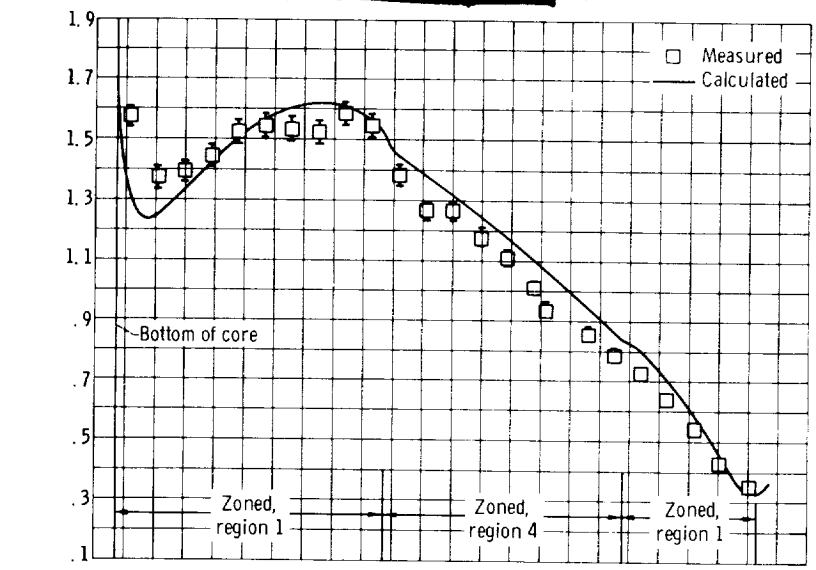

(a) Center fuel element, G-7.

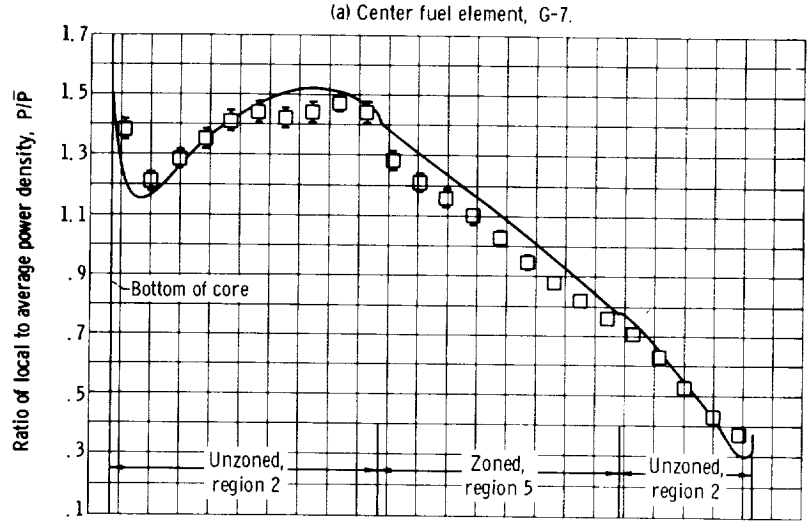

(b) Fuel element, G-4; radius, 22.86 centimeters.

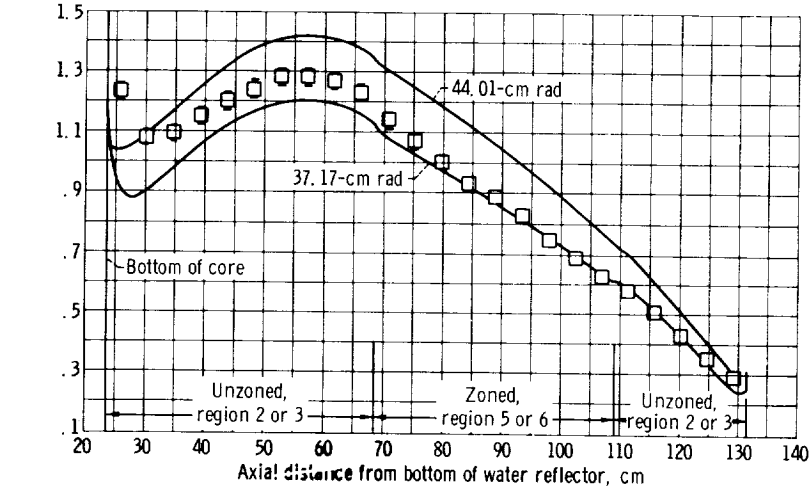

(c) Fuel element, J-1; radius, 40.32 centimeters.

Figure 21. - Axial power traverse. Comparison of measured results with calculation for 7.62-centimeter-pitch, beryllium-reflected, fully zoned core (core VI).

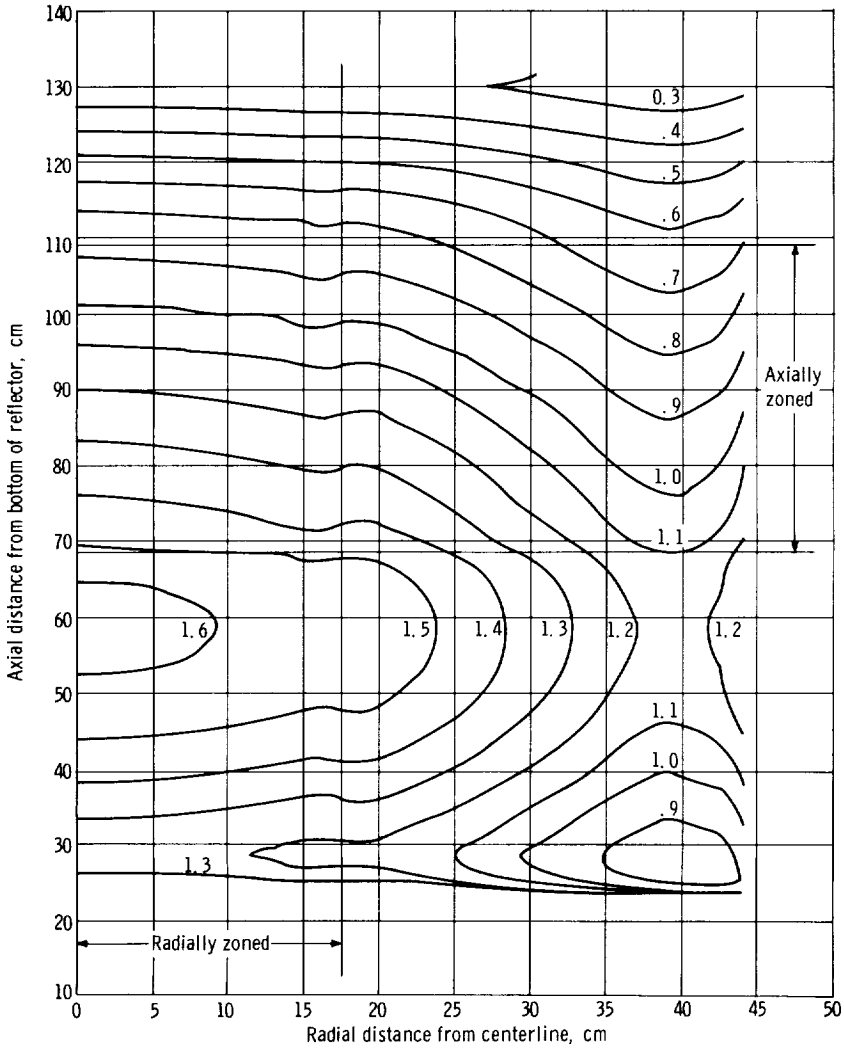

Figure 22. - Calculated local to core average isopower plot of 7.62-centimeter-pitch, fully zoned, beryllium-reflected core (core VI) using GAMBLE code. Poison tubes contain 0.1278 mole per liter $CdNO_3$.

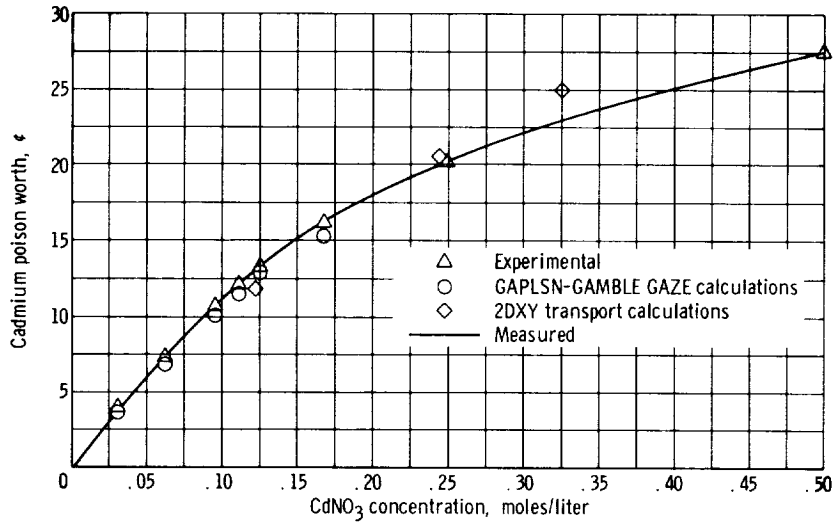

Figure 23. - Comparison of experimental and calculated center poison rod worth as function of poison concentration in 7.62-centimeter-pitch, water-reflected core (core I).

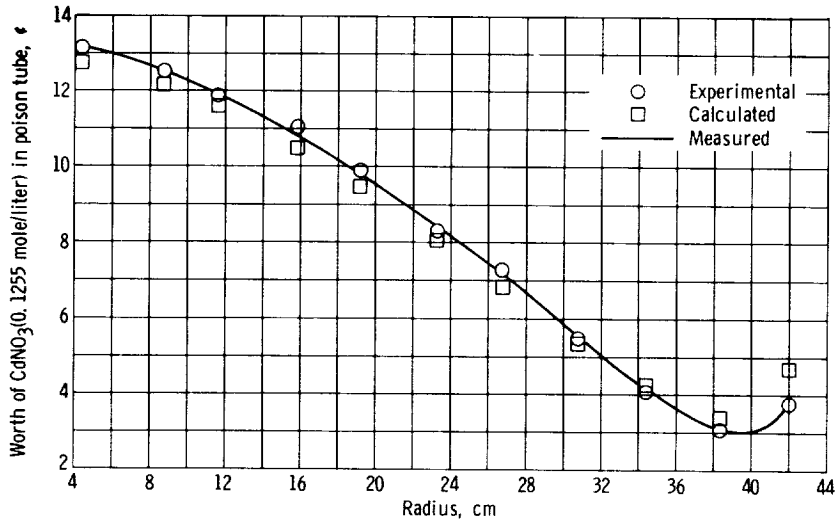

Figure 24. - Comparison of experimental and calculated poison rod worths as function of radial position in 7.62-centimeter-pitch, water-reflected core (core I).

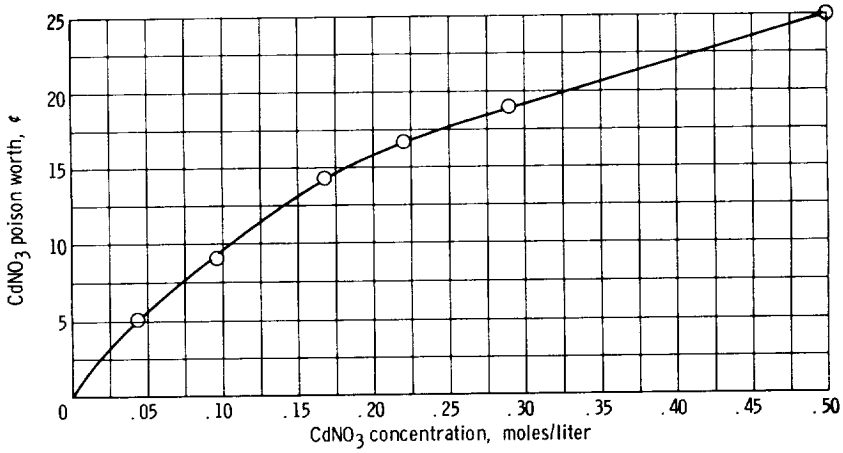

Figure 25. - Measured center poison rod worth as function of poison concentration in 7.62-centimeter-pitch, beryllium-reflected core (core IV).

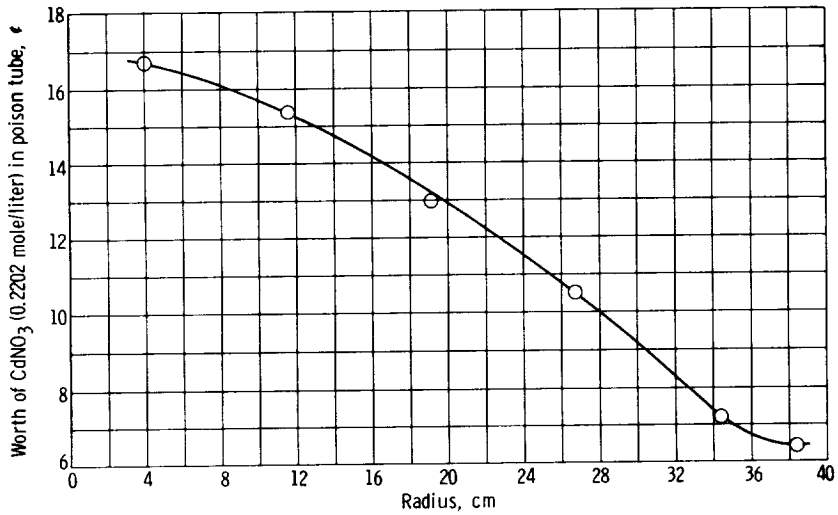

Figure 26. - Measured poison rod worths as function of radial position in 7.62-centimeter-pitch, beryllium-reflected core (core IV).

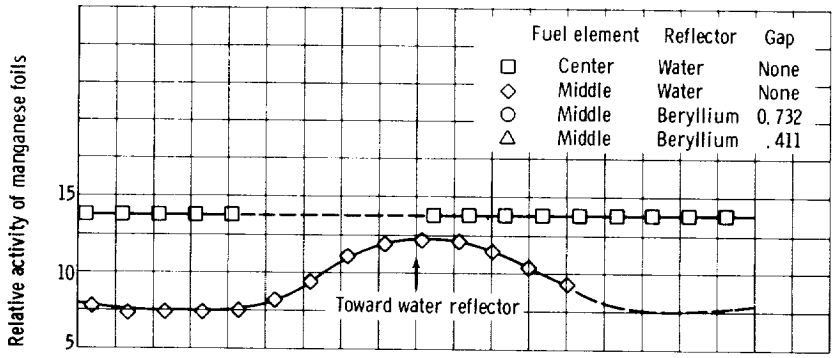

(a) Core I. 7.62-Centimeter-pitch water-reflected core.

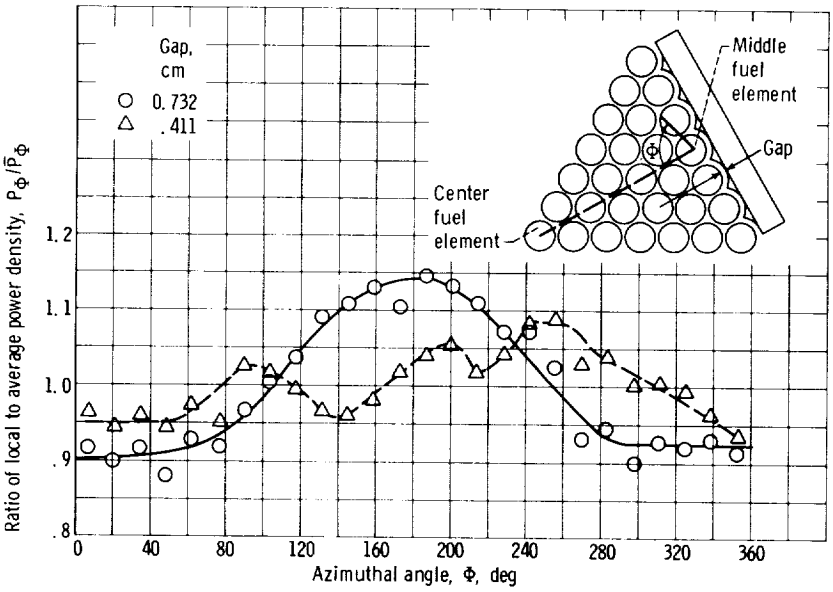

(b) Core IV. 7.62-Centimeter-pitch beryllium-reflected core.

Figure 27. - Azimuthal activation of manganese foils taped to U^{238} ring of tenth fuel stage from top of core.

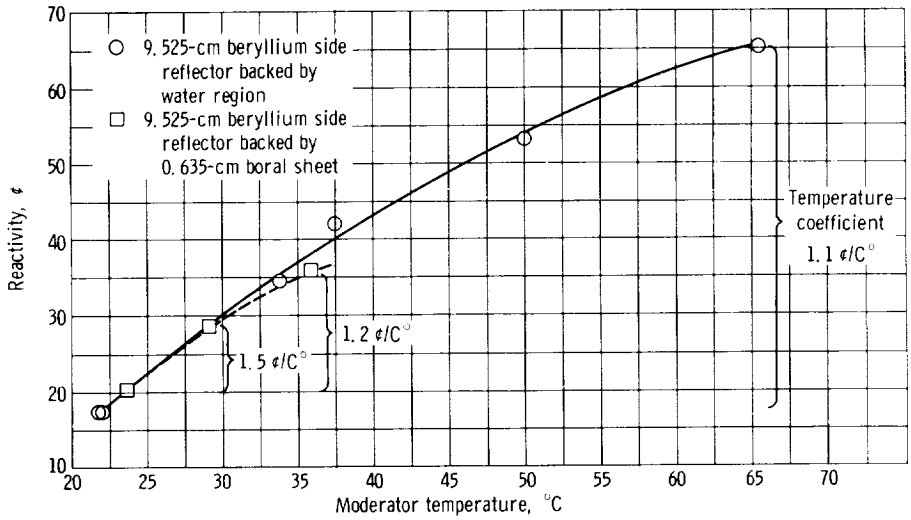

Figure 28. - Measured isothermal temperature defect in General Electric critical configuration; 37 test fuel elements; 7.87-centimeter hexagonal pitch.

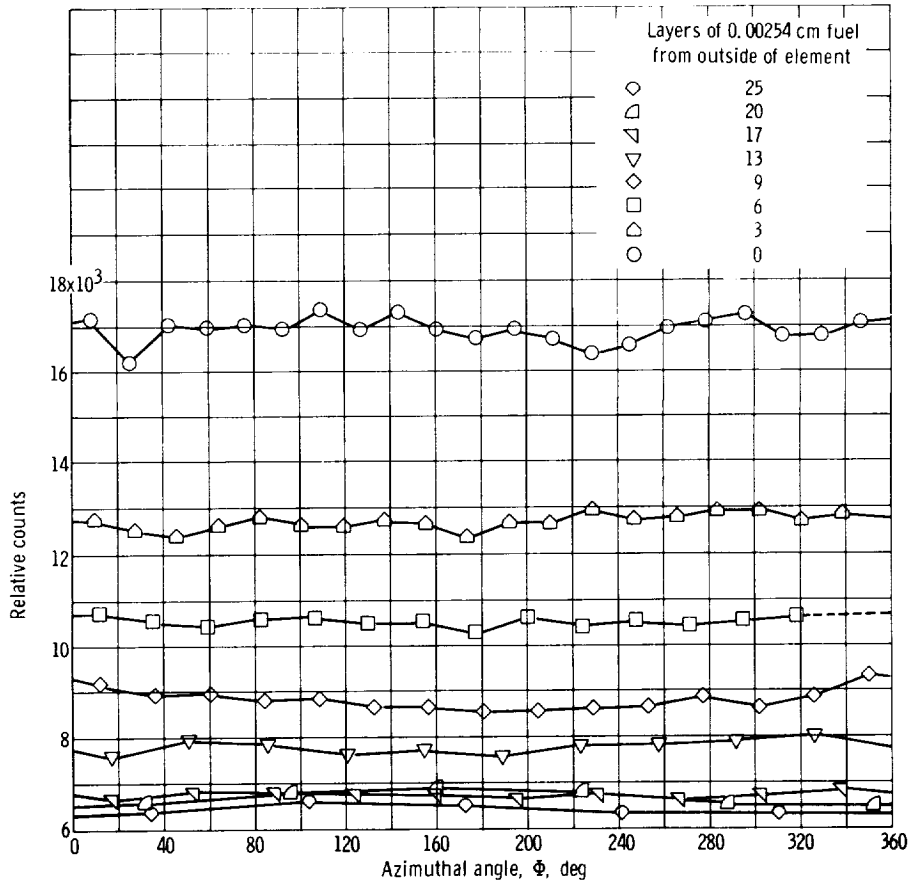

Figure 29. - General Electric central-fuel-element azimuthal power distribution. Middle stage, 65.8° C.

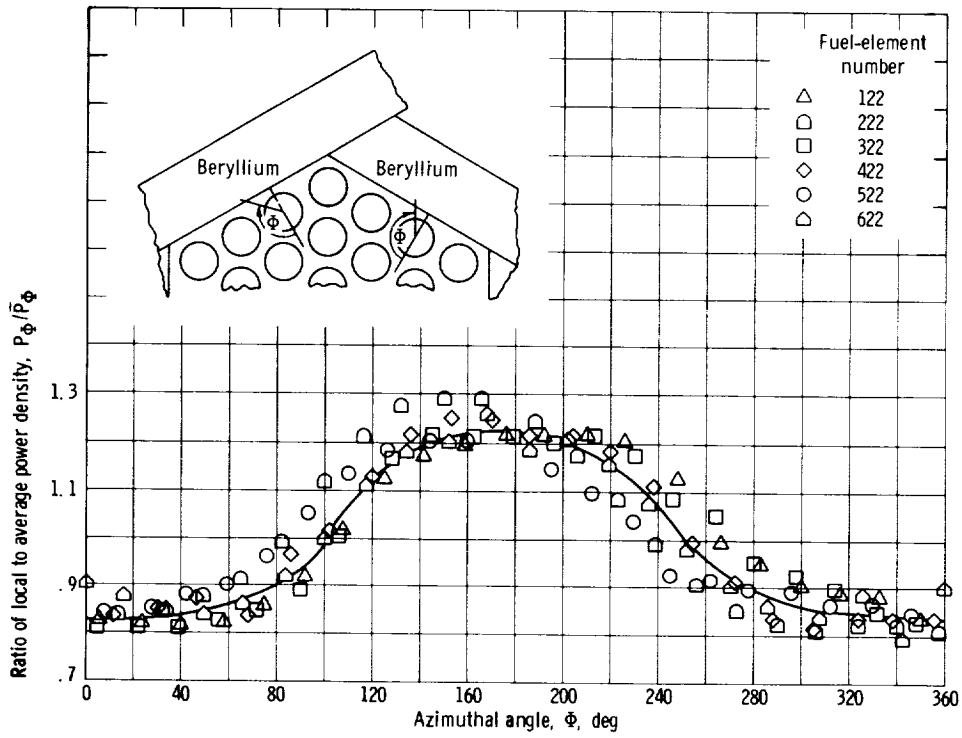

Figure 30. - Azimuthal power distribution at middle stage for outer fuel elements symmetrically located on hexagonal flat faces of 37-element core.

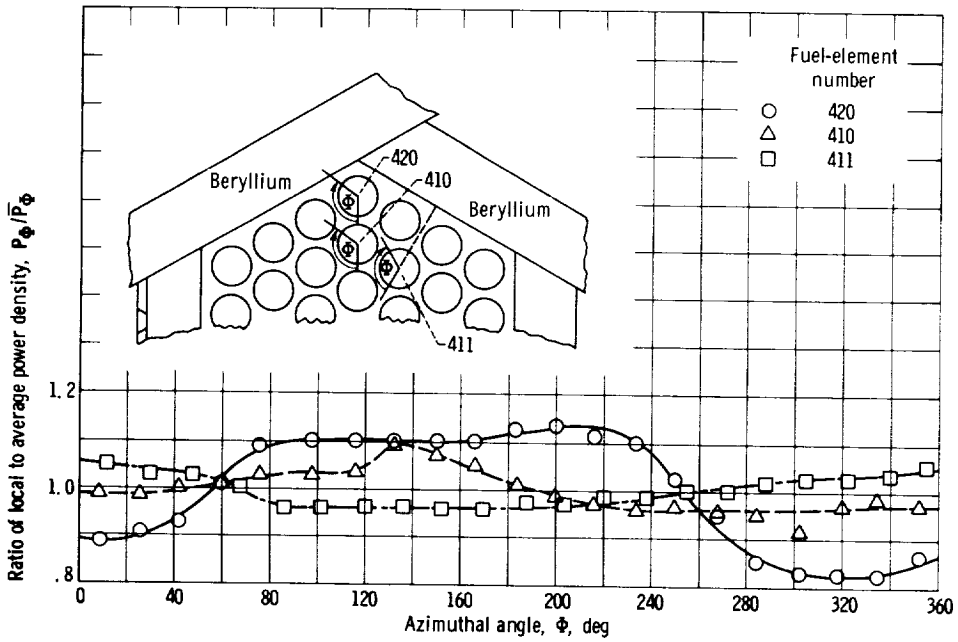

Figure 31. - Measured azimuthal power distribution for indicated fuel elements in 37-element core at middle stage.

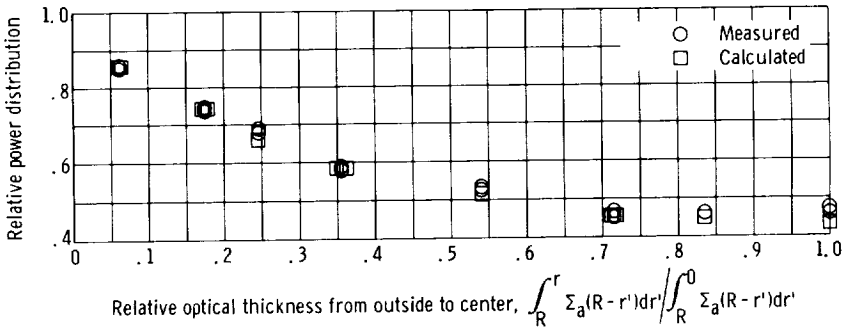

Figure 32. - Power distribution at 25° C within center of fuel element of 37-element insert in General Electric 630-A core.

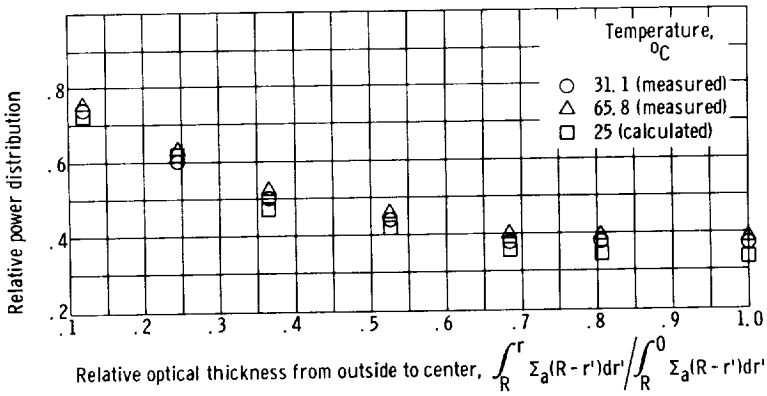

Figure 33. - Power distribution within center fuel element of General Electric 37-fuel-element mockup core.

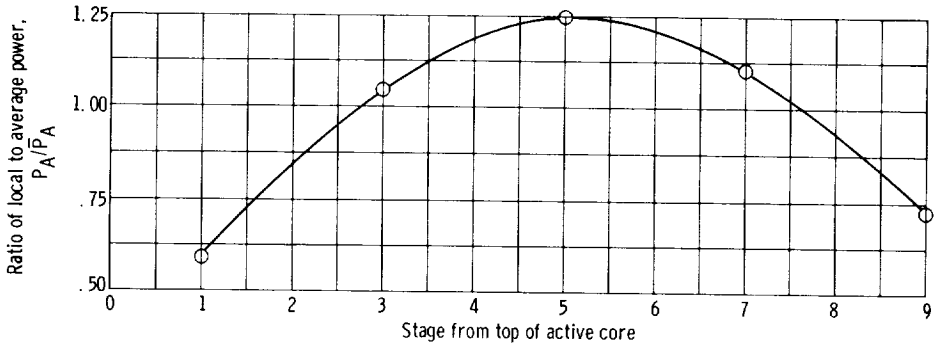

Figure 34. - Measured axial power distribution in center fuel element of 37-fuel-element core.

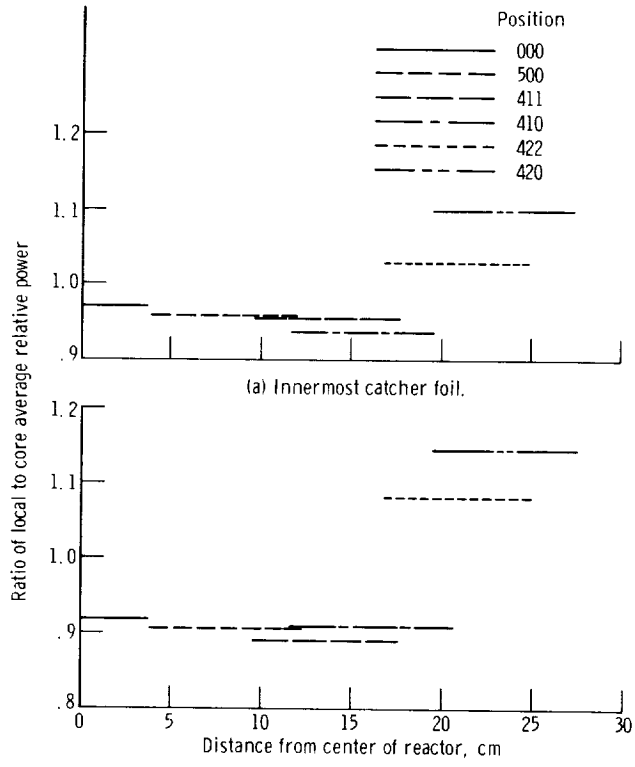

(a) Innermost catcher foil.

(b) Outermost catcher foil.

Figure 35. - Radial power distribution for General Electric 37-test-element critical configuration.

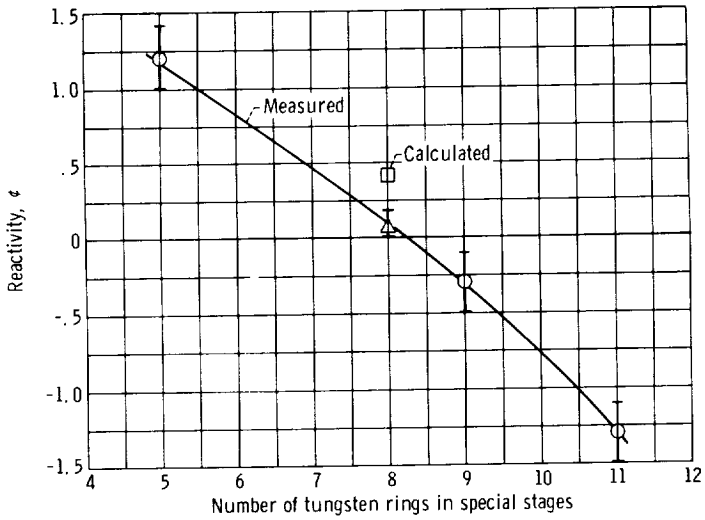

Figure 36. - Difference in reactivity on replacement of five central mockup stages with five special reference stages indicated (core IV).

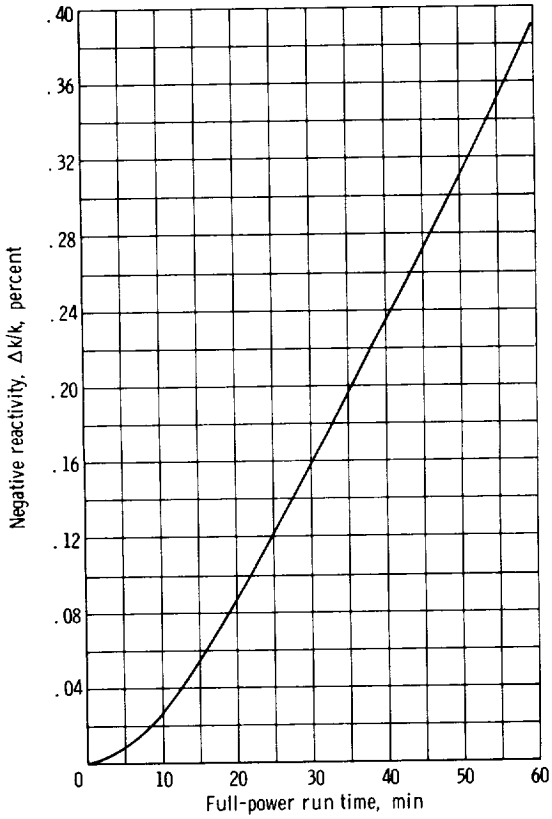

Figure 37. - Loss in reactivity due to xenon poisoning during run at full power. (Equilibrium xenon is 4.8 percent and is reached at 40 hr of full-power operation. Operating conditions: thermal flux, 8.7×10^{14} cm^{-2} sec^{-1}; power density in fuel, 7.14 MW/liter; thermal fission factor, 0.8; both xenon and iodine concentrations are zero at time zero.)

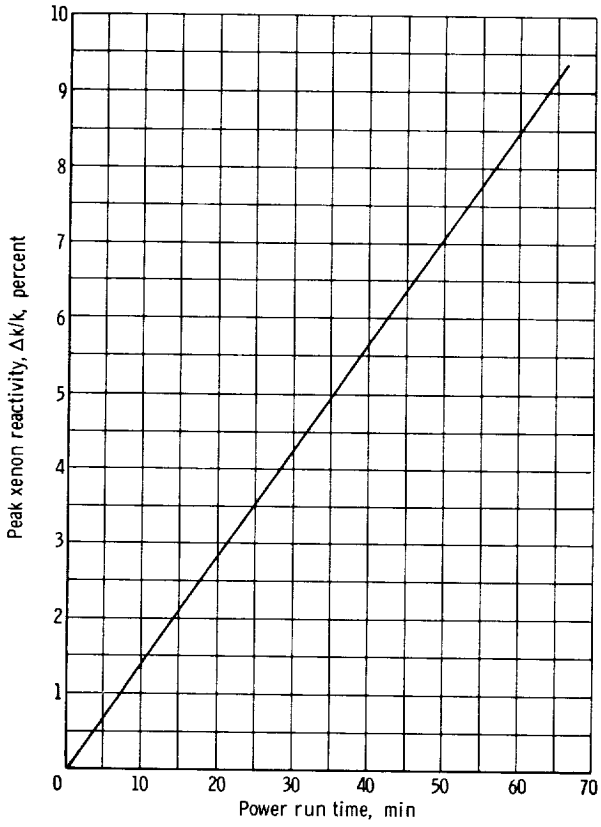

Figure 38. - Approximate reactivity required for peak xenon override after full-power run as function of power run time.

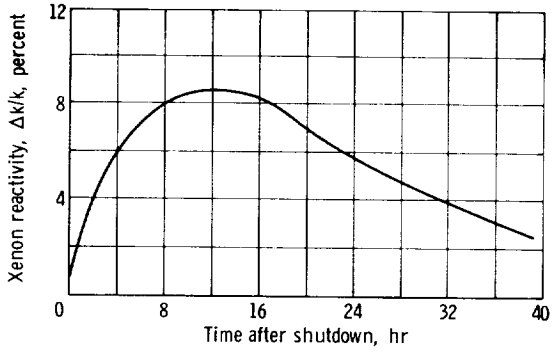

Figure 39. - Transient xenon reactivity as function of time after shutdown from 1-hour power run. (Operating conditions: power density in fuel, 7.14 MW/liter; thermal neutron flux, 8.7×10^{14} cm^{-2} sec^{-1}.)

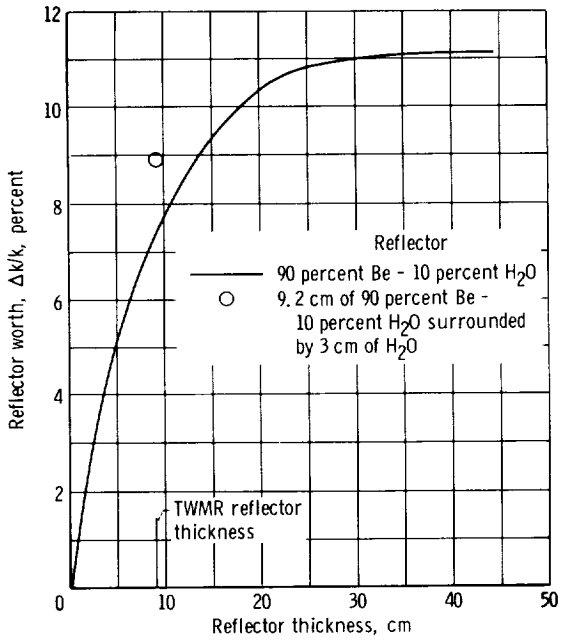

Figure 40. - Reflector worth as function of thickness for 121-fuel-element assembly, 7.8-centimeter-pitch core.

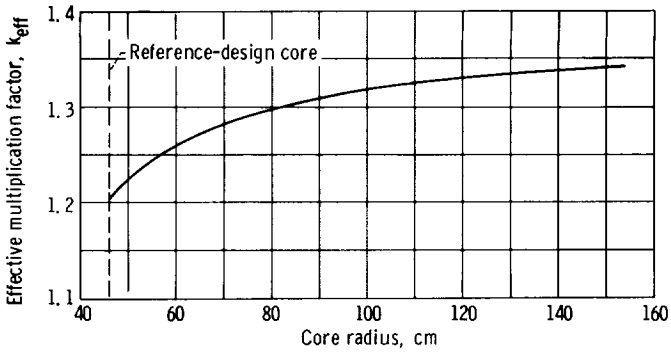

Figure 41. - Variation of reactivity with core radius for 7.87 centimeter-pitch and 6.35-centimeter-thick 90-percent-beryllium - 10-percent-water reflector.

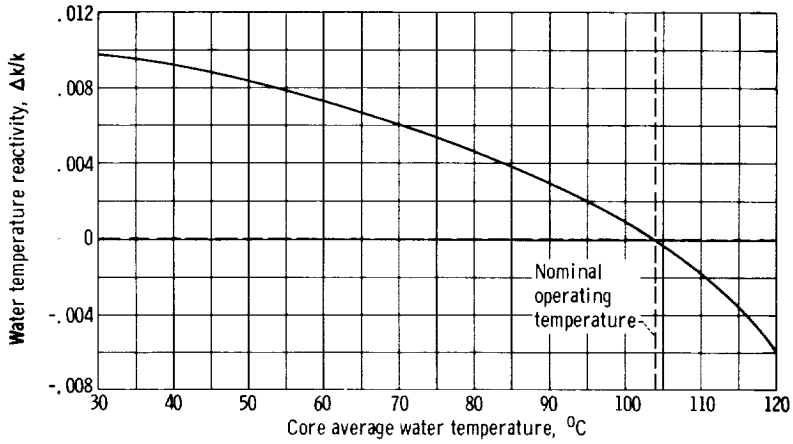

Figure 42. - Change in reactivity of TWMR with core average water temperature.

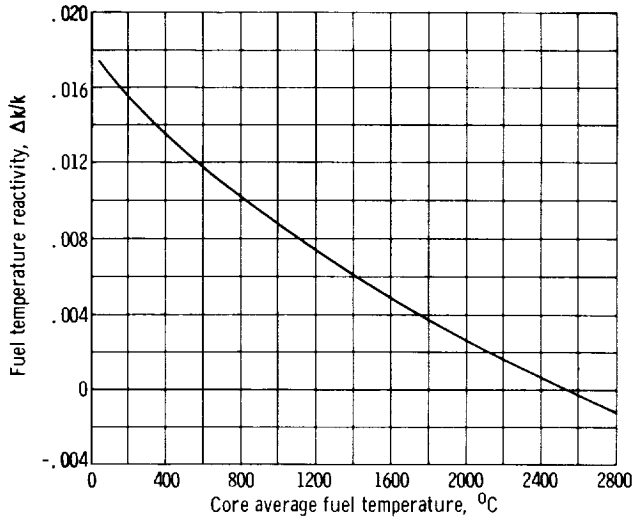

Figure 43. - Change in reactivity of TWMR with core average fuel temperature. Core water temperature, 100° C.

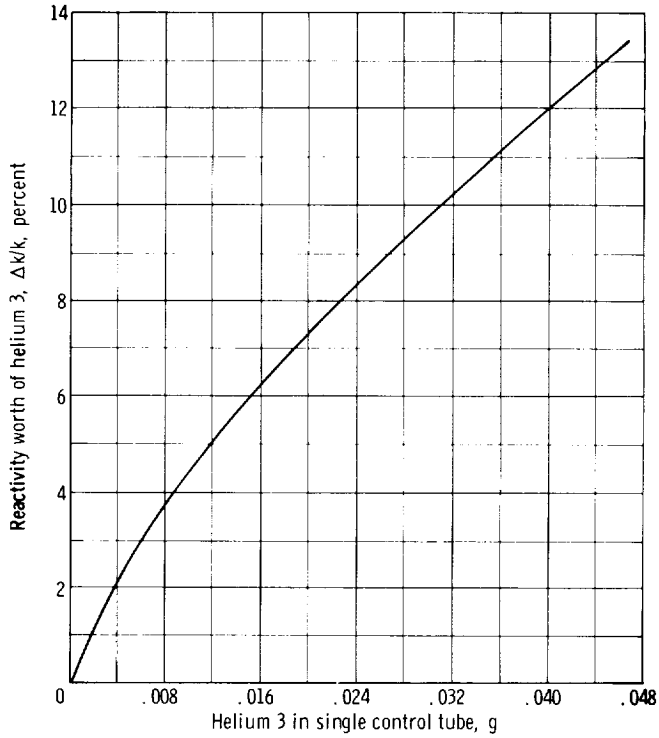

Figure 44. - Typical reactivity curve for helium 3 control system (204 control tubes in reference reactor).

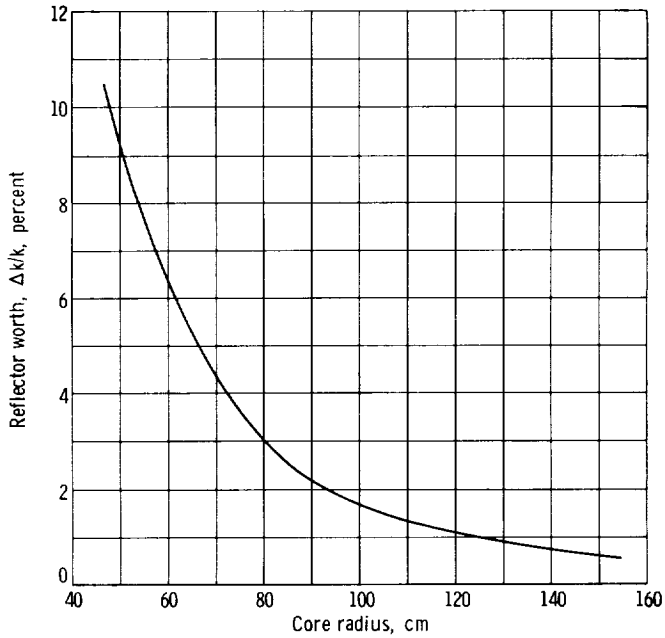

Figure 45. - Variation of reflector worth with unzoned core radius for 7.87-centimeter-pitch cell and 22.9-centimeter, 90-percent-beryllium - 10-percent-water reflector.

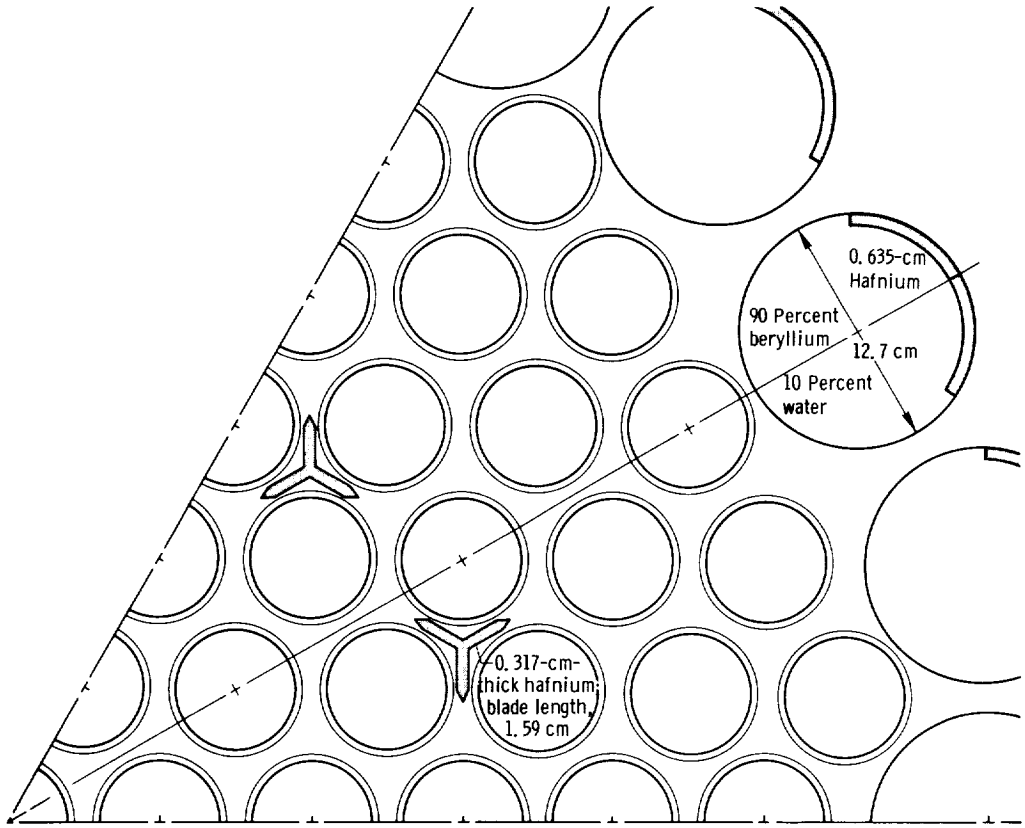

Figure 46. - Reflector-drum controlled core with supplementary interstitial control rods. (Core has twelve full-length control rods and twenty-four 12.7-cm-diam control drums. Rod control of reactivity used between shutdown and hot-critical; rods completely withdrawn from top reflector during power operation.)

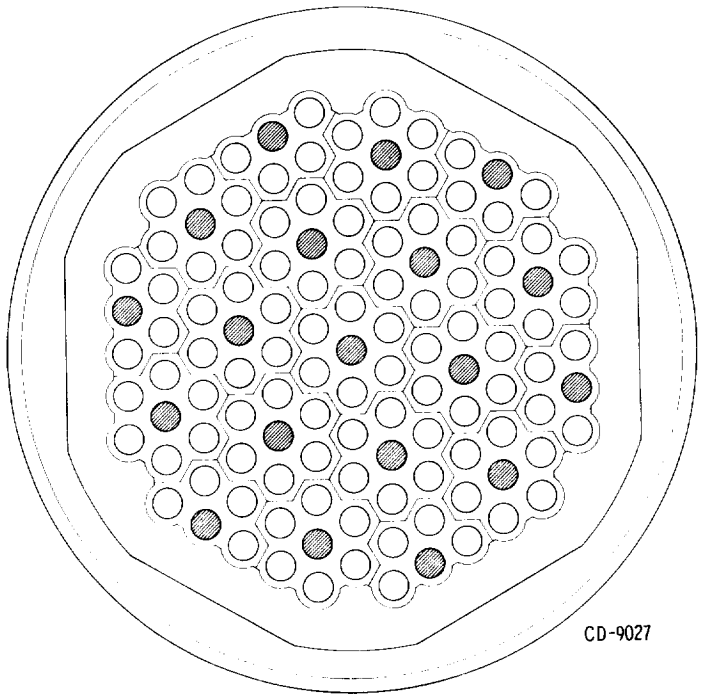

Figure 47. - Core layout with 19 control rods.

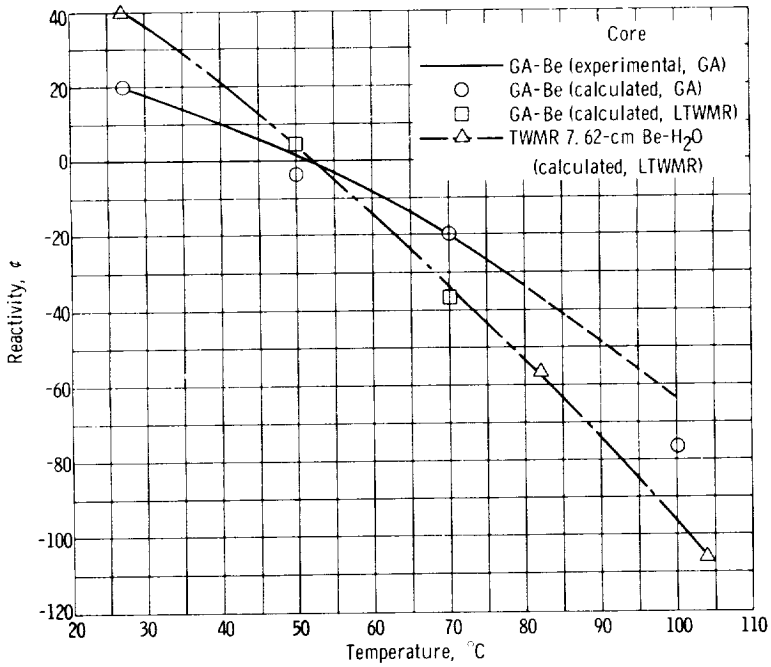

Figure 48. - Reactivity of isothermal reactors as function of temperature for General Atomic beryllium, and TWMR 7.62-centimeter beryllium-water cores. Calculations normalized at 52° C.

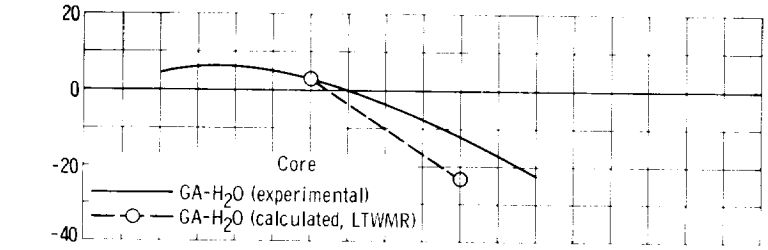

(a) General Atomic water core.

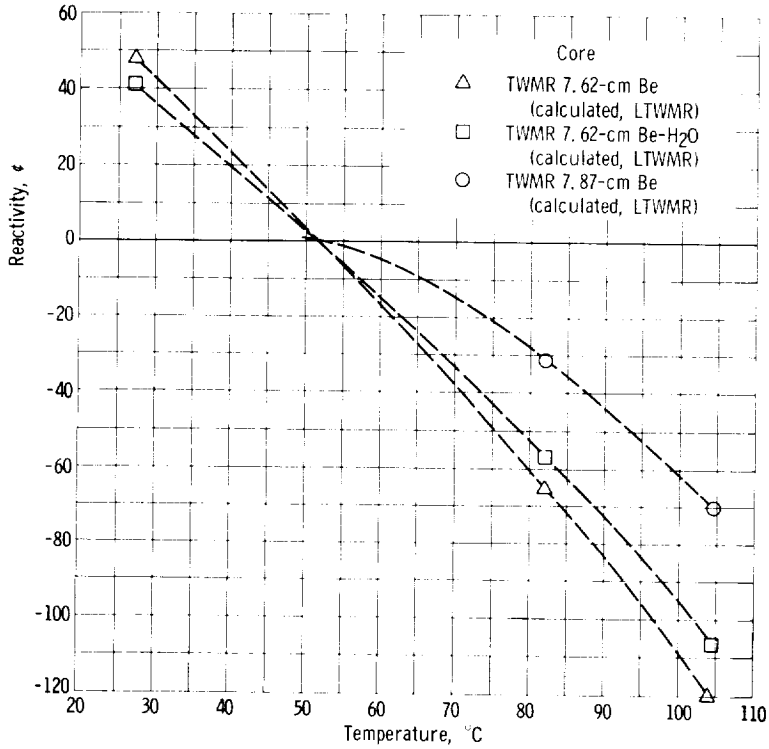

(b) TWMR 7.62-centimeter beryllium, TWMR 7.87-centimeter beryllium, and TWMR 7.62-centimeter, beryllium-water cores.

Figure 49. - Reactivity of isothermal reactor as function of temperature. Calculations normalized at 52° C.

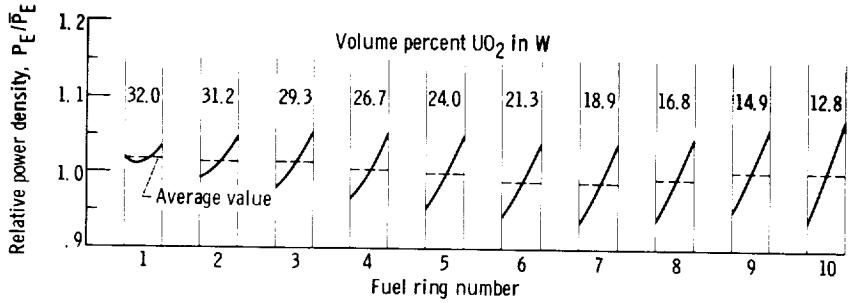

Figure 50. - Calculated radial power distribution within zoned reference-design fuel assembly; average loading, 20.28 volume percent UO_2 in W; multiplication factor of cell, 1.442; pitch, 7.87 centimeters; cell temperature, 27° C; fuel ring thickness, 0.0533 centimeter.

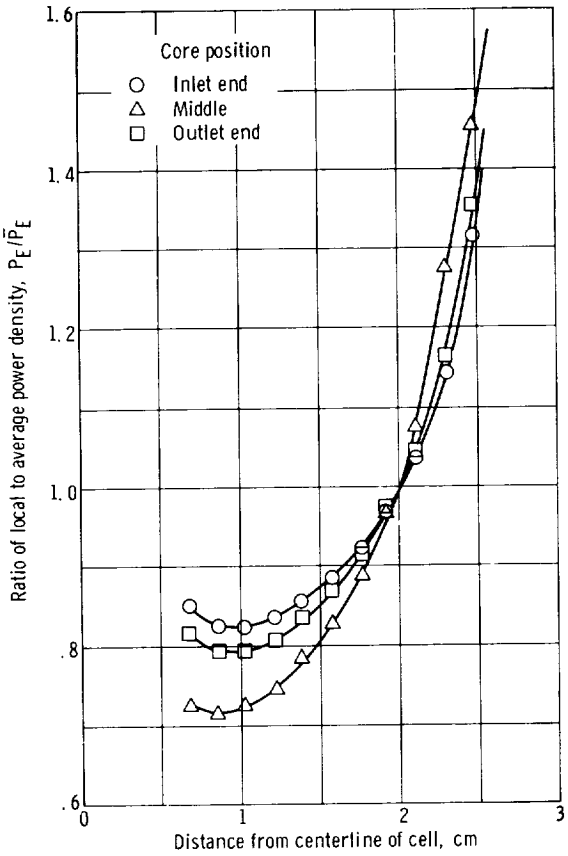

Figure 51. - Calculated radial power density distributions within fuel assembly at several axial locations.

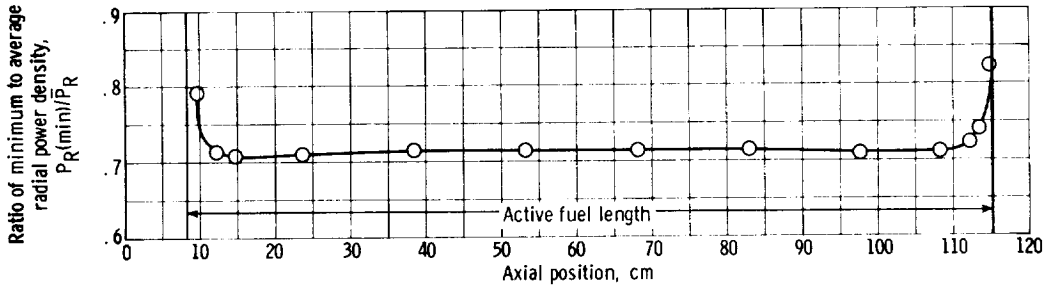

Figure 52. - Variation of fuel assembly radial power profile as function of axial position.

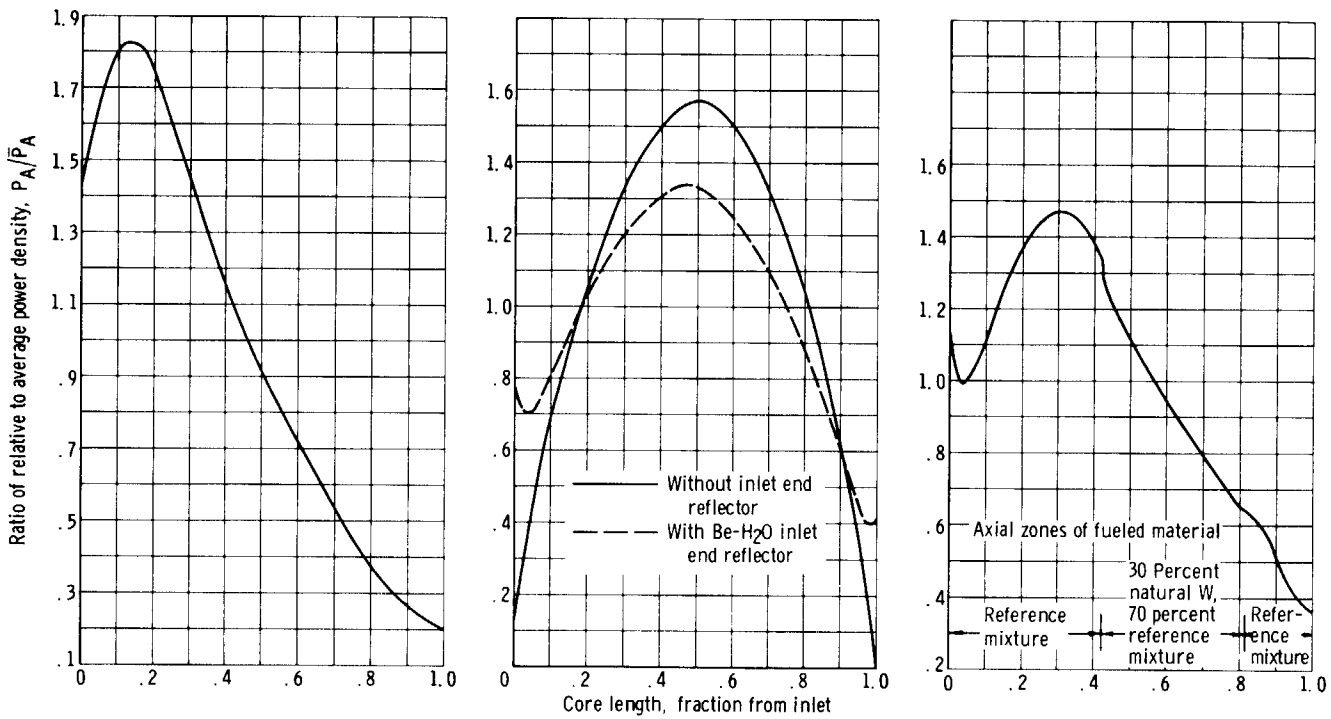

(a) Optimum.

(b) Calculated comparison of TWMR with and without inlet end reflector.

(c) Calculated with two isotopic tungsten mixtures in fuel material. Reactivity loss due to zoning, 4 percent.

Figure 53. - Axial power distribution.

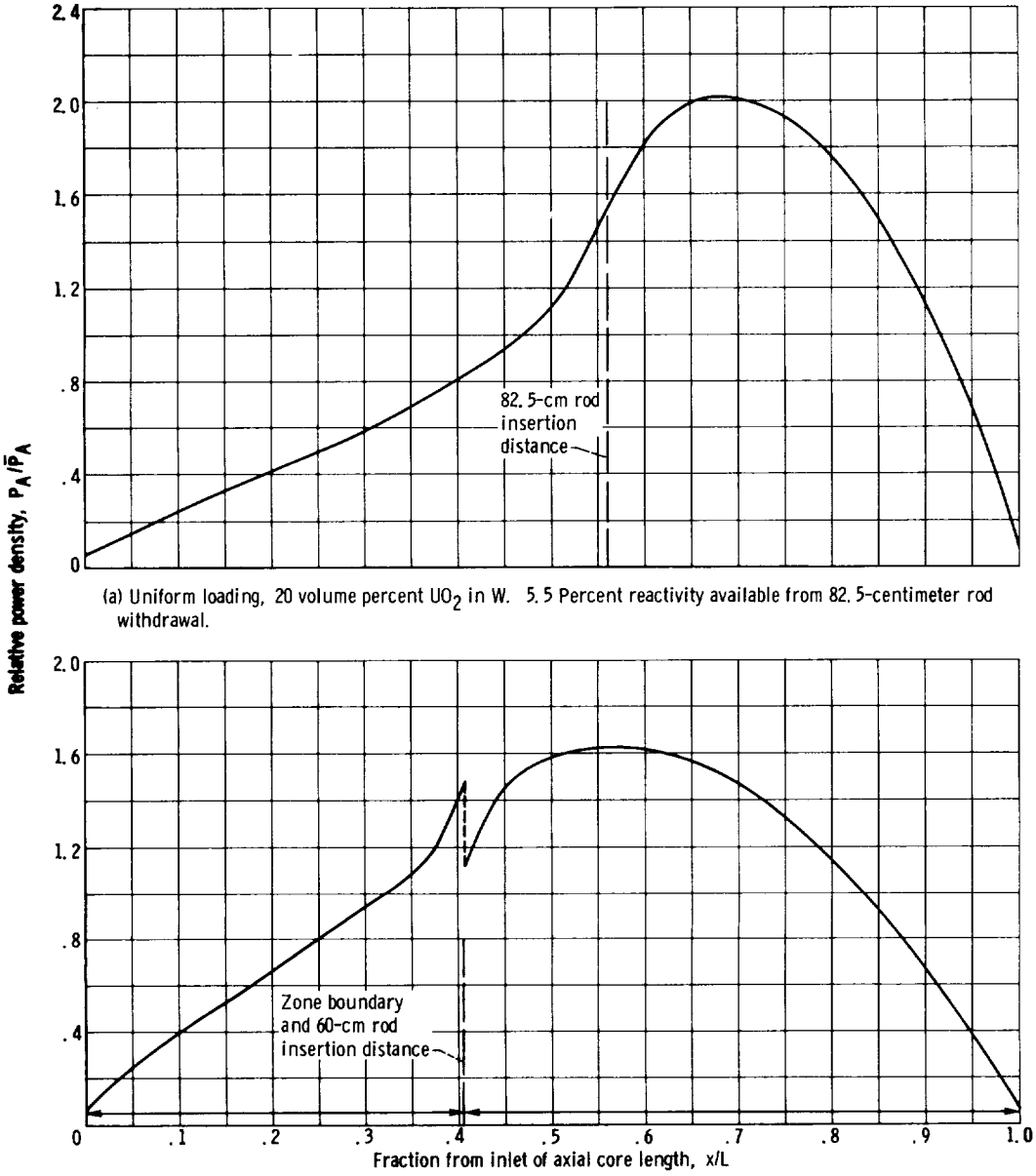

(a) Uniform loading, 20 volume percent UO_2 in W. 5.5 Percent reactivity available from 82.5-centimeter rod withdrawal.

(b) Zoned core. 4 Percent reactivity used for axial zoning, 6 percent available from 60-centimeter rod withdrawal.

Figure 54. - Calculated axial power distribution.

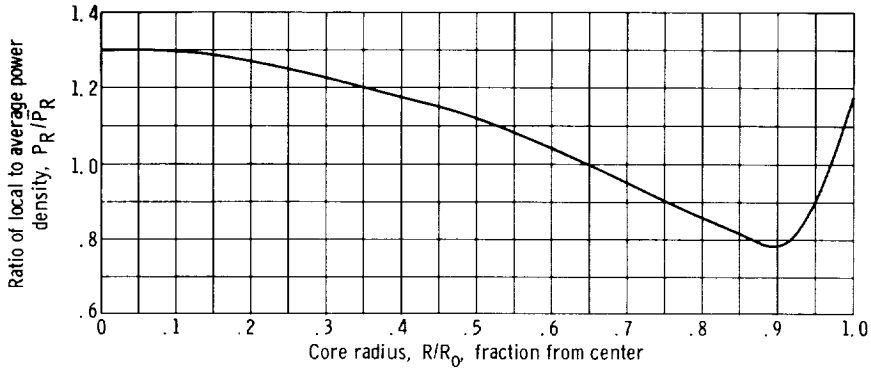

Figure 55. - Calculated gross radial power density distribution for core with 121 fuel assemblies on 8.05-centimeter pitch in hexagonal array. Unzoned core with 9.2-centimeter 0.9-beryllium 0.1-water reflector backed by 2.8 centimeters of H_2O.

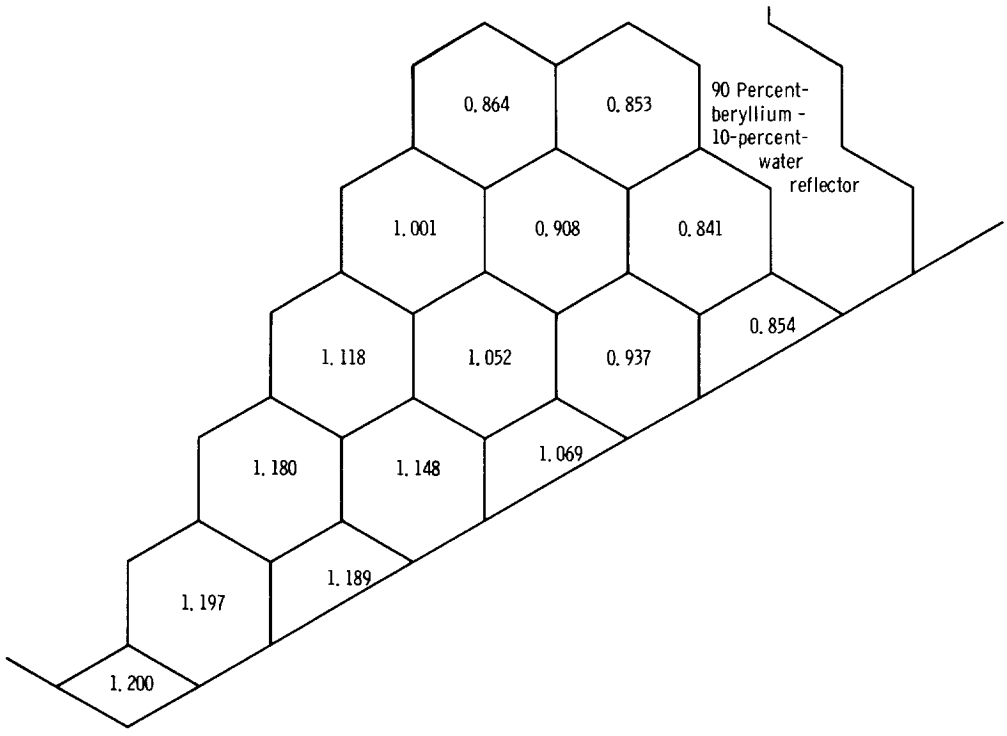

Figure 56. - Calculated gross radial power distribution for one-twelfth of symmetrical core for continuously varied resonance absorption (reference-design distribution). Values are ratios of cell center power to average gross radial power.

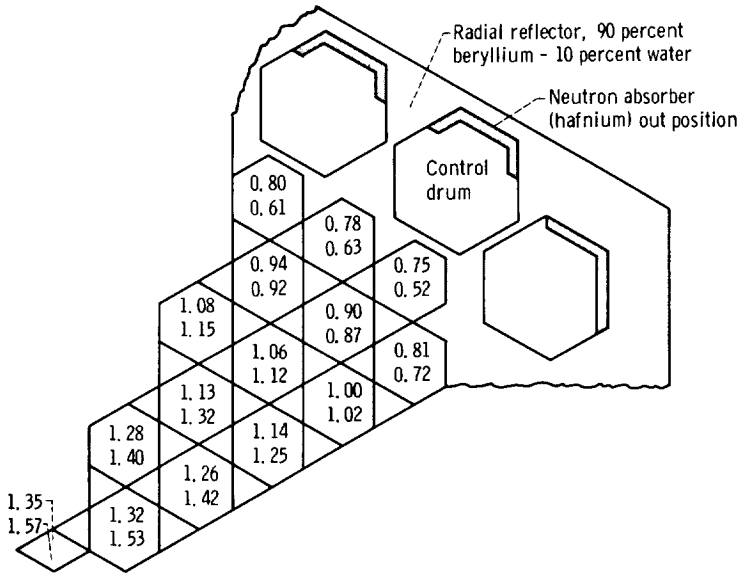

Figure 57. - Calculated gross radial power distributions with reflector control drums. Power densities of each fuel assembly shown are relative to average. Upper numbers denote drums-out position; lower numbers denote drums-in position.

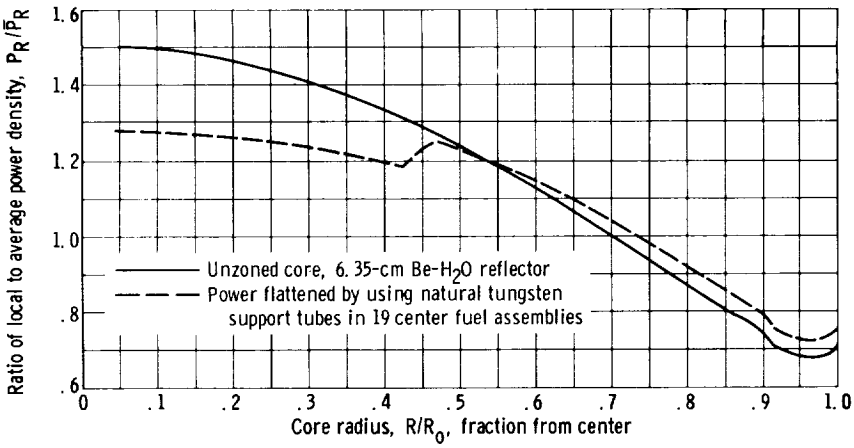

Figure 58. - Calculated gross radial power density distributions for core with 121 fuel assemblies on 8.05-centimeter pitch.

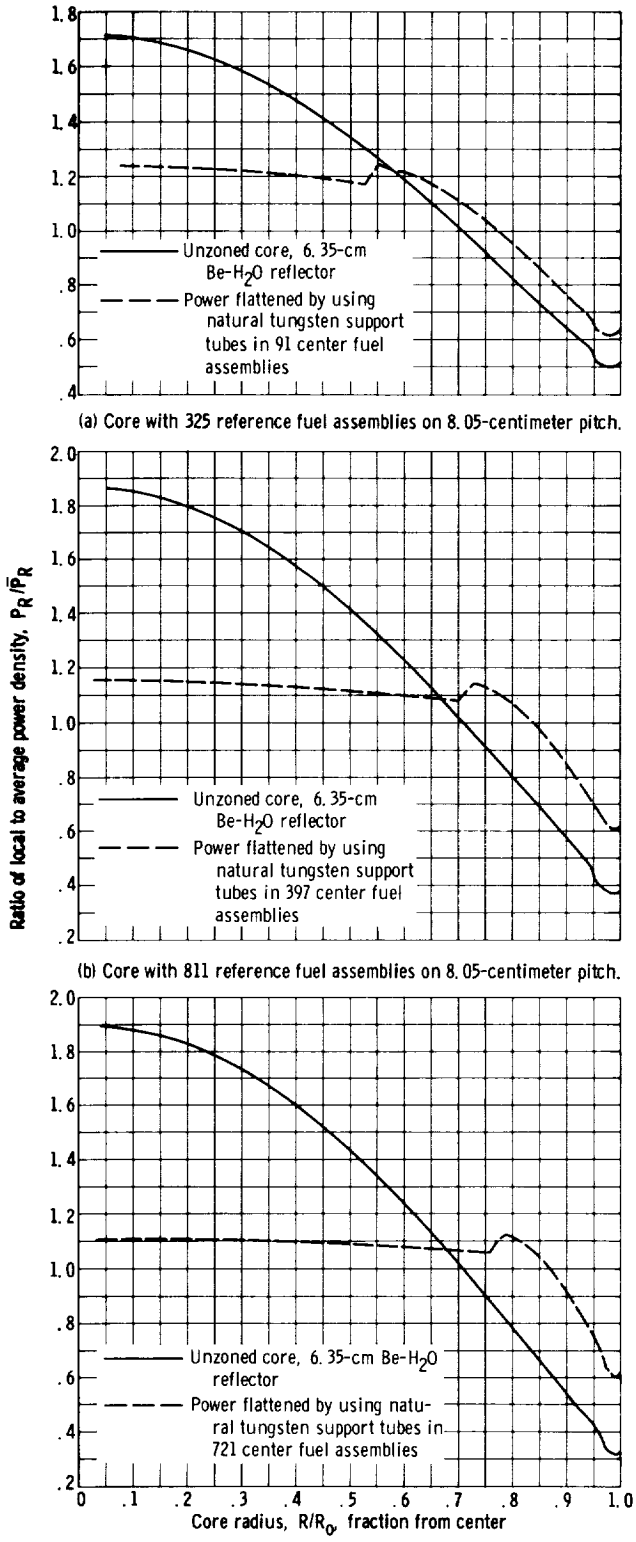

(a) Core with 325 reference fuel assemblies on 8.05-centimeter pitch.

(b) Core with 811 reference fuel assemblies on 8.05-centimeter pitch.

(c) Core with 1255 reference fuel assemblies on 8.05-centimeter pitch.

Figure 59. - Calculated gross radial power density distribution.

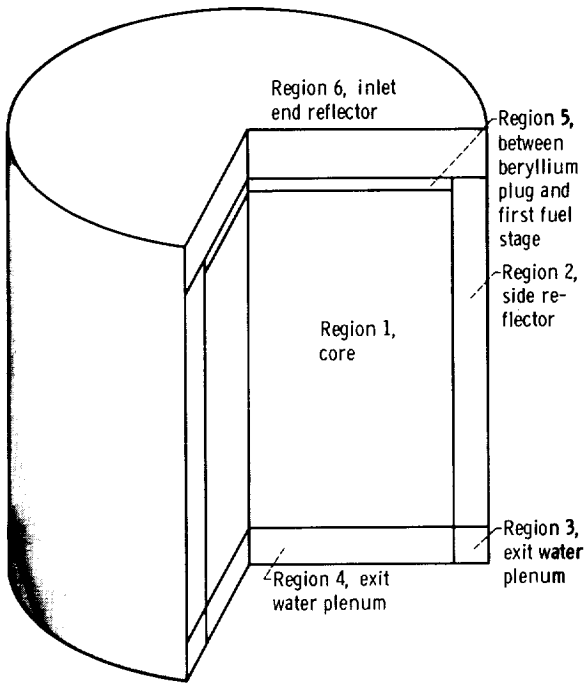

Figure 60. - Reactor representation for point kernel calculations.

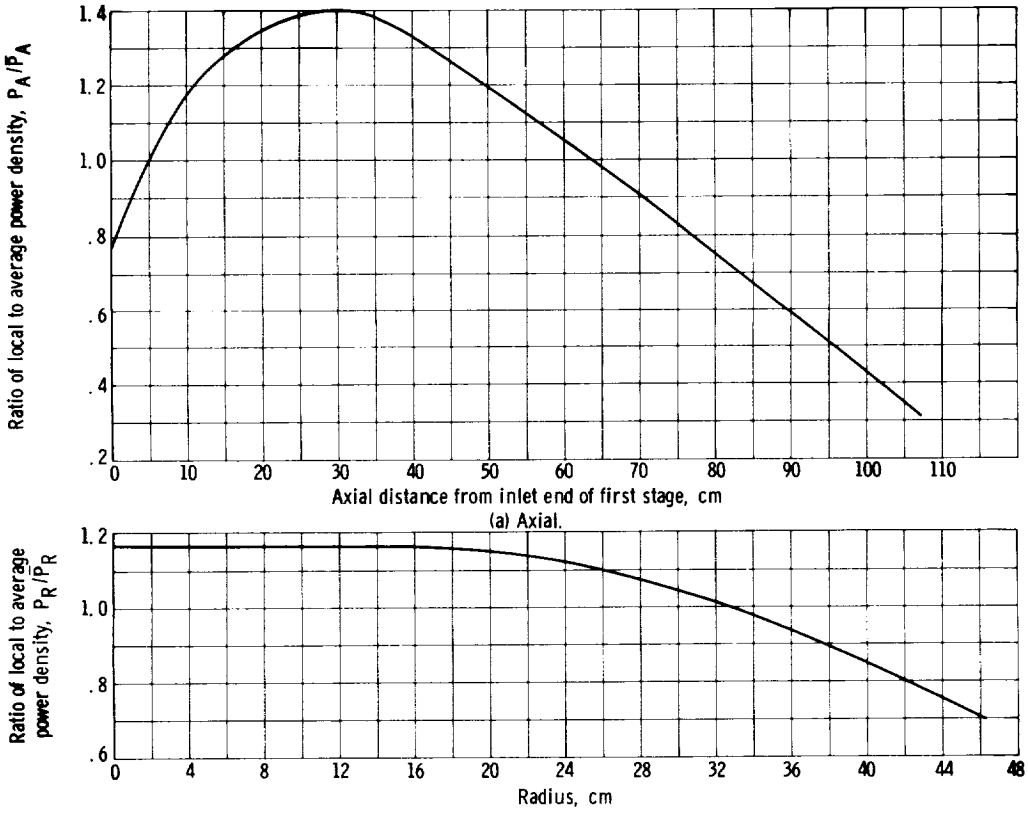

Figure 61. - Power distribution.

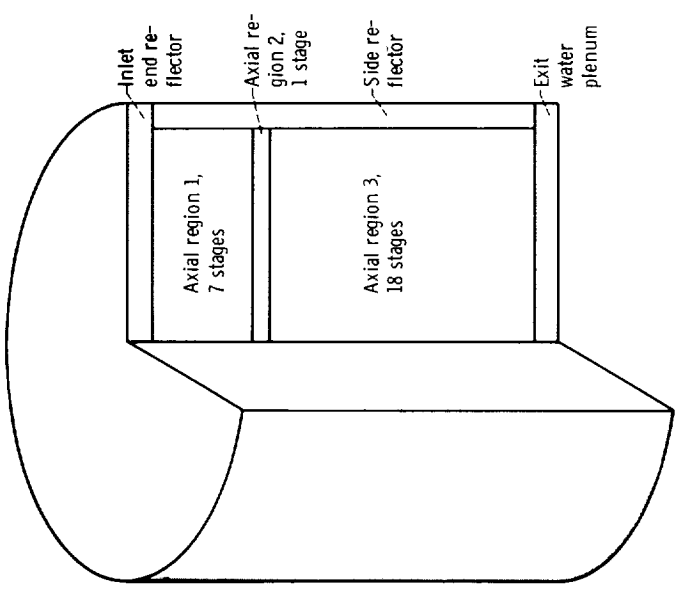

Figure 63. - Axial subdivision of core for Monte Carlo calculations.

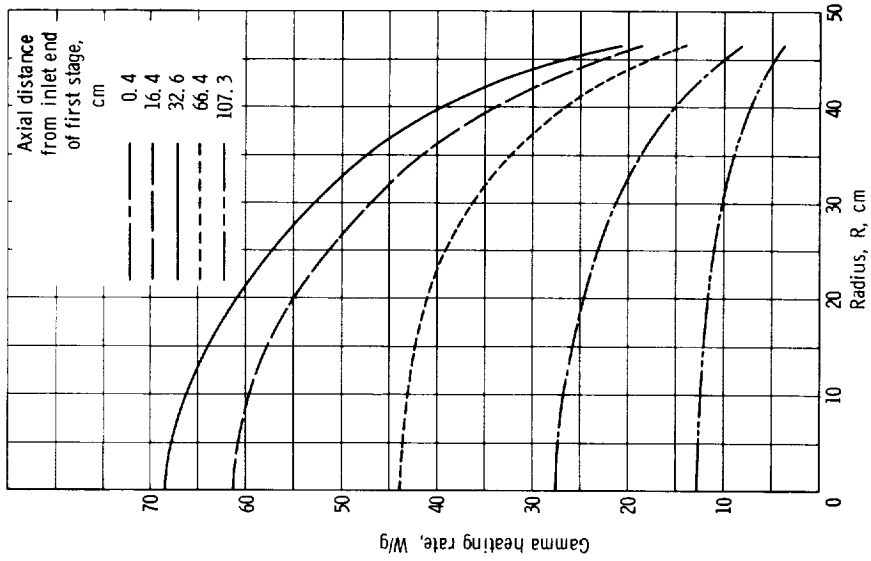

Figure 62. - Calculated gamma heating rate in aluminum. Reactor power, 1540 megawatts.

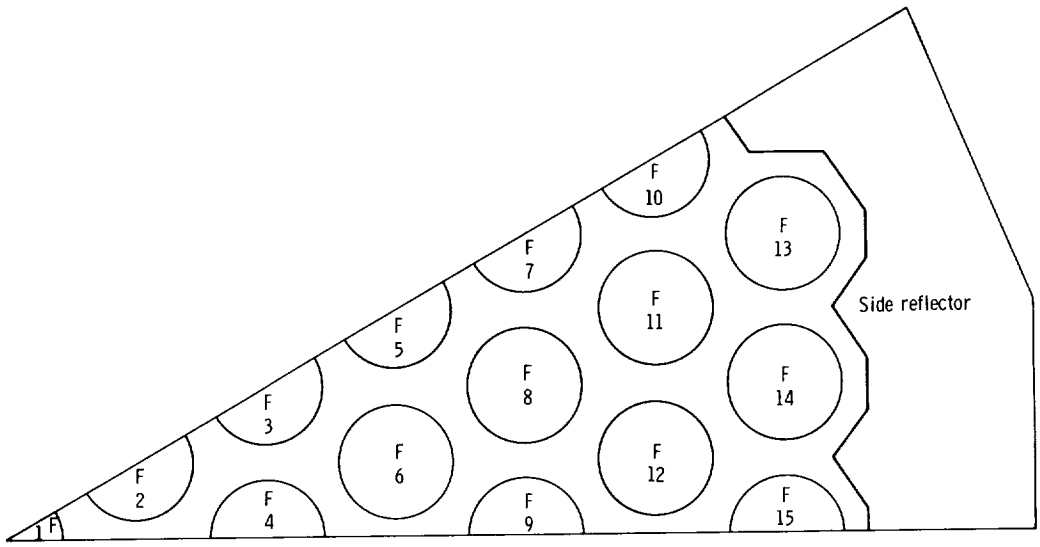

(a) Axial regions 1 and 3.

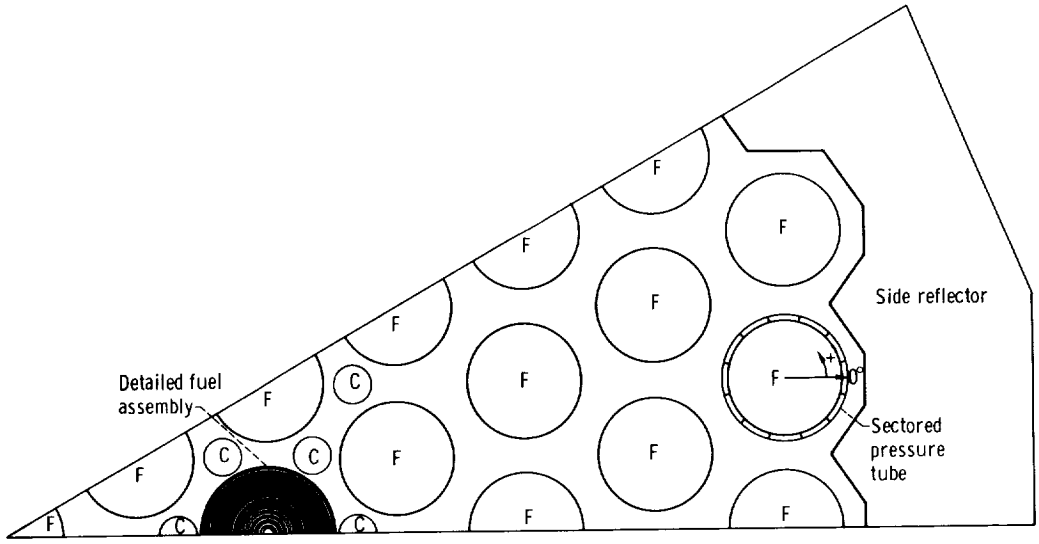

(b) Axial region 2.

Figure 64. - 30° Sector cross section. Homogenized fuel assembly, F; control tube, C.

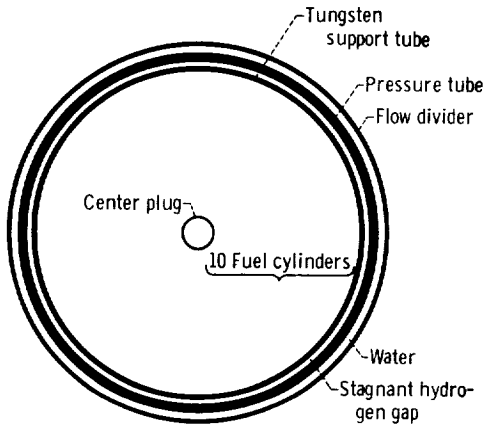

Figure 65. - Detailed representation of fuel stage.

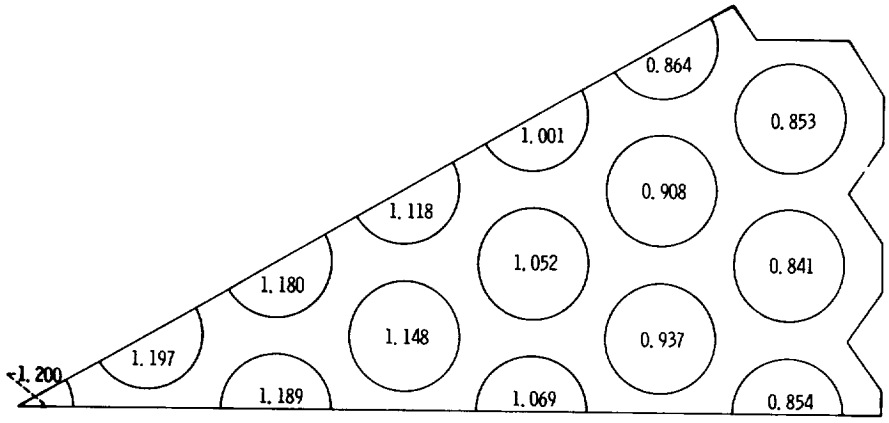

Figure 66. - Gross radial power distribution. Values are ratios of cell power to gross radial average power.

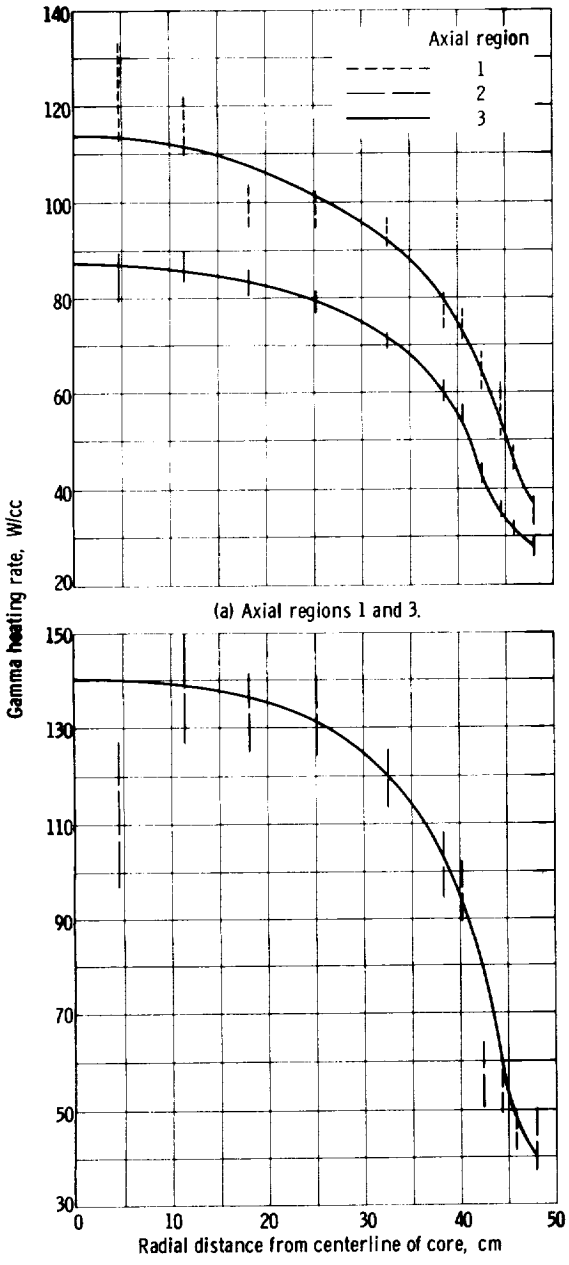

(a) Axial regions 1 and 3.

(b) Axial region 2.

Figure 67. - Monte Carlo calculated gamma heating rates in water regions.

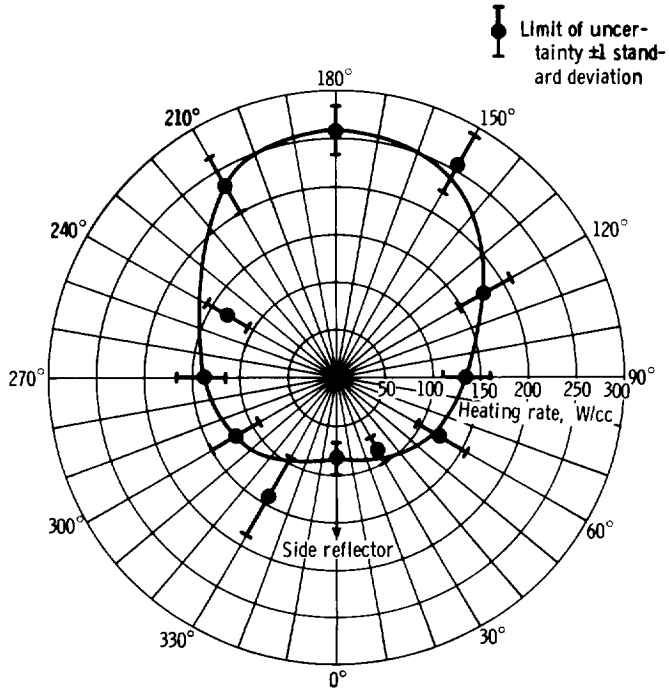

Figure 68. - Pressure tube circumferential gamma heating variation.

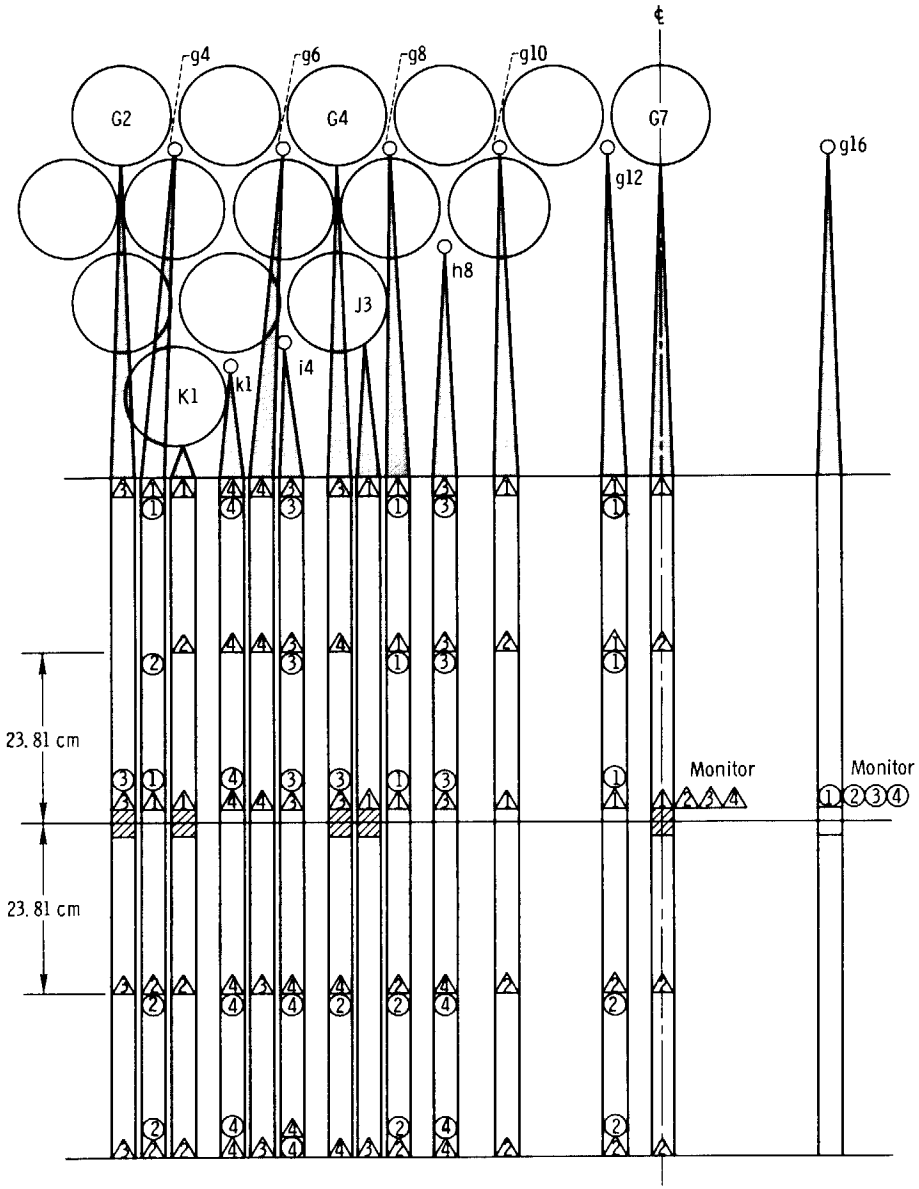

Run	Number of graphite chambers in -	
	Fuel element	Poison tube
1	6	10
2	7	9
3	8	8
4	4	12

Run	Number of polyethylene chambers in -	
	Fuel element	Poison tube
1	---	9
2	1	8
3	2	7
4	---	9

Figure 69. - Placement of gamma and gamma-neutron ionization chambers in core III of TWMR.

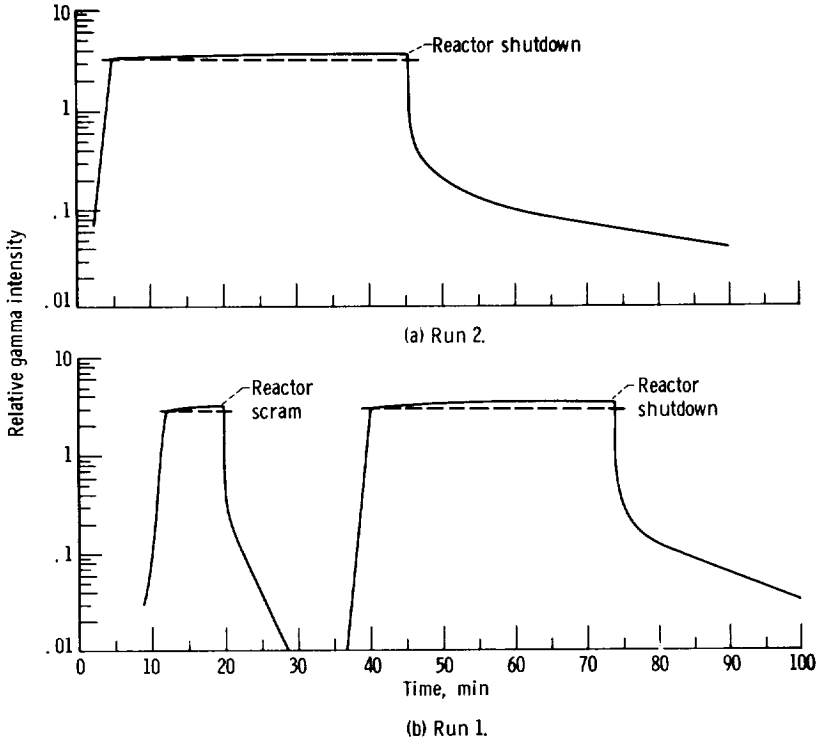

(a) Run 2.

(b) Run 1.

Figure 70. - Gamma intensity time history for ionization chamber runs.

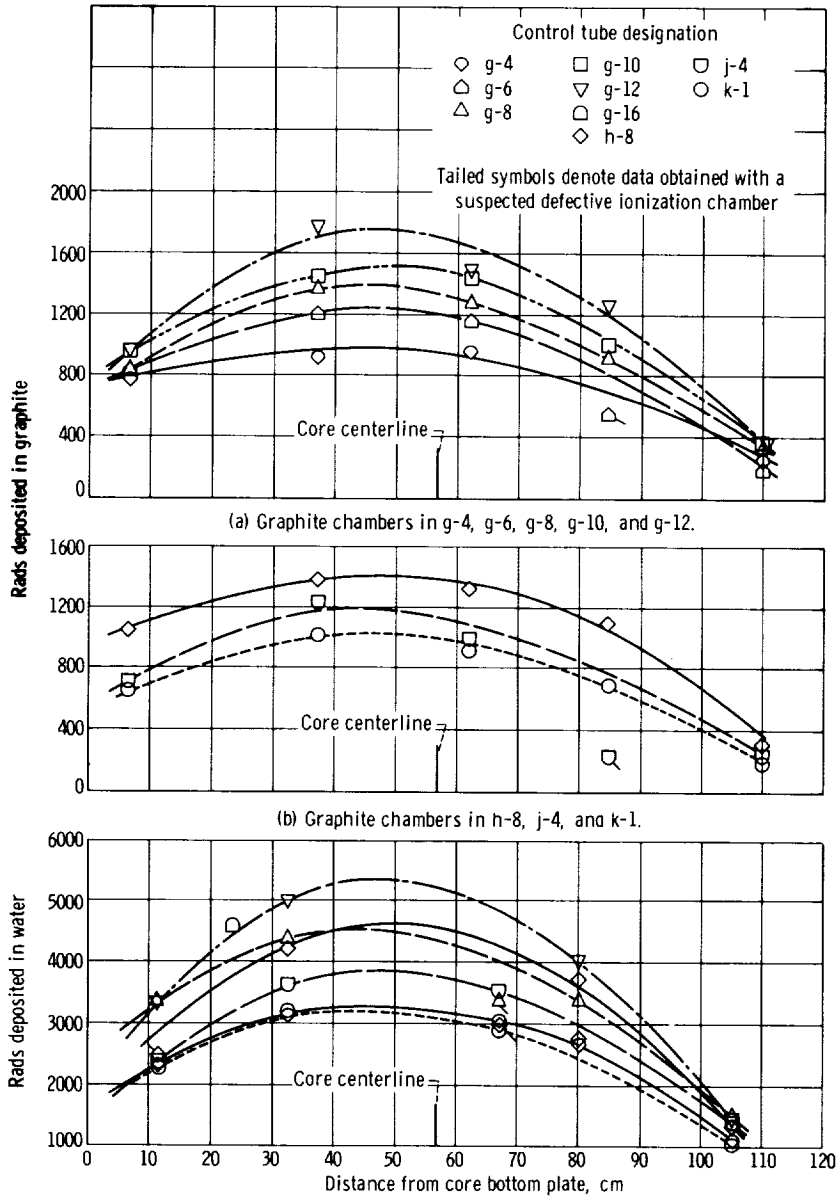

Figure 71. - Axial measurements of gamma and neutron absorbed doses in graphite and polyethylene ionization chambers in nuclear rocket core poison tubes.

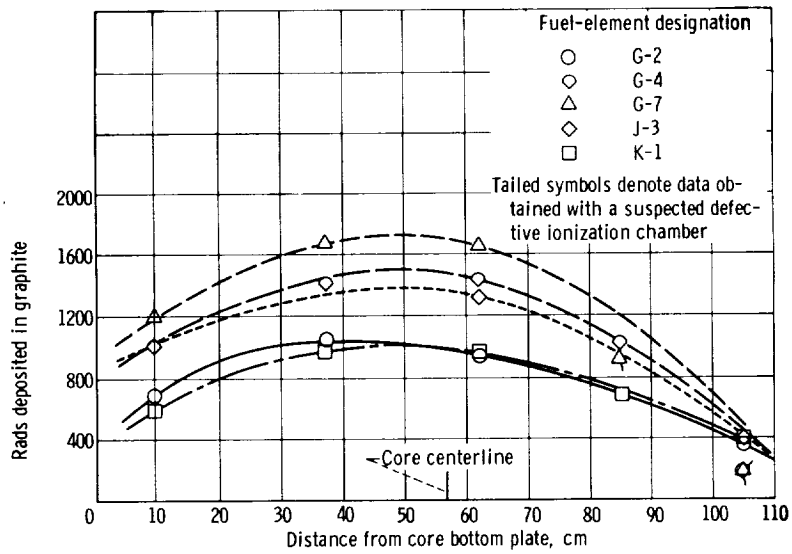

Figure 72. - Axial measurements of gamma and neutron absorbed doses in graphite ionization chambers in nuclear rocket core fuel elements. Graphite chambers in G-2, G-4, G-7, J-3, and K-1.

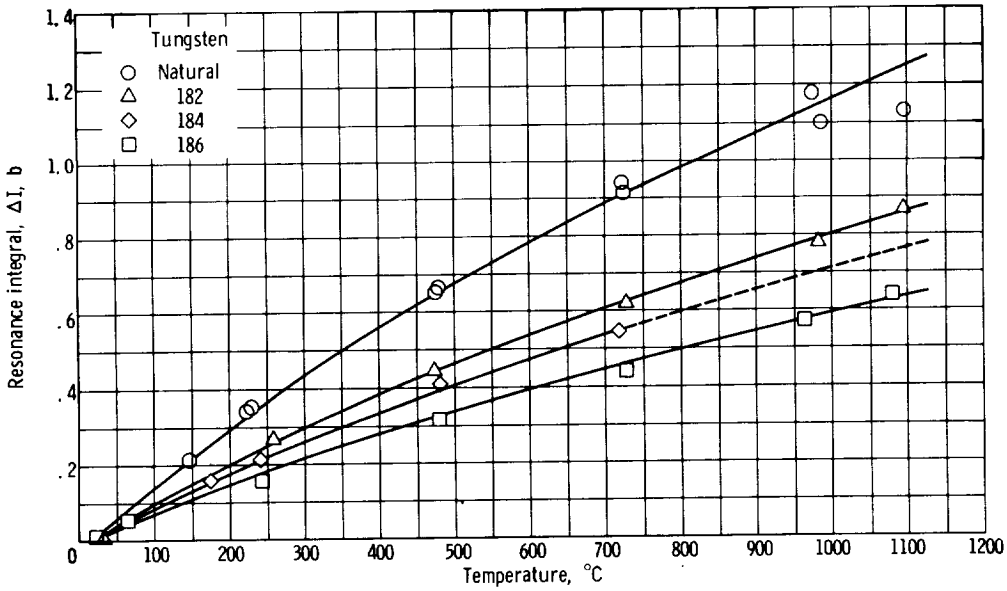

Figure 73. - Change in resonance integral as function of absolute temperature for 1.113-centimeter-diameter samples of natural and enriched tungsten. Curves are least-squares fits to data of the form $I = a + b\sqrt{T}$.